DEVELOPMENT

OF A MATHEMATICAL MODEL

OF A

STEAM-REFORMING FURNACE

Author: M. W. NEWMAN.

M W Newman

Date: SEPTEMBER 1971.

ACKNOWLEDGEMENT

My thanks are due to many people who have assisted me in this work.

The co-operation and financial help of the North Eastern Gas Board in this study is gratefully acknowledged. It was only by the access to the N.E.G.B. Dewsbury Works and the willingness to install additional instrumentation that this project was possible.

The advice and help of Professor Andrew is gratefully recognised. His practical knowledge of reforming plant was an invaluable complement to the theoretical analysis developed in this work.

I would like to thank the staff of the Chemical Engineering Department, especially Professor Haselden and my supervisor Dr. C. McGreavy, who has helped me through many difficult problems. I also wish to thank Mrs. J. Murray, Houldsworth School Librarian for her help.

Finally, I must acknowledge the debt I owe to my wife and parents whose encouragement at critical moments in this work is greatly appreciated.

ABSTRACT

Mathematical models are developed for a steam reforming furnace in both the steady state and unsteady state modes of operation. The one-dimensional radiation field in a participating medium is resolved into various classes of rays which distribute radiant energy to the furnace tubes carrying the process gas.

Results predicted by the model are found to compare satisfactorily with values measured on an actual plant.

A preliminary analysis of the thermal shock effects that arise during transient conditions in the furnace is made and limits on the safe rate of change of load level are indicated.

CONTENTS

LIST OF FIGURES

LIST OF TABLES

CHAPTER 1. INTRODUCTION - SCOPE OF THE PROJECT

1.1 The Industry Based on the Reforming of Hydrocarbons

The major sources of industrial hydrocarbons are deposits of fossil fuels. There is a close correspondence between the volatility of a fuel and its carbon to hydrogen ratio. On a weight for weight basis, this ratio is approximately 3.0 for natural gas, rising to 5.6 for light petroleum distillate, 7.8 for heavy fuel oil, 15.5 for a typical bituminous coal and over 30 for anthracite (1).

Concurrently with the increase in the carbon to hydrogen ratio there is an increase in the average number of carbon atoms per molecule. Natural gas consists largely of methane with small amounts of ethane, propane and butane. Light distillates, in general, are straight-chained paraffins in the C_6 to C_9 range, containing also small quantities of benzene. Heavy oils are complex mixtures of the higher paraffins, whilst the solid fuels are multi-ringed structures containing several hundred carbon atoms per molecule.

An important part of the chemical and allied industries is concerned with transforming the complex carbon compounds found in naturally occurring fuels into simpler gaseous mixtures. The procedure involves two principal operations - "cracking", the breaking down of carbon chains or rings into smaller molecules by the action of heat; and reforming, the reduction of the carbon to hydrogen ratio, generally using steam as the source of additional hydrogen. By manipulating the severity of the cracking conditions and the amount of steam employed and by using special catalysts to promote certain reactions while inhibiting others, the product composition can be varied to suit different demands (2). These demands fall into two categories: the gas may be used as a fuel or it may serve as the starting material for the manufacture of other chemicals.

At moderate temperatures with no steam present, large paraffin

molecules are ruptured by the breaking of carbon-carbon bonds near the middle of the chain and the fragments form a lower paraffin and an olefine. As the temperature increases, the lower paraffins formed tend to crack further producing still lower paraffins and increasing amounts of free hydrogen as the carbon-hydrogen bonds now break. The olefines now become diolefines and then aromatic compounds and if the temperature increases still further, the aromatics are progressively dehydrogenated to multi-ringed tarry substances and eventually to carbon. At these temperatures even the simplest paraffins are cracked into their constituent elements - carbon and hydrogen.

The picture changes when a hydrocarbon is heated together with steam. Initially, the chief products are still the lower paraffins and olefines, but the excess hydrogen tends to saturate the olefines forming more paraffins. As the temperature increases, the paraffin molecules become smaller and a significant increase in the breaking of carbon-hydrogen bonds occurs. Free hydrogen is produced whilst the released carbon atoms form oxides with oxygen from the steam. This is an idealisation of the reactions - in practice, a considerable amount of tar and carbon is formed in a purely thermal cracking process even when a large excess of steam is employed.

In general, the higher the hydrocarbon used as a feedstock, the more difficult it is to stop the reactions at intermediate stages. With regard to reforming reactions, coal may only be fully gasified with steam to produce "water gas" - a mixture of carbon monoxide and hydrogen. Naphtha (light petroleum distillate) on the other hand, yields substantial quantities of methane at moderate temperatures. As the operating temperature of the naphtha-steam reaction is raised, the methane is progressively converted to carbon oxides and hydrogen. The methane rich-product forms the basis of the town gas manufacturing process whereas the hydrogen-rich gas can be treated to produce either pure hydrogen or

a hydrogen-carbon monoxide mixture known as "synthesis gas". Hydrogen is used to manufacture ammonia and for various hydrogenation processes; synthesis gas is the starting point for several important reactions, including methanol production and the "Oxo" process for making other alcohols and carbonyl compounds (4) (5).

The advantages of naphtha and natural gas over solid fuels due to their lower carbon to hydrogen ratios are enhanced by the greater ease with which they can be handled in the fluid state. This facilitates full mechanisation and automatic control in these plants with the result that they have generally replaced coal-based processes for the manufacture of town gas and hydrogen (6).

The particular reforming process studied in this project involves the manufacture of town gas. An important feature of such plants is the frequency with which their operating levels must be changed to meet varying demands, unlike ammonia plants, for example, which normally operate continuously at their design capacities. If in the future manufactured gas is only required for peak loads this aspect will become even more marked and hence considerable savings may be made by changing from one operating level to another in an optimal manner. This point will be discussed further in Sec. 1.3 when the overall objectives of the research are stated.

1.2 Process Description

The actual plant studied is the No.1 stream of the North Eastern Gas Board's Dewsbury Works. It can use either naphtha or natural gas as the reformer feedstock. In common with most other plants nowadays, Town's gas is made by a two-stage process. First, the hydrocarbon is reformed to give a "lean gas" of calorific value approximately 380 Btu / ft^3; this is then enriched to a calorific value of 500 Btu / ft^3 by butane or natural gas. It is possible to make a full town gas in a single, continuous reforming operation (7), but carbon deposition on the catalyst tends to

be excessive unless uneconomically high steam/hydrocarbon ratios are used. Hence most plants that manufacture rich gas in one stage must employ periodic regeneration of the catalyst - they are cyclic in operation and work at low pressures.

Lean gas production requires a reformer exit temperature of about 750°C, midway between the temperatures necessary to produce a full town gas (600°C) and hydrogen (900°C). The catalyst in the present plant is a specially promoted nickel-based ceramic which was developed by Imperial Chemical Industries Ltd. in the late 1950's, known as ICI 46/1. This catalyst permits the use of an economically low steam/hydrocarbon ratio without significant carbon deposition on the catalyst. In addition the process can be run at higher pressures, which increases the throughput for a given area of plant and saves compression costs where the gas is to be fed into a high pressure town gas grid.

Fig. 1.1 is a simplified flowsheet of the process. Naphtha is first preheated, then mixed with a stream of hydrogen-enriched recycle gas prior to being vaporised and superheated to the required temperature for hydro-desulphurisation. This is done before entry to the reformer to avoid poisoning the catalyst; it means that subsequent sulphur removal from the make gas is unnecessary.

Desulphurisation is accomplished in two stages. First, the naphtha vapour and recycle gas pass through a bed of zinc oxide in the primary desulphuriser at 350-400°C which absorbs most of the sulphur compounds. Then in the secondary desulphuriser certain "hard" organic sulphides are reduced to hydrogen sulphide by reaction over a special molybdenum catalyst. Another bed of zinc oxide below the catalyst removes the hydrogen sulphide produced. This vessel is also maintained at around 350-400°C. For successful operation of the molybdenum catalyst, the amount of CO_2 in the recycle gas stream should be kept to a minimum.

The desulphurised vapour is mixed with superheated steam to give an

approximate ratio of 3:1 between the lb.-moles of steam and lb.-atoms of carbon in the feed. If the reformer feedstock is natural gas, it enters the process train at this point since vaporisation and desulphurisation are unnecessary. The steam and hydrocarbon pass to the reforming furnace at 400°C and a pressure in the region of 450 psi.

All reforming reactions are endothermic to some degree so that heat must be supplied to maintain them. A reformer, then, comprises essentially a furnace in which the heat sink is an array of catalyst-filled tubes through which the reacting gases are passed. A more detailed description of the furnace geometry is given in Chapter 2.

Waste heat from the reformer flue gases is recovered in a convection section consisting of a steam superheater, the naphtha vaporiser and the combustion air preheater. Gases leaving the air heater are discharged into the atmosphere via a chimney.

Lean gas leaves the reformer tubes at 750°C and 400 psi. It first passes through the primary make gas waste heat boiler, which raises high pressure steam and cools the lean gas to 390°C, the required temperature for the shift reaction. This makes use of the well-known water gas reaction whereby the conversion of carbon monoxide and steam to carbon dioxide and hydrogen is favoured by low temperatures. The catalyst is chromia-promoted iron oxide. Due to the exothermic nature of the process the gas temperature on exit from the CO shift converter has risen to 430°C.

Heat is recovered from the lean gas stream in a series of plant items. The shift converted gas passes through the secondary make gas waste heat boiler which raises more high pressure process steam; then through a heat exchanger which preheats the feedwater to the boilers; subsequently through the naphtha preheater, the carbonate reboiler and two other heat exchanger items not shown in Fig. 1.1 . These are firstly, a low-pressure boiler which raises steam to de-aerate the raw boiler feedwater and

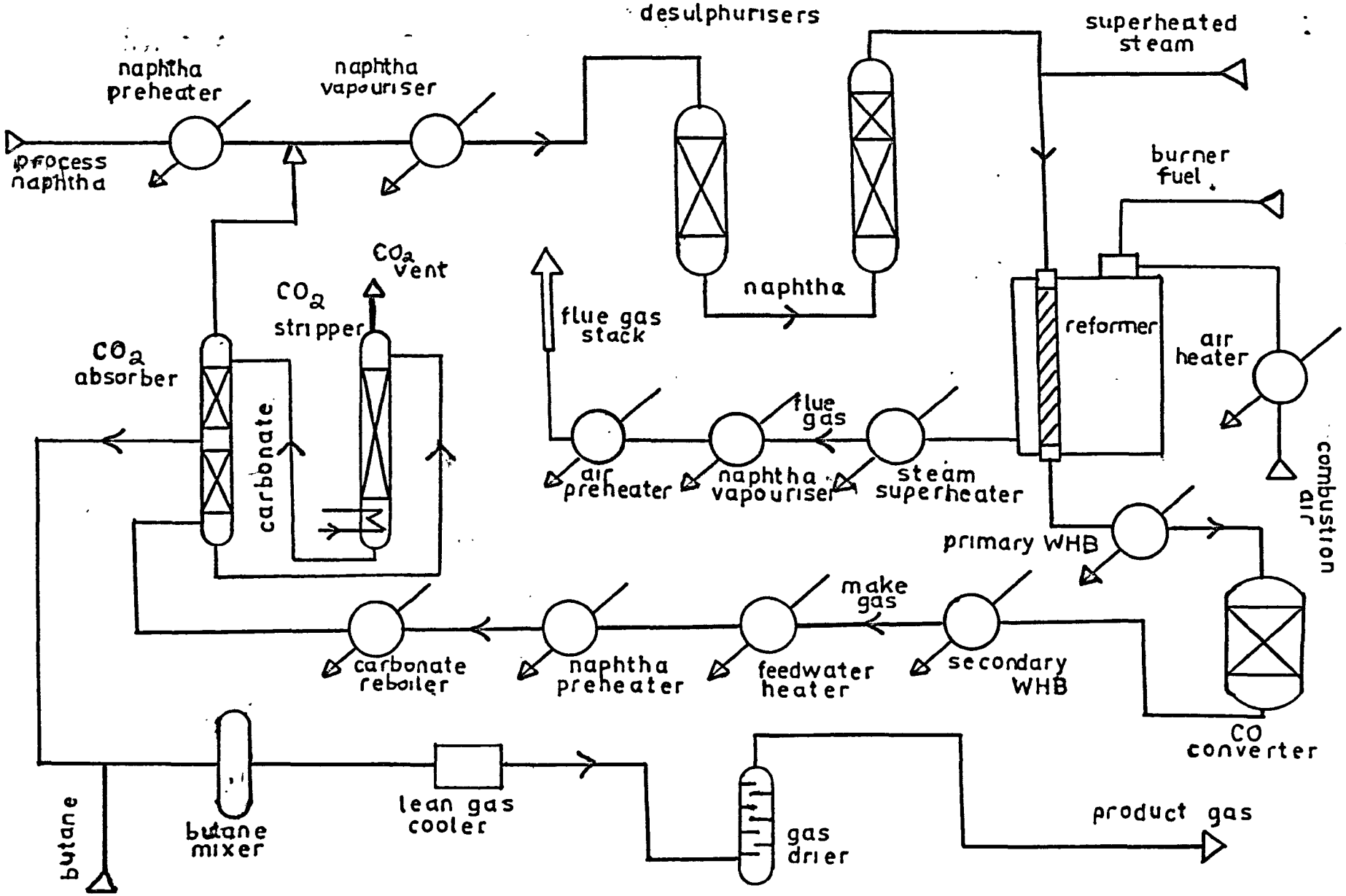

Fig 1.1 Lean gas production

secondly an air-cooled series of finned tubes.

Then the gas enters the base of the carbon dioxide absorption column, its temperature having fallen, by this time, to about 100°C. Condensation begins in the gas stream after the feedwater heater. Therefore, the water produced in this and all downstream exchangers has to be removed by knock-out drums and after suitable degassing, the condensate is returned to the boiler feed tanks. By-passes are installed around each heat exchanger to facilitate temperature control of the gas.

Carbon dioxide is dissolved out of the make gas for two reasons: to control the specific gravity, and to provide a recycle hydrogen stream substantially free from CO_2 for the desulphurisation processes. However, only part of the carbon dioxide is to be removed from the main make gas stream, whilst the minimum possible concentration is desired in the recycle stream. The arrangement adopted is a division of the absorber into two sections, with the gas off-take pipe for the recycle stream situated at the top of the tower and a second off-take pipe for the make gas in between the sections. In this way the lean gas stream is split, the recycle gas being almost completely stripped of CO_2, but the make gas only partially so. Further adjustment in the upward direction of the make gas CO_2 content is possible by means of a by-pass around the lower section of the absorber.

Absorption of CO_2 is carried out by scrubbing the gas with a solution of 30% potassium carbonate which is pumped to the top of the column and allowed to trickle down through the packing. The potassium bicarbonate formed is transferred from the base of the absorber to the top of the stripper column by the difference in pressure between the two columns. In the base of the stripper there is a reboiler to regenerate the potassium carbonate. The stripped CO_2 is vented to atmosphere from the top of the stripper and the regenerated carbonate

solution is returned to the absorber.

Recycle gas from the absorber is passed through an air cooler and then a knock-out drum to remove condonsate. It is then compressed to over 500 psi before joining the liquid naphtha downstream of the naphtha preheater.

Provision is made in the present plant for enriching the lean gas stream with either natural gas, liquified petroleum gas (usually butane) or by the Gas Council's hydrogenation process which uses part of the naphtha feedstock as the basis of the enrichment. If the lean gas is "cold-enriched", i.e. with an external source of natural gas, or butane, it passes through an air cooler from which it emerges a few degrees above ambient temperature. After condensate removal, it is mixed with the enriching element before proceeding to the gas drying column where traces of water vapour are removed by scrubbing with glycol. The final gas enters a delay volume to guard against off-specification gas and is then odorised, metered and fed into the grid.

The hydrogenation process is a thermal cracking reaction in which naphtha vapour and lean gas are contacted at 750^{o}C and 350 psi. Both high temperatures and high pressures are necessary for the hydrogenation to occur; otherwise large quantities of unsaturated hydrocarbons will appear. The mechanism of the reactions is barely understood. No catalyst material is actually used but it seems necessary that a trace of sulphur be present in the naphtha and a fairly high percentage of CO_2 in the lean gas stream (9).

A small amount of raw naphtha is therefore blended with the desulphurised stream before entry to the hydrogenator vessel. The required CO_2 content is obtained by adjusting the by-pass around the absorber. In addition a small quantity of steam is left in the lean gas stream to prevent carbon formation. Fig 1.2 gives the flowsheet of the hydrogenation process.

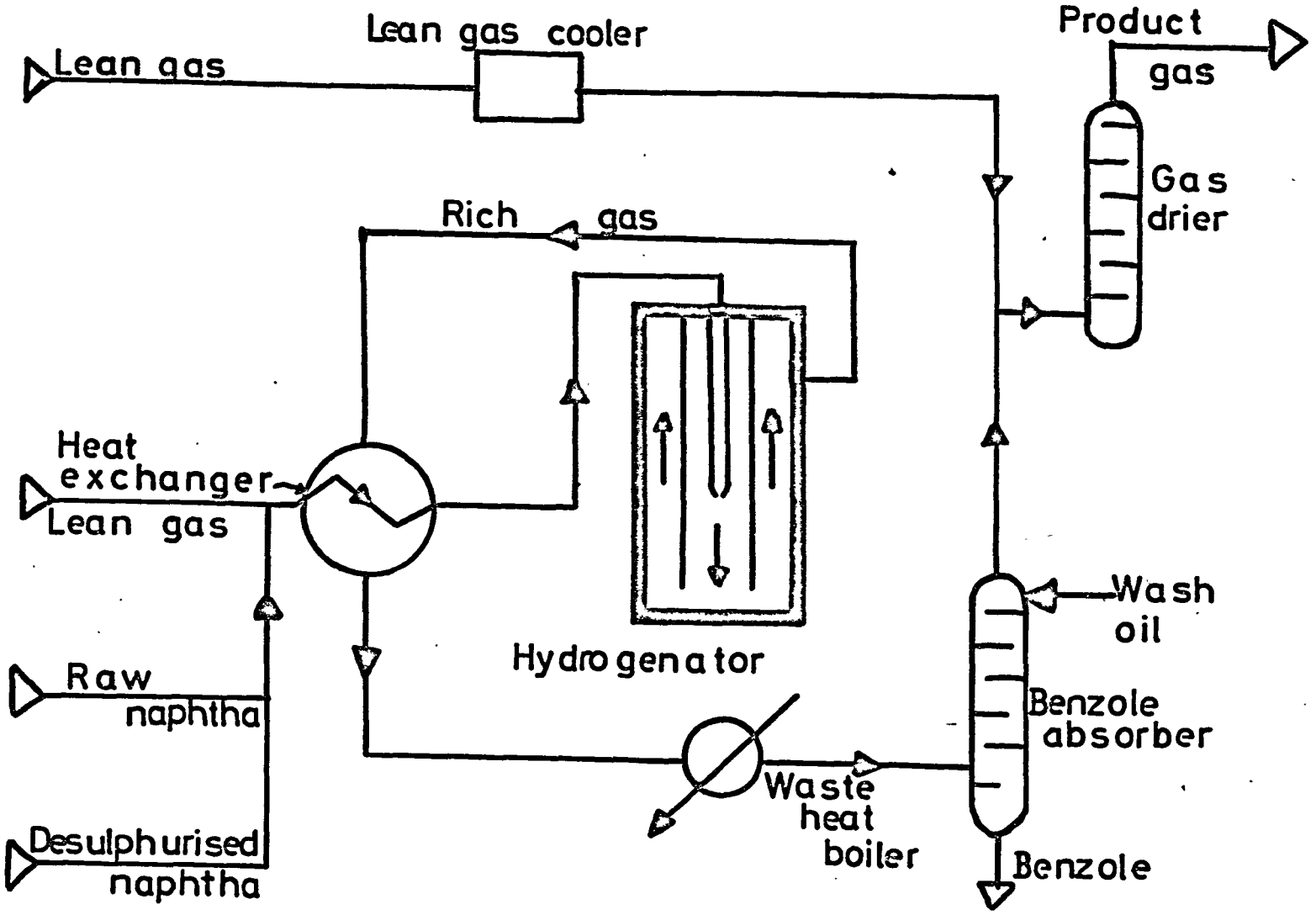

Fig 1.2 : ENRICHMENT BY THE GAS COUNCIL HYDROGENATOR.

Products obtained from the hydrogenator are principally methane and ethane, with a little ethylene and some aromatic compounds which are subsequently stripped from the gas and added to the furnace burner fuel. The reactions are somewhat exothermic so by using the sensible heat of the product gases to preheat the ingoing reactants, no external heat source is required. The calorific value of the rich gas lies between 750 and 800 Btu / ft^3. Finally, the rich and lean gas streams combine and are dried in the glycol absorber before feeding to the grid.

Clearly, the hydrogenation enrichment process is the most economic if cold enriching feedstocks command a significant price premium. However, this is becoming less so as the availability of natural gas increases so that the present trend is to enrich the reformed naphtha with natural gas.

1.3 Research Objectives

There are several aspects of gas-making plants that make computer control and modelling appear attractive. As stated previously, variations in ambient temperature result in fluctuating demand for town gas. Consequently, reforming plants must be capable of operating over a wide range of throughputs and be able to switch from one operating level to another as rapidly as possible. The establishment of an optimum set of controlled variables at a given operating level is the objective of steady state optimisation, whilst moving from one operational level to the desired level along an optimal path is the basis of dynamic optimisation and control studies.

If the Gas Council's hydrogenator is used, there arises an interesting feed-forward control problem, since the variation in the lean gas state on exit from the shift convertor will affect the products emerging from the hydrogenator. To operate the hydrogenator in an optimum manner, therefore, it is necessary to anticipate and counteract

the effects of these disturbances by altering its control settings.

The steam-raising system on the other hand is a good illustration of feedback control. As indicated in Fig 1.1, process steam is raised in boilers using the waste heat of both the flue gas and make gas streams. These boilers are all connected to a common steam drum, so from the steam-raising viewpoint only the total excess heat available from the furnace is important. This quantity is defined by the difference between the heat released by the burners and the heat required to maintain the endothermic chemical reactions. Thus the steam pressure is determined primarily by a feedback loop to the burner fuel flowrate.

It was decided that the ultimate aim of the project should be the implementation of supervisory control on a gas-making stream with special attention being paid to the dynamic behaviour of the system as it moves from one load level to another. It was considered that steady state optimisation would not bring about a comparable reduction in operating costs because the system is fairly tightly constrained, primarily by the need to achieve correct gas specification and to maintain sufficient waste heat capacity for steam generation. Hence the range of possible operating conditions for a given throughput is limited and conventional analogue instruments will normally maintain the process close to these set points.

Essentially, the thermal economy of the process determines its viability. A certain fraction of the hydrocarbon feedstock has to be burnt in order to reform the remainder. Waste heat from the furnace is then utilised in the generation of process steam. It is evident that the reforming furnace plays a key role in this system and it is on this that the major effort should be concentrated.

A key element in optimisation and control studies is the development of a mathematical model of the process. If the aim is supervisory control in the unsteady state, the model must be able to perform the following functions:

i) Prediction of the dependent process variables from the independent ones. Obviously, effective control action can be exercised only if the consequences of a given action can be foreseen. In particular, the transient behaviour of the system in response to a change in the input variables must be analysed to ensure that constraints on certain parameters are not violated.

ii) Computation of the optimal, time-dependent control vector required to bring the process to a new operating level. The literature on this subject is extensive (10) (11), but is almost always concerned with lumped-parameter representations and often with such inconveniences as time lags and non-linearities discounted. Since many chemical plants cannot be described adequately in these terms some simplification of the model is called for. Several techniques are available for doing this (12).

The present work is concerned with the development of a detailed dynamic model of the reforming furnace at Dewsbury which can be checked against data recorded from the plant. First a generalised model is formulated in terms of state variable equations, then a subset of these solved for the steady state case. Results from this model are checked against in-plant data. A second steady state model is also described which follows more closely the actual geometry of the furnace. Finally, the full dynamic model is solved and this too compared with values recorded from plant tests.

CHAPTER II. FORMULATION OF A GENERALISED MODEL.

2.1 Special Features of a Reforming Furnace

Furnaces consist essentially of refractory-lined enclosures, inside which there is a means of transporting the heat sink into and out of the furnace volume in batch-wise or continuous manner. Apart from electric furnaces, the heating medium is the body of hot combustion gases within this volume so that the predominant mode of heat transfer, even at moderate temperatures is by radiation.

Fig 2.1 shows a schematic side elevation of a typical reformer. It is of rectangular construction and contains three rows of catalyst-packed vertical tubes down which the process gas (heat sink) flows. Burners are distributed over the roof area, firing downwards into the furnace volume between the tube lanes. The number of burners employed is less than the number of tubes; normally between one quarter and one third as many. One of the aims of successful reformer design is to ensure that, at a given horizontal level, the configuration of burners used gives as nearly uniform a heat flux as possible to every tube.

The fuel used by the burners is either natural gas or naphtha, mixed with a small amount of aromatic hydrocarbons if the Gas Council rich gas hydrogenation process is in operation. Liquid naphtha is first atomised with air before reaching the burner nozzles. The flue gases pass downwards and are removed through ducts built into the floor of the furnace.

It is clear that the layout of a reformer is rather different from that of steam-raising furnaces which have their bank of tubes around the walls of the combustion chamber and the flue gas outlet somewhere in the upper part of the furnace. Such an arrangement means that the gases are well-mixed, of substantially constant composition and temperature. In fact, the Topsoe reformers are side-fired with the flue

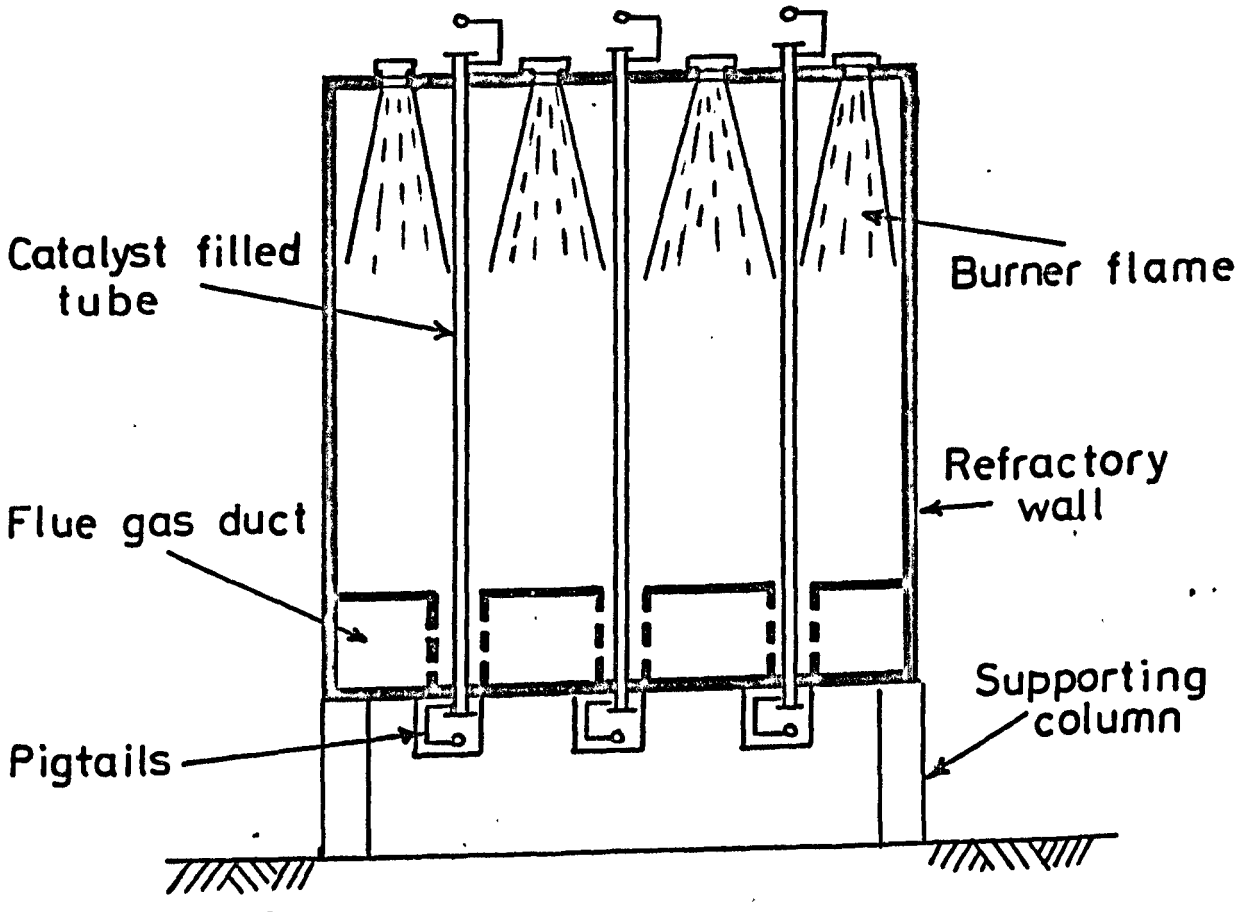

Fig 2·1 SCHEMATIC DIAGRAM OF REFORMER

at the roof of the furnace (14) so that these furnaces do, to a reasonable approximation, approach uniform conditions.

Calculation of the radiant heat transferred between the gases and tube bank is then possible by defining a single geometrical quantity known as the "mean beam length". This was done by LOBO and EVANS (15) and still forms the basis of design and performance modelling methods for these furnaces.

A straightforward lumped parameter treatment like this cannot hold good for a top-fired reformer. In the upper region of the furnace, the jetting action of the burners will induce turbulent recirculation of the combustion gases so that here their temperature will be fairly constant. Below this region, however, the gas temperature falls steadily with increasing distance down the furnace as heat is transferred to the tubes. This stable temperature pattern causes the gas to travel in plug flow down the furnace, parallel with the flow of steam and naphtha with little recirculation or back-mixing. Any formulation of a model for a reforming furnace must take account of these gradients in the radiation field, which transforms it into a distributed parameter problem.

2.2 Some Methods of Furnace Modelling

There are many methods of analysis available for evaluating the heat transfer characteristics of industrial furnaces. The degrees of sophistication and consequent mathematical complexity of these will vary enormously: a satisfactory model is one that retains all essential features of the system but is nevertheless open to numerical evaluation in terms of the computing facilities available.

The inadequacy of simple lumped parameter treatments of the Lobo and Evans type has already been mentioned. This is true even for the steady state case. Certain refinements are possible to take account of the mutual shielding of adjacent tubes, reflection of radiant flux

from the refractory walls on to the tubes and the fact that the gas does not absorb and emit radiation at constant rate for all wavelengths (relaxation of the grey gas assumption). These are all described in HOTTEL's chapter in the book by McAdams (16). It is always necessary however, to assume constant temperature throughout the furnace volume.

One method which does, in principle, deal with non-uniform temperature distributions in furnaces is the "zoning" method developed by HOTTEL and co-workers (17) (18). This involves dividing the boundary surfaces and furnace volume into a matrix of isothermal compartments. Exchange equations for each pair of compartments are set up and the result is a system of linear equations whose variables are the various radiant fluxes. By further sub-division of the compartments, the accuracy of the solution can be improved to any desired extent.

While this technique is perfectly sound in the steady state case, it does not readily lend itself to extension to the unsteady state. Also there are two drawbacks when applied to a reformer; first, the isothermal compartments must be at least two-dimensional because the tube planes are perpendicular to the gas temperature variation. This means that the nett transfer of heat in the gas phase is vertical, whereas that between gas and solid boundaries is horizontal so the essentially one-dimensional nature of the problem is destroyed. Secondly, there is the convective flow of heat transported by the bulk flow of process gas - this is not easily superimposed on the flux balance equations.

The completely general problem of radiative transfer in a non-isothermal, absorbing and scattering medium has been considered by numerous authors in recent years. Basically, the problem is treated in a similar manner to conduction and convection studies by compiling an energy balance on an arbitrarily located volume element in the radiation field. However, absorption and emission of flux will take place over finite path lengths resulting in an integral expression for

the heat generation term, and consequently, the equation expressing conservation of energy will be an integro-differential one. Fundamental derivations are to be found in the works of CHANDRASEKHAR (19) and KOURGANOFF (20). The one-dimensional problem with a non-scattering medium is outlined in Appendix A.

Even if all the system parameters are available, the solution of equations such as these is very difficult. Therefore, although the problem can be formulated, its application to engineering systems is limited. Some examples are available in the literature (21) (22) (23), and the review article by CESS (24) presents perhaps the simplest cases that can be considered. Any realistic treatment of a reformer needs to consider simultaneous radiative and convective transport of heat with space-varying boundary temperatures. Papers by CHEN (25) and VISKANTA (26) studied a problem similar to this assuming steady state conditions prevailed, but found that the mathematical difficulties were severe.

Clearly certain simplifying assumptions must be made in the analysis before solution is possible and fortunately these are available. First, however, the general problem in terms of state equations will be discussed.

2.3 The State Variable Equations

The physical state of a system at time θ may be characterised by a finite number of real quantities, $x_1, x_2 \ldots\ldots x_n$. These variables constitute the state vector $\underline{x}$. To control the system, there must be a number of quantities that are susceptible to independent, external manipulation; this control vector $\underline{u} = (u_1, u_2 \ldots\ldots u_m)$ is also a function of time.

Any set of mathematical equations which relate the output state variables to the input variables, controlled variables and time is known as a dynamic model of the system. The basic laws which govern the behaviour of physical systems such as the conservation of matter, energy

and momentum, lead to formulation of the model in terms of differential equations. If the state variables are spatially variant, the model will be described by a set of partial differential equations in space and time; otherwise they becomes ordinary differentials with time as the only independent variable.

For reasons that were discussed in Section 2.1, it is not possible to regard a reformer as other than a distributed parameter problem. Thus the simplest form that the state equations can take is the vector equation

$$\dot{\underline{x}} = \underline{f}(\underline{x}, \underline{u}, \theta) \qquad \text{-------} \quad (2.1)$$

where $\underline{f}$ is in general a non-linear vector function and $\dot{\underline{x}}$ the substantial (total) derivative of the state vector. Considering only one space dimension, this becomes,

$$\frac{\partial \underline{x}}{\partial \theta} + \frac{\partial \underline{x}}{\partial z} \cdot \frac{\partial z}{\partial t} = \underline{f}(\underline{x}, \underline{u}, \theta) \qquad \text{-------} \quad (2.2)$$

$$\frac{\partial \underline{x}}{\partial \theta} + \underline{V} \frac{\partial \underline{x}}{\partial z} = \underline{f}(\underline{x}, \underline{u}, \theta) \qquad \text{-------} \quad (2.3)$$

The reformer may be characterised by two separate streams of gases flowing down the furnace which interact thermally. As in all furnace problems, the important variables are the enthalpies of the two gas streams that constitute the source and sink of heat, plus the radiation flux within the furnace enclosure. The components of the state vector become,

$$\underline{x} = (H_g, H_p, Q) \qquad \text{-------} \quad (2.4)$$

In addition to the vector of state variables, the model equations must contain those quantities that are externally manipulated, namely the control vector $\underline{u}$. For a reformer the principal ones are the steam/carbon process feed ratio, inlet temperature and flowrate of process feed and the mass flow of fuel to the burners. All of these can in fact, be directly related to the state variables chosen; for instance the process feed parameters may be incorporated within the process enthalpy H_p and the burner fuel flowrate determines the flame

temperature and hence the enthalpy of the flue gas, H_g. It is not therefore proposed to distinguish explicitly a separate control vector within the model equations at this stage. With this simplification, the model equations now assume the general form

$$\dot{\underline{x}} = \underline{f}\left(\underline{x}, \Theta\right) \qquad \text{------- (2.5)}$$

where $\underline{f}$ is still, of course, a non-linear vector function.

An expression for the conservation of energy taken over an incremental volume of the furnace is (27),

$$\rho_g c_g \frac{\partial T_g}{\partial \Theta} + \rho_g V_g c_g \frac{\partial T_g}{\partial z} + \frac{\partial H_p}{\partial \Theta} + V_p \frac{\partial H_p}{\partial z} + \frac{dQ}{dz} = 0 \qquad \text{------- (2.6)}$$

or, more concisely,

$$\frac{D}{D\Theta}\left(H_g + H_p + Q\right) = 0 \qquad \text{------- (2.7)}$$

This assumes that the stream temperatures and the radiation flux are constant over any cross section of the furnace so that the problem is limited to one spatial dimension. Energy changes within the gas streams due to thermal conduction, thermal expansion and viscous dissipation are neglected.

It is useful to de-couple the direct thermal effects of the flue gas and process gas - that is, to assume that there is no direct transfer of heat from the flue gas to the furnace tubes and thence to the process gas by simple conduction or convection. Instead the flue gas only absorbs and emits radiation flux in certain regions of the spectrum and it is this flux that interacts with the tubes which effectively comprise the heat sink of the furnace.

Thus the two energy balances for the gas streams become;

$$\frac{D}{D\Theta} H_g = \int \left(\beta_\lambda Q_\lambda - 4 K_\lambda \sigma T_g^4\right) d\lambda \qquad \text{------- (2.8)}$$

$$\frac{D}{D\Theta} H_p = \int \left(a_t \varepsilon_{t\lambda} - 2\sigma T_t^4\right) d\lambda \qquad \text{------- (2.9)}$$

where the subscript λ refers to the monochromatic values and T_g and T_t

are the flue gas and tube skin temperatures at time θ and distance x from the furnace roof.

To obtain a similar relation for the radiation flux term the equations of transfer for the radiation beams in the furnace enclosure must be considered in more detail. The total flux term Q can be expressed in terms of the monochromatic intensity of radiation I_λ, propagated over a solid angle w at direction ϕ to the normal. Thus:

$$Q = \int_0^\infty \int_{4\pi} I_\lambda \cos\phi \, dw \, d\lambda \qquad \text{------- (2.10)}$$

Putting $\mu = \cos\phi$ and $dw = \sin\phi \, d\phi$ eq. (2.10) becomes

$$Q = 2\pi \int_0^\infty \int_{-1}^{1} I_\lambda \mu \, d\mu \, d\lambda \qquad \text{------- (2.11)}$$

It is shown in Appendix A that the equation for I_λ between two parallel plates in a non-scattering medium is given by the two equations:

$$I(\tau, \mu) = I(0, \mu) e^{-\tau/\mu} + \frac{1}{\pi} \int \eta_\lambda(t) e^{-\frac{(\tau_\lambda - t)}{\mu}} \frac{dt}{\mu} \qquad \text{------- (2.12)}$$

$$I(\tau, -\mu) = I(\tau_0, -\mu) e^{-\frac{(\tau_0 - \tau)}{\mu}} - \frac{1}{\pi} \int \eta_\lambda(t) e^{-\frac{(\tau_\lambda - t)}{\mu}} \frac{dt}{\mu} \qquad \text{------- (2.13)}$$

where the optical depth parameter τ is defined as $\tau = \int_0^x \beta_\lambda \, dx$ and t is a dummy variable of integration. The integral terms in Eqs (2.12) and (2.13) are due to energy emitted in the direction of the beam from the finite volume contained in the solid angle dw. Because this energy originates over a finite path lengths, it causes the equation of transfer to become an integral equation.

In the context of a reforming furnace, the source function η_λ must contain terms for radiant emission from the tubes and furnace refractory walls and similarly, the absorption coefficient includes absorption by the solid surfaces as well as by the furnace gas.

The integro-differential equations developed above are extremely difficult to solve unless considerable simplifications are made. There are three general categories of simplifying assumptions: they are, (i) a directional averaging of the angular distribution of flux intensity, (ii) approximations for the radiant heat source terms, and (iii) assumptions regarding the spectral energy distribution of the

absorption and emission of radiation by the flue gas.

Those of the first category recognise the inherent difficulty of evaluating the term $\int_{4\pi} I_\lambda d\omega$ (or $\int_{-1}^{1} I_\lambda \, d\mu$ if axial symmetry exists). If I_λ can be considered as independent of μ this problem, of course, disappears. By defining "mean intensities" I_λ^+ and I_λ^- of the radiation field for the downward and upward hemispheres respectively, such a relation is obtained. These beams are,

$$I_\lambda^+(\tau) = \int_0^1 I(\tau,\mu)\, d\mu \qquad I_\lambda^-(\tau) = \int_{-1}^{0} I_\lambda(\tau,\mu)\, d\mu \qquad \text{-----(2.14)}$$

so that the radiation intensity is a function of the distance τ only. This technique is called the Schuster - Swarzchild approximation and provides a very useful tool for the solution of many engineering problems in radiation transfer.

The original differential equation of transfer developed in detail in Appendix A is:

$$\frac{\mu\, dI_\lambda(\tau,\mu)}{d\tau} + \beta_\lambda I_\lambda(\tau,\mu) = \eta_\lambda(\tau,\mu)$$

Since from Eqs (2.14)

$$\int_0^1 \mu \frac{dI}{d\tau}(\tau,\mu)\, d\mu = \frac{1}{2}\int_0^1 \frac{dI}{d\tau}(\tau,\mu)\, d\mu = \frac{1}{2}\frac{dI_\lambda^+(\tau)}{d\tau}$$

and

$$\int_{-1}^0 \mu \frac{dI_\lambda}{d\tau}(\tau,\mu)\, d\mu = \frac{1}{2}\int_{-1}^0 \frac{dI_\lambda}{d\tau}(\tau,\mu)\, d\mu = \frac{1}{2}\frac{dI_\lambda^-(\tau)}{d\tau} \qquad \text{-----(2.15)}$$

the equation of transfer may be re-written as two equations, namely,

$$\frac{1}{2}\frac{dI_\lambda^+}{d\tau} + \beta_\lambda I_\lambda^+ = \eta_\lambda(\tau,\mu)$$

$$-\frac{1}{2}\frac{dI_\lambda^-}{d\tau} + \beta_\lambda I_\lambda^- = \eta_\lambda(\tau,\mu) \qquad \text{------- (2.16)}$$

Now an approximation is required for the source term η_λ in order to avoid integration over the finite path lengths used in setting up Eqs (2.12) and (2.13). One well-known technique makes use of the Rosseland equation, or optically thick approximation. This postulates that the radiation is fully attenuated after passing only a short distance through the medium, so that the transfer processes will depend only on the local temperature of the medium, thus providing a relation between the radiant energy emitted from a particular element with the emissive power at that point (28). However this does not take into account

radiation fluxes from the solid surfaces and cannot be valid anywhere near the boundaries. Hence the usefulness of the Rosseland equation in the case of an industrial furnace is doubtful (29).

The other limiting case (the "optically thin" approximation) when the medium has negligible self absorption and interchanges flux only with the boundary walls is also inapplicable to this case.

The basic assumption made in the present treatment is that in passing through each incremental volume of the furnace, the radiation beams will be attenuated by an amount proportional to the absorbing power of the flue gas, furnace tube surface and refractory surface within that increment. The beams will be augmented by emission terms dependent upon the emissive powers and local temperatures of these materials within the same increment. This means that instead of integrating the source term over a finite path length, the mean value of the emission at a given horizontal level is taken as the sum of the individual emission terms for the gas tube and refractory surfaces at that level.

This also circumvents one problem of using the Schuster-Swarzschild approximation. Since the horizontal components of flux intensity no longer exist, the beams should not intercept the catalyst tubes. Clearly this is unacceptable, but if the solid surfaces are considered to be uniformly dispersed throughout the radiation field, which is effectively what has been done, the radiant beams and solid components can now interact.

The monochromatic flux balance equations become;

$$\frac{dI_\lambda^+}{dt} = (-\beta_\lambda - \varepsilon_t a_t - \varepsilon_r a_r) I_\lambda^+ + \beta_\lambda \sigma T_g^4 + \varepsilon_t a_t \sigma T_t^4 + \varepsilon_r a_r \sigma T_r^4 \quad \text{---(2.17)}$$

$$-\frac{dI_\lambda^-}{dt} = (-\beta_\lambda - \varepsilon_t a_t - \varepsilon_r a_r) I_\lambda^- + \beta_\lambda \sigma T_g^4 + \varepsilon_t a_t \sigma T_t^4 + \varepsilon_r a_r \sigma T_r^4 \quad \text{---(2.18)}$$

To obtain the total flux intensity it is necessary to integrate I_λ^+ and I_λ^- over the entire spectrum, i.e.

$$I^+ = \int_0^\infty I_\lambda^+ \, d\lambda \quad \text{and} \quad I^- = \int_0^\infty I_\lambda^- \, d\lambda$$

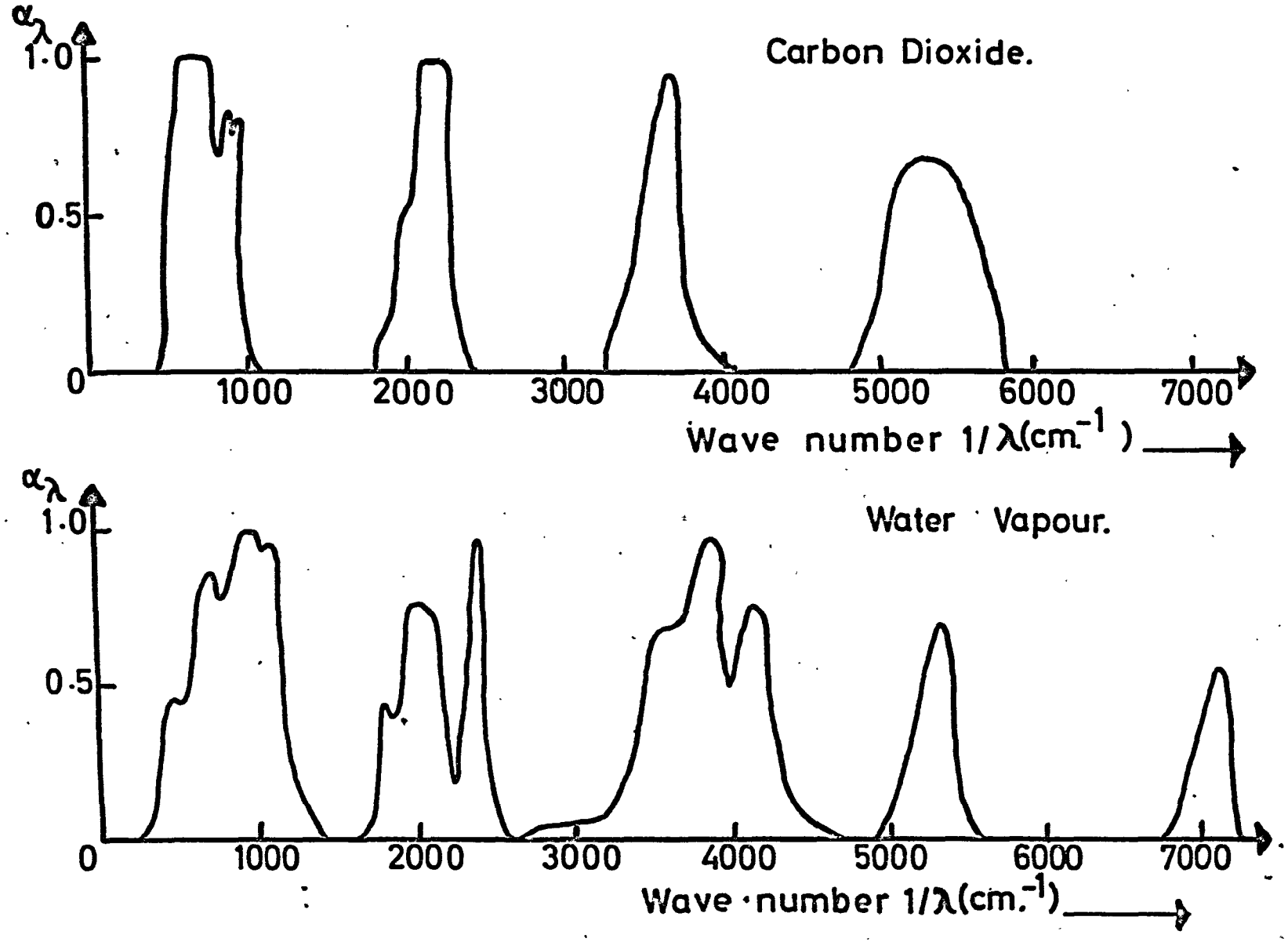

Fig. 2.2: ABSORPTION SPECTRA FOR CO_2 AND H_2O.

$$I^+ = \int_0^\infty I_\lambda^+ d\lambda \qquad I^- = \int_0^\infty I_\lambda^- d\lambda \qquad \text{------- (2.19)}$$

Carbon dioxide and steam, the principal products of hydrocarbon combustion are found to absorb and emit thermal radiation only in certain discrete wavebands (see Fig 2.2). In the intervening parts of the spectrum, the gases are substantially transparent, in the way that gases like oxygen with symmetrical molecules are for all wavelengths. A useful approximation to the spectral distribution of absorbing power consists of dividing the entire waveband of interest into two regions; (a) the absorption region, which comprises, a fraction ψ of the total spectrum, and (b) the transparent region fraction $(1 - \psi)$.

By this means I may be classified into two groups, I_a and I_b which represent averages of the radiation intensities falling respectively inside or outside the absorption bands. Applying this process to the two beams I^+ and I^-, the flux intensity is finally decomposed into four groups, thus:

$$I = I_a^+ + I_a^- + I_b^+ + I_b^- \qquad \text{------- (2.20)}$$

Hence the state vector $\underline{x}$ becomes,

$$\underline{x} = (H_g, H_p, I_a^+, I_a^-, I_b^+, I_b^-) \qquad \text{------- (2.21)}$$

The full set of equations for the system will comprise six differential equations, one for each component of the state vector. Together these will satisfy the conservation of energy equation (2.7). For the steady state case, the equations will be ordinary differentials with distance down the furnace as the independent variable. The dynamic equations will be partial differentials although the time derivatives of the radiant beams are neglected. The terms in the equations are shown diagramatically in Fig. 2.3.

$$\frac{\partial H_g}{\partial \theta} + V_g \frac{\partial H_g}{\partial x} = -2\beta\sigma\psi T_g^4 + \beta I_a^+ + \beta I_a^- \qquad \text{------- (2.22)}$$

$$\frac{dI_a^+}{dx} = (-\beta - \varepsilon_t a_t - \varepsilon_r a_r) I_a^+ + \beta\sigma\psi T_g^4 + \varepsilon_t a_t \sigma\psi T_t^4 + \varepsilon_r a_r \sigma\psi T_r^4 \qquad \text{--- (2.23)}$$

Unit volume of gas.

Tube surface area (T) per unit volume = $2a_t$.

Refractory surface area (R) per unit volume = $2a_r$.

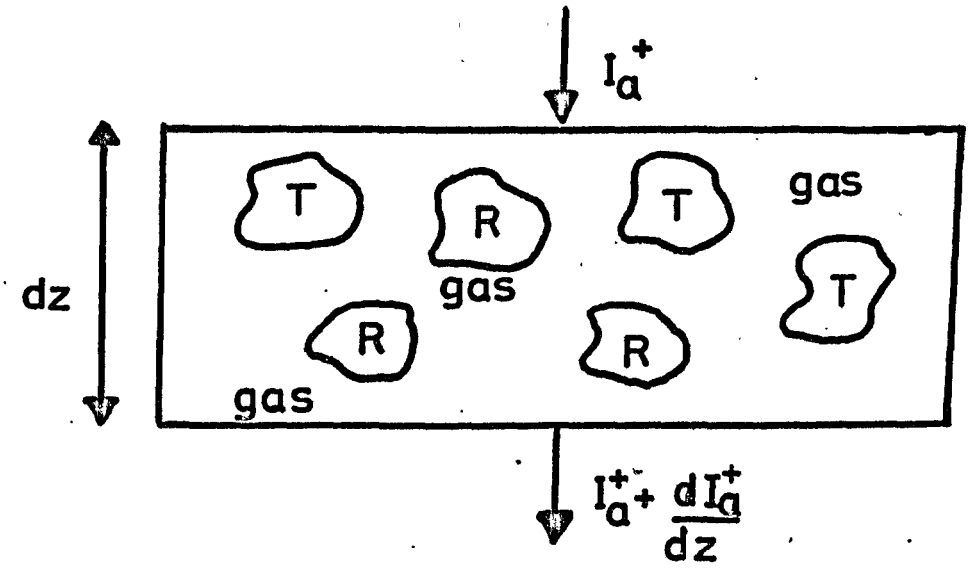

Absorbing Power.		Emitting Power.
β	gas	$\beta \psi \sigma T_g^4$.
$\epsilon_t a_t$	T	$\epsilon_t a_t \sigma T_t^4$
$\epsilon_r a_r$	R	$\epsilon_r a_r \sigma T_r^4$

Fig. 2.3 : RADIATIVE TRANSFER TERMS FOR GAS AND SOLID COMPONENTS.

$$-\frac{dI_a^-}{d\tau} = (-\beta-\varepsilon_t a_t-\varepsilon_r a_r)I_a^- + \beta\sigma\psi T_g^4 + \varepsilon_t a_t\sigma\psi T_t^4+\varepsilon_r a_r\sigma\psi T_r^4 \quad \text{---- (2.24)}$$

$$\frac{dI_b^+}{d\tau} = (-\varepsilon_t a_t-\varepsilon_r a_r)I_b^+ + \varepsilon_t a_t(1-\psi)\sigma T_t^4 + \varepsilon_r a_r(1-\psi)\sigma T_r^4 \quad \text{---- (2.25)}$$

$$-\frac{dI_b^-}{d\tau} = (-\varepsilon_t a_t-\varepsilon_r a_r)I_b^- + \varepsilon_t a_t(1-\psi)\sigma T_t^4 + \varepsilon_r a_r(1-\psi)\sigma T_r^4 \quad \text{---- (2.26)}$$

$$\frac{\partial H_p}{\partial\Theta} + V_p\frac{\partial H_p}{\partial\tau} = \varepsilon_t a_t\left(I_a^+ + I_a^- + I_b^+ + I_b^- - 2\sigma T_t^4\right) \quad \text{---- (2.27)}$$

It is seen that the six equations (2.22) to (2.27) contain the refractory wall and tube skin temperatures as dependent variables. Before any solution can be attempted, T_g and T_t must be obtained in terms of the dependent state variables. This is discussed in Sec. 3.1 for the steady state model, and Sec. 8.3 for the dynamic. Similarly, discussion of the appropriate boundary conditions for the six differential equations for both steady state and unsteady state are left until these cases are considered in more detail.

CHAPTER III. THE STEADY STATE MODEL (1).

3.1 Reduction of the State Equations to the Steady State Case

The manufacture of lean gas is, of course, a continuous process. Even though the load levels are changed more frequently than those of most chemical processes (see Sec. 1.3) steady state conditions should exist for a major proportion of the time. For most design purposes, a model which enables furnace performance characteristics to be evaluated for different geometries and input conditions will suffice. Provided that changes in the control variables are made slowly, capacity lags within the system may be neglected and the model becomes a steady state analysis. Only when optimisation and control strategies are to be considered does a dynamic model of the system become mandatory.

It is therefore proposed to study the steady state model first. This should be mathematically more tractable and provide results which are more easily checked against values logged from the plant itself and against published data. Moreover, many of the parameters required in the steady state model are unchanged in the dynamic analysis, so that useful indications of the sensitivity of the furnace to perturbations in these parameters may be obtained.

The assumption that the furnace is operating under conditions of steady state means that every point on the boundary surfaces is in thermal equilibrium with the radiation field at that point. Hence there is no accumulation of heat in the solid components or gas streams. With reference to the set of equations (2.22 to 2.27) developed in Sec. 2.3, it is clear that all partial derivatives with respect to time may be set equal to zero.

Equations relating the tube skin temperature and refractory wall temperature which appear in Eqs. (2.22 to 2.27) to the other dependent variables are obtained by writing local flux balances. For T_t, at any horizontal level of the furnace this equation takes the form,

$$h_{tc}(T_t - T_p) = \frac{\varepsilon_t}{2}(I_a^+ + I_a^- + I_b^+ + I_b^- - 2\sigma T_t^4) \qquad \text{----------(3.1)}$$

The term on the right hand side of Eq.(3.1) is the nett heat flux absorbed by the tubes. It is linked with the heat absorbed by the process gas stream by a convective heat transfer coefficient, h_{tc}. If the process gas temperature profile is known, or may be calculated independently of the radiation field equations, this relation will enable T_t to be evaluated.

Similarly, the refractory temperature at any position z down the furnace is given by the equation,

$$\xi = \frac{\varepsilon_r}{2}(I_a^+ + I_a^- + I_b^+ + I_b^- - 2\sigma T_r^4) \qquad \text{---------(3.2)}$$

where ξ is the nett flux absorbed by the refractory slab. Because there is a temperature gradient between the hot inside face of the refractory and the outside face at ambient conditions, there must be a nett flow of heat through the slab thickness. However, it is a reasonable approximation to assume that the convection of heat from the furnace gas on to the inside face balances the heat conducted through the wall (30), both being small in comparison with the radiant fluxes involved. Then, the nett radiant interchange between the inside refractory surface and the furnace volume is zero. With $\xi = 0$, the refractory temperature in terms of the radiation beams follows immediately.

In the differential equations, absorption and emission terms for the refractory become, for example,

$$\frac{dI_a^+}{dz} = \text{--------} - \varepsilon_r a_r I_a^+ + \psi\frac{\varepsilon_r a_r}{2})(I_a^+ + I_a^- + I_b^+ + I_b^-) \qquad \text{----------} \quad (3.3)$$

$$\text{Or,} \quad \frac{dI_a^+}{dz} = \text{---------} - \varepsilon_r a_r I^+ + \psi\frac{\varepsilon_r a_r \cdot I}{2} \qquad \text{----(3.4)}$$

The full set of steady state equations may now be stated:

$$\frac{dI_a^+}{dz} = (-\beta - \varepsilon_t a_t - \varepsilon_r a_r)\, I_a^+ + \beta\psi\sigma T_g^4 + \psi \frac{\varepsilon_r a_r}{2} \cdot I + \psi \varepsilon_t a_t \sigma T_t^4 \quad \text{------- (3.5)}$$

$$-\frac{dI_a^-}{dz} = (-\beta - \varepsilon_t a_t - \varepsilon_r a_r)\, I_a^- + \beta\psi\sigma T_g^4 + \psi \frac{\varepsilon_r a_r}{2} \cdot I + \psi \varepsilon_t a_t \sigma T_t^4 \quad \text{------- (3.6)}$$

$$\frac{dI_b^+}{dz} = (-\varepsilon_t a_t - \varepsilon_r a_r)\, I_b^+ + (1-\psi) \frac{\varepsilon_r a_r}{2} \cdot I + (1-\psi)\varepsilon_t a_t \sigma T_t^4 \quad \text{------- (3.7)}$$

$$-\frac{dI_b^-}{dz} = (-\varepsilon_t a_t - \varepsilon_r a_r)\, I_b^- + (1-\psi) \frac{\varepsilon_r a_r}{2} \cdot I + (1-\psi)\varepsilon_t a_t \sigma T_t^4 \quad \text{------- (3.8)}$$

Heat balances on the furnace gas and process gas streams are:

$$\frac{dH_g}{dz} = -2\beta\psi\sigma T_g^4 + \beta(I_a^+ + I_a^-) \quad \text{------- (3.9)}$$

$$\frac{dH_p}{dz} = \frac{\varepsilon_t a_t}{2}(I - 2\sigma T_t^4) \quad \text{------- (3.10)}$$

This set of six, simultaneous, ordinary differential equations, (3.5) to (3.10) is essentially that given by ROESLER (31) who presents a steady state model for a reformer assuming that the complete process gas temperature profile is available in advance.

Six boundary conditions must be specified. Those for the radiation beams are derived from flux balances at the floor and roof of the furnace, assuming that no nett radiant flux is absorbed there. Consider the position at the furnace roof. The flux striking the roof is $I_a^- + I_b^-$, of which a fraction ε_r is absorbed. On re-emission, fractions $\psi\varepsilon_r(I_a^- + I_b^-)$ can interact with the gas and $(1-\psi)\varepsilon_r(I_a^- + I_b^-)$ cannot. Therefore, the beam I_a^+ will comprise the reflected portion of the I_a^- beam, plus the term $\psi\varepsilon_r(I_a^- + I_b^-)$ That is,

$$I_a^+ = (1-\varepsilon_r) I_a^- + \psi\varepsilon_r(I_a^- + I_b^-) \quad \text{-------- (3.11)}$$

Similarly, I_b^+ will comprise the reflected portion of I_b^- plus the term $(1-\psi)\varepsilon_r(I_a^- + I_b^-)$.

$$I_b^+ = (1-\varepsilon_r)I_b^- + (1-\psi)\varepsilon_r(I_a^- + I_b^-) \quad \text{------(3.12)}$$

Exactly analogous relations are found by writing flux balances at the furnace floor.

$$I_a^- = (1-\varepsilon_r)I_a^+ + \psi\,\varepsilon_r\,(I_a^+ + I_b^+) \quad \text{------(3.13)}$$

$$I_b^- = (1-\varepsilon_r)I_b^+ + (1-\psi)\,\varepsilon_r\,(I_a^+ + I_b^+) \quad \text{------(3.14)}$$

The initial condition for H_p is defined by the enthalpy of the process feed prior to its entry into the reformer tubes. In the case of H_g, the initial value may be set equal to $G_g\,C_g\,T^*$ where T^* is the theoretical flame temperature. However, turbulence induced by the burner jets destroys the plug flow regime in the top part of the furnace causing heat to be spread over a finite volume, and thus lowering the actual flue gas temperature considerably. ROESLER suggests that this is most easily taken account of by first, setting the initial condition for Hg equal to $G_g\,C_g\,T_{go}$, where T_{go} $(<T^*)$ is the gas temperature at the furnace roof; then distributing the resulting heat deficit over a depth of furnace corresponding to the penetration depth of the flames. If the gas adjacent to the furnace roof is in equilibrium with the local radiation field there, an estimate for T_{go} will be given by

$$T_{go} = \sqrt[4]{\frac{(I_a^+ + I_a^-)}{2\sigma}} \quad \text{------(3.15)}$$

The relationship between the furnace gas temperature profile T_g and the variables of the state equations is readily obtainable since H_g directly represents the sensible heat flow of the gas. Hence,

$$T_g = H_g \;/\; G_g\;C_g \quad \text{------(3.16)}$$

The process gas temperature profile, T_p which enters the state equations via Eq. (3.1) must also be derived in terms of these variables. In Roesler's paper, the functional relationship of the

process gas temperature to its enthalpy is not defined. Clearly, however, it is considerably more complex than for the furnace gas stream.

An endothermic chemical reaction occurs between naphtha and steam so that a given quantity of heat absorbed by the process gas stream will not be fully reflected by a rise in its temperature; some of the heat is absorbed by the chemical reaction. The means by which this function is determined is described in the following section.

3.2 Thermodynamics of Steam Reforming.

Any estimate of the heat load on the furnace requires a knowledge of the various chemical reactions occurring within the catalyst-filled tubes and the consequent amounts of heat absorbed or released by these reactions. Experience has shown that with modern reforming catalysts the process gas mixture approaches local chemical equilibrium at the prevailing temperature and pressure (32, 33, 34). The approach to final equilibrium is limited, not by kinetic reaction rates but by the rate at which heat can be transferred to the reactants. By assuming, therefore, that the kinetics of all important reactions are infinitely fast, the gas composition may be predicted directly from its temperature, pressure and the inlet feedstock composition.

The mixture of paraffinic hydrocarbons of the C_5 to C_9 range that constitute naphtha may be reformed in a variety of ways. There is a reasonable measure of agreement however, (35, 36, 37) that the process can be conveniently classified into three main steps. These are:

3.2.1 Methanation

The initial stage of the process involves the breaking up of the carbon chain into methane. A little carbon dioxide, hydrogen and a trace of ethane are thought to be formed also. The methanation reaction proceeds essentially to completion between 400°C and 600°C. DENT (35) gives the stoichiometric formula,

$$C_n H_{2n+2} + \left(\frac{n-1}{2}\right) H_2O \rightarrow \left(\frac{3n+1}{4}\right) CH_4 + \left(\frac{n-1}{4}\right) CO_2 \qquad \text{------(3.17)}$$

Other authors include molecular hydrogen on the right hand side. The reaction is slightly exothermic.

3.2.2. Reforming of Methane

Above 600°C the methane/steam reaction proceeds rapidly to equilibrium. Carbon monoxide and hydrogen are the principal products the stoichiometry being written as:

$$CH_4 + H_2O \rightleftharpoons CO + 3H_2 \qquad \text{------(3.18)}$$

This reaction (left to right) is strongly endothermic and it is during this stage that the major heat input is required.

3.2.3. Shift Equilibrium

Parallel with the methane/steam equilibrium, the well known water gas shift equilibrium must also hold true, i.e.

$$CO + H_2O \rightleftharpoons CO_2 + H_2 \qquad \text{------(3.19)}$$

Once the methanation process is complete, the gas will consist of five chemical species, - CH_4, CO, CO_2, H_2 and H_2O which was initially in considerable excess. A typical overall equation for lean gas production is given by ANDREW (38), on the basis of each atom of carbon processed.

$$CH_{2.1} + 1.13\ H_2O \longrightarrow 0.27\ CO + 0.43\ CO_2 + 1.58\ H_2 + 0.30\ CH_4 \qquad \text{------(3.20)}$$

In a second paper, ANDREW (39), discusses how the reforming process may be used to manufacture a wide range of product gases by carefully selecting the operating conditions for the reaction. The particular equilibrium mixture of gases obtained is strongly dependent on the process parameters - temperature, pressure and the ratio of the molecules of steam to atoms of carbon in the feed. There are two limiting possibilities:

(a) At low temperature, high pressure and low steam to carbon ratio, the naphtha is reformed to give the maximum amount of methane but comparatively little of this is further reformed to oxides of carbon or

hydrogen. Eq.(3.17) goes to completion but the methane/steam equilibrium is well over to the left.

(b) At very high temperatures, lower pressures and a high steam to carbon ratio, the methane formed by Eq.(3.17) is almost fully converted to carbon oxides and hydrogen. The equilibrium of the methane/steam reaction is pushed well over to the right.

3.3 Equilibrium Calculations

If the temperature, pressure and number of lb - atoms of each element present in a reacting mixture are specified, the composition at thermodynamic equilibrium in terms of certain chemical species is determined. The identities of the species presumed to be present have to be selected *a priori*. The method of obtaining the equilibrium state of the system is outlined in Appendix B.

For a steam to carbon ratio of 3, percentage compositions (by volume) of the process gas for naphtha reforming at various temperatures are shown in Fig. 3.1 . The unreacted steam has been eliminated. Fig.3.2 gives the equivalent results for reforming natural gas. Qualitatively, the two graphs are almost identical which is to be expected since the first step in naphtha reforming is methanation, and natural gas is largely methane anyway. The amount of methane present falls off drastically with increasing temperature indicating its progressive conversion to carbon oxides. The CO_2 content goes through a distinct peak, which shows that it is formed initially by the methane/steam reaction but at higher temperatures, the shift equilibrium favours conversion to CO.

Figs. 3.3 and 3.4 illustrate how the compositions vary with pressure and steam to carbon ratio for naphtha reforming. Clearly the changes are far less pronounced than with temperature. It is seen that the methane content is the most strongly varying component and is in greatest concentration at low temperatures, low steam ratios and high pressures - a result in agreement with that given by ANDREW (39).

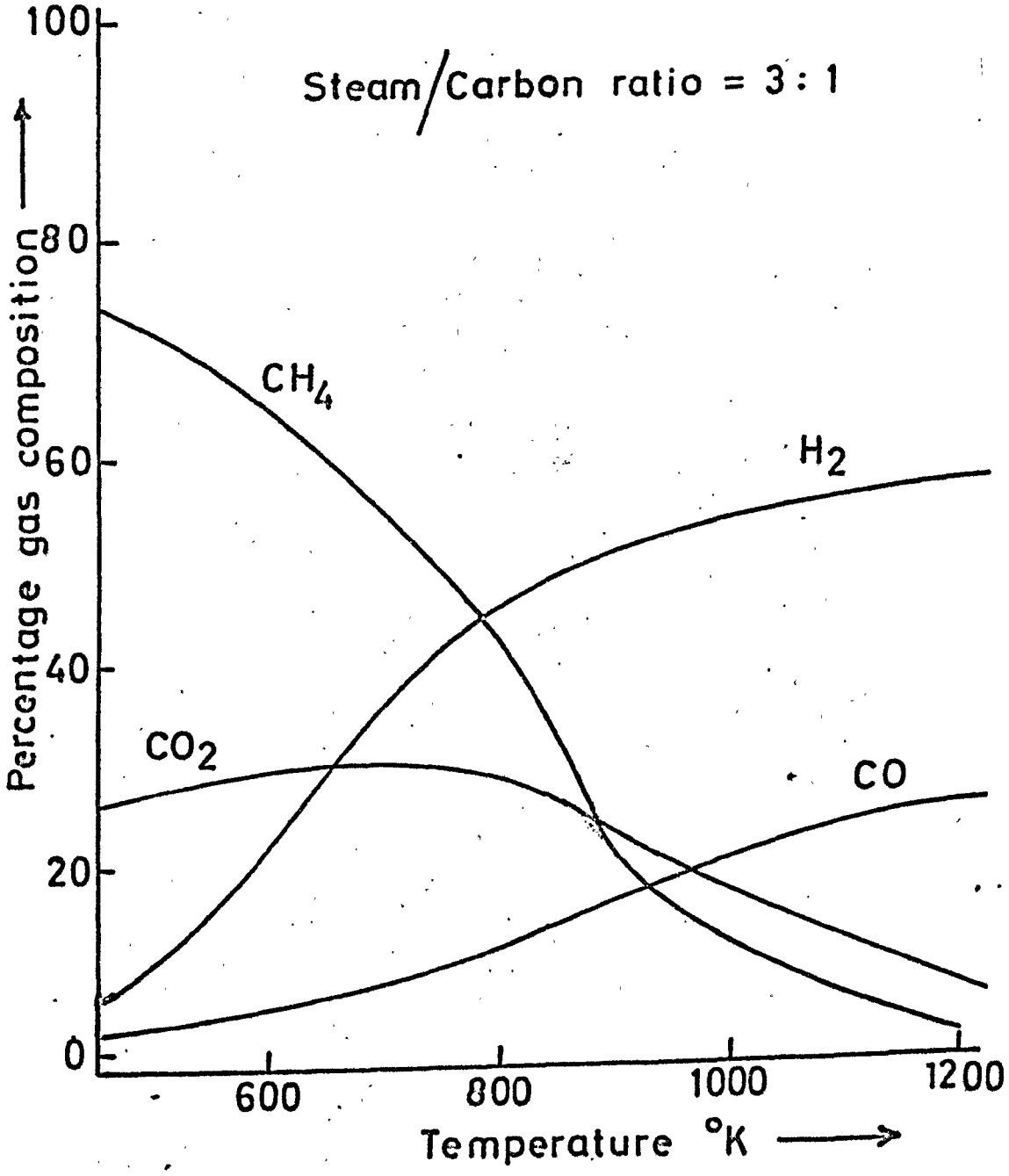

Fig 3.1: PERCENTAGE GAS COMPOSITIONS AT EQUILIBRIUM ON STEAM-FREE BASIS

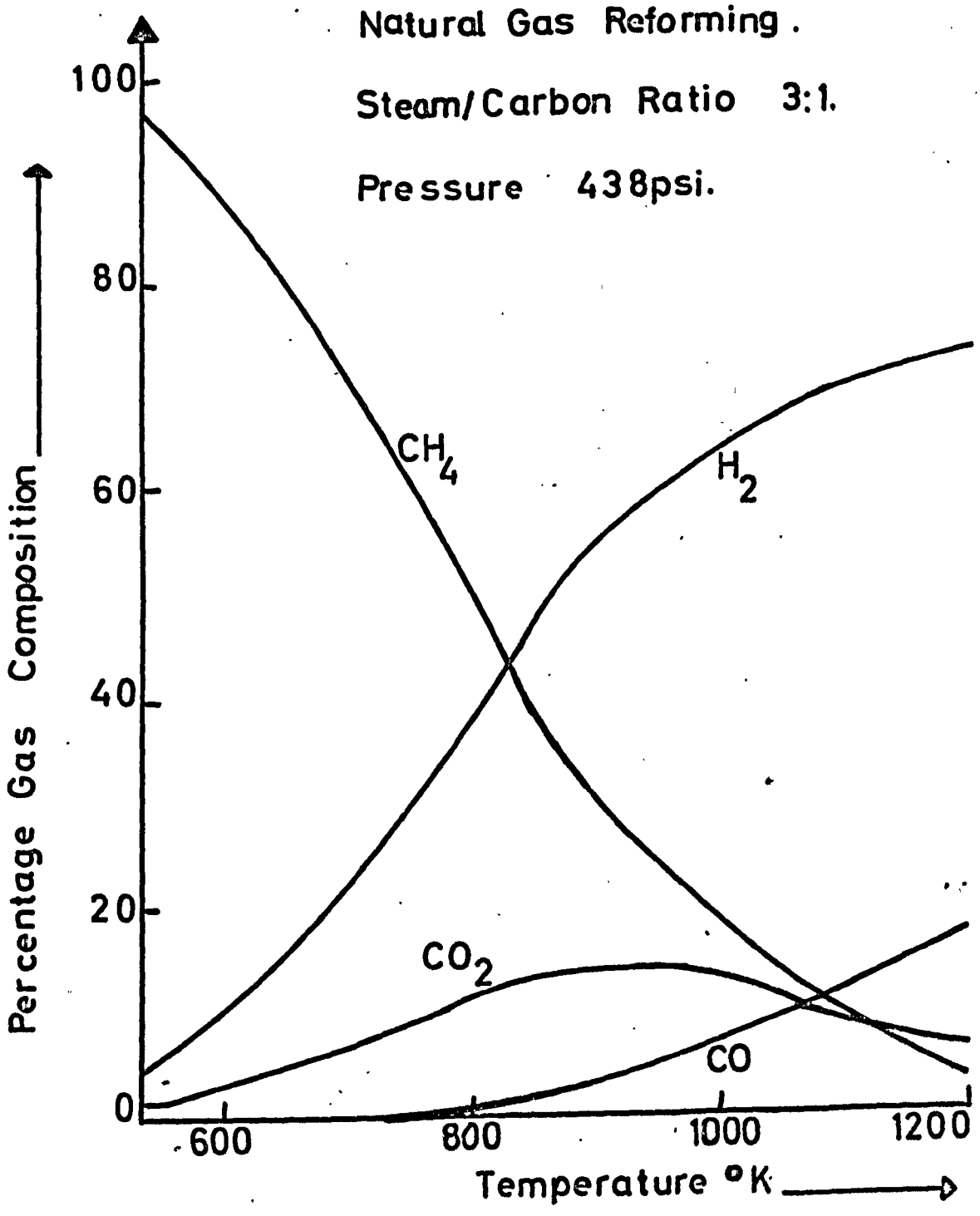

Fig 3.2 : PERCENTAGE GAS COMPOSITION AT EQUILIBRIUM ON A STEAM-FREE BASIS.

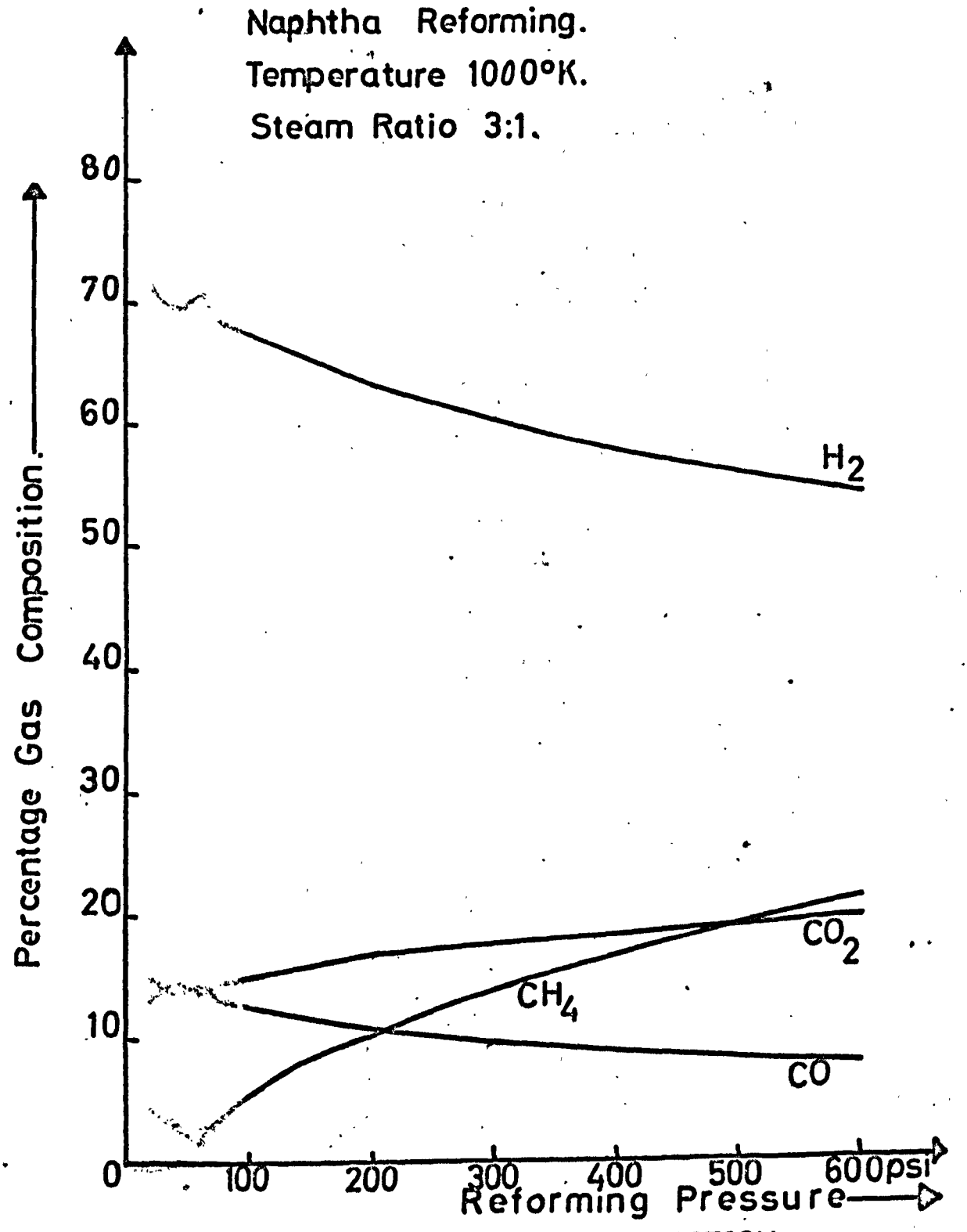

Fig3.3:EQUILIBRIUM DRY GAS COMPOSITION: VARIATION WITH REFORMING PRESSURE.

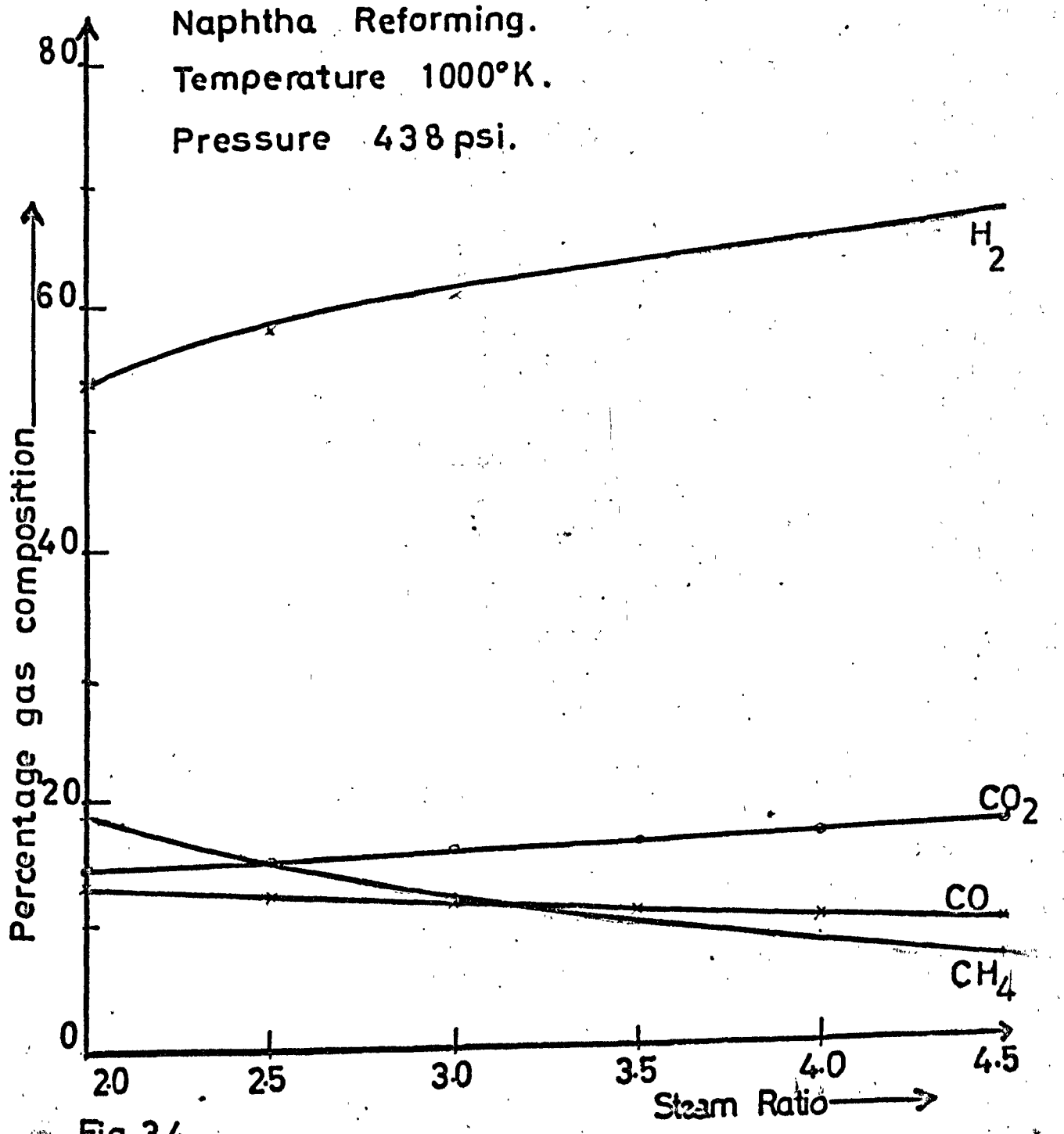

Fig 3.4.
EQUILIBRIUM DRY GAS COMPOSITIONS:
VARIATION WITH STEAM/CARBON RATIO.

Since the heat of combustion per mole of methane is much higher than for CO or hydrogen, the methane content has the greatest influence on the calorific value of the lean gas. Therefore careful control of the furnace to ensure that the final equilibrium conditions are correct is essential. This is especially true during start up or when a load increase is scheduled. During start-up, steam and nitrogen are passed through the tubes initially, the hydrocarbon feed is then switched in and the steam/carbon ratio gradually narrowed. Until the plant is very nearly at steady-state, the make gas is vented.

Once the make gas compositions have been obtained it is easy to compute the heat of reaction for the process.

If y_{ei} is the number of moles of component i present at equilibrium and x_{fi} the moles of i in the feed, the standard heat of reaction at 298°K is given by:

$$\Delta H^{o}_{298} = \sum_{i=1}^{n} y_{ei} H_{fi} - \sum x_{fi} H_{fi} \qquad \text{------(3.21)}$$

where H_{fi} is the standard enthalpy of formation of component i at 298°K. To convert this to the required heat of reaction at T_p (°K) the formula

$$\Delta H_{T_p} = \Delta H^{o}_{298} + \int_{298}^{T_p} \Delta Cp \; d\,Tp \qquad \text{------(3.22)}$$

is used, where Δ Cp is the difference in the molar specific heats of products and reactants. Usually these are supplied as quadratic functions in temperature; DODGE (40) for example tabulates these coefficients. Working to this precision is worthwhile because of the importance of obtaining ΔH_{T_p} accurately.

The variation of ΔH_{T_p} with temperature for different steam ratios for reforming naphtha is shown in Fig.3.5. The corresponding graph for natural gas reforming is given in Fig.3.6.

At low temperatures, the overall reaction for naphtha reforming (but not for natural gas) is slightly exothermic (ΔH_{Tp} negative),

becomes thermally neutral at around 500°C and only strongly endothermic above 600°C. This corresponds roughly to the preheating of the naphtha and steam in the upper parts of the tubes, with the main reactions occuring further down. Therefore, the assumption that equilibrium exists at all points down the tube length is a reasonable one to make as regards the distribution of heat consumed by the process gas.

The enthalpy of the process gas is the sum of its sensible heat plus the heat of reaction term. If the enthalpy per unit mass is U, this sum may be expressed as,

$$U + \text{const} = \frac{H_p}{G_p} = \int_0^L C_p \frac{dT_p}{dz}\, dz + \gamma \int_0^L \Delta \frac{H_{Tp}}{L} \cdot dz \qquad \text{-------(3.23)}$$

where γ is the ratio of the 16 - atoms of carbon in the process gas to its total mass. Taking a mean value for Cp, the first integral may be evaluated and Eq. (3.23) becomes,

$$H_p = G_p C_p (T_p - T_{p0}) + G_p \gamma \int_0^L \frac{H_{Tp}}{L} \cdot dz \qquad \text{-------(3.24)}$$

Eq.(3.24) provides the necessary relationship between Tp and Hp. In conjunction with Eqs. (3.10) and (3.1) it enables a check to be made to determine whether the flux received by the process gas stream is in agreement with its assumed temperature profile. The computational procedure must, of course, be iterative, but discussion of this is delayed until Chapter 5 when all other parameters required in the model have been assembled.

3.4 Comments on the simplifying assumptions made in the steady state model.

Apart from the basic assumptions stated in Sec.2.2 which were inherent in using the Schuster-Swarzschild approximation for the radiation field, there are several other physical phenomena that have been neglected without affecting the descriptive detail in order that the mathematics remain tractable. Many of these simplifications have already been mentioned, others have been included by implication rather than stated explicitly. A list of the most important assumptions made

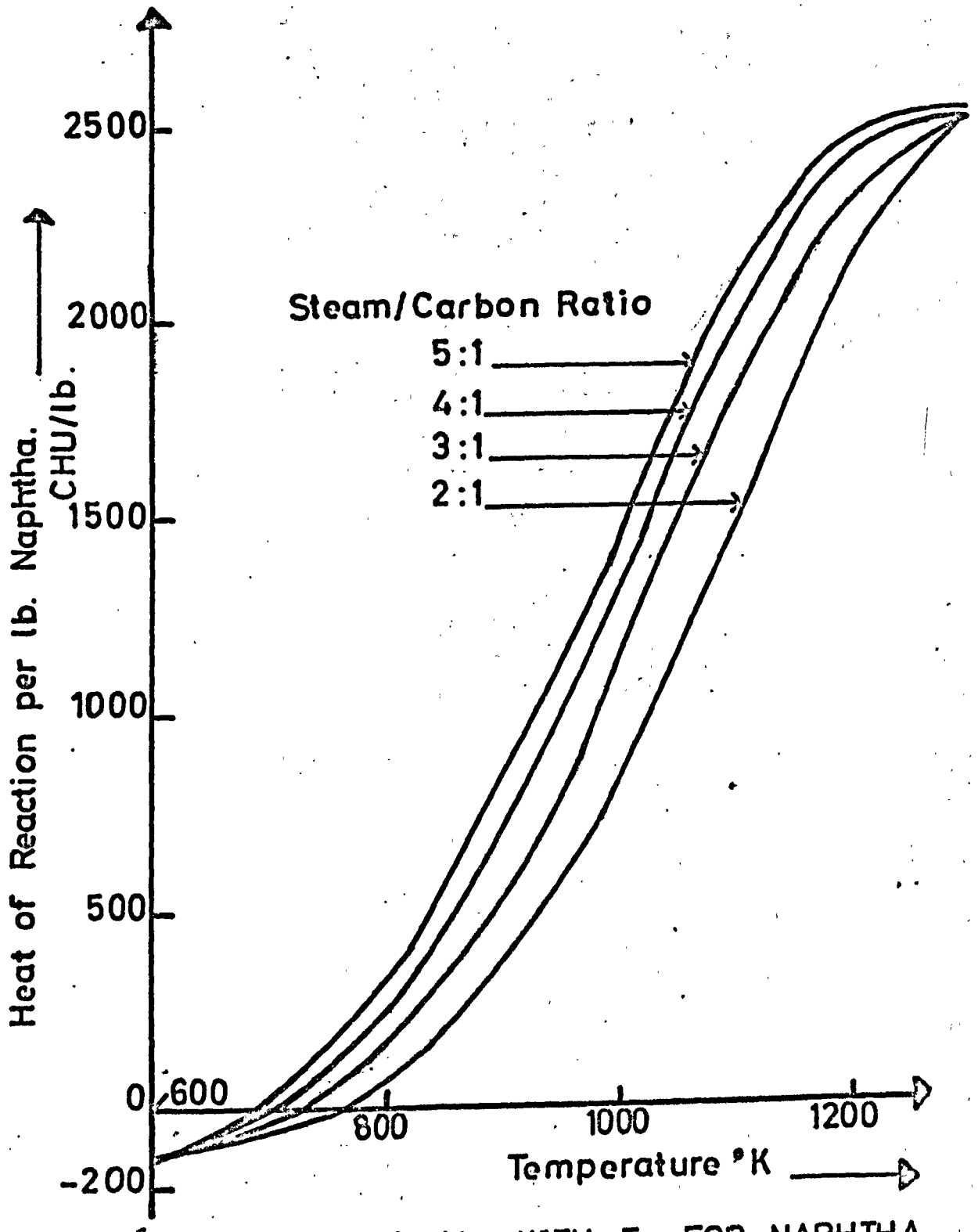

Fig 3.5 : VARIATION OF ΔH WITH T_p FOR NAPHTHA REFORMING.

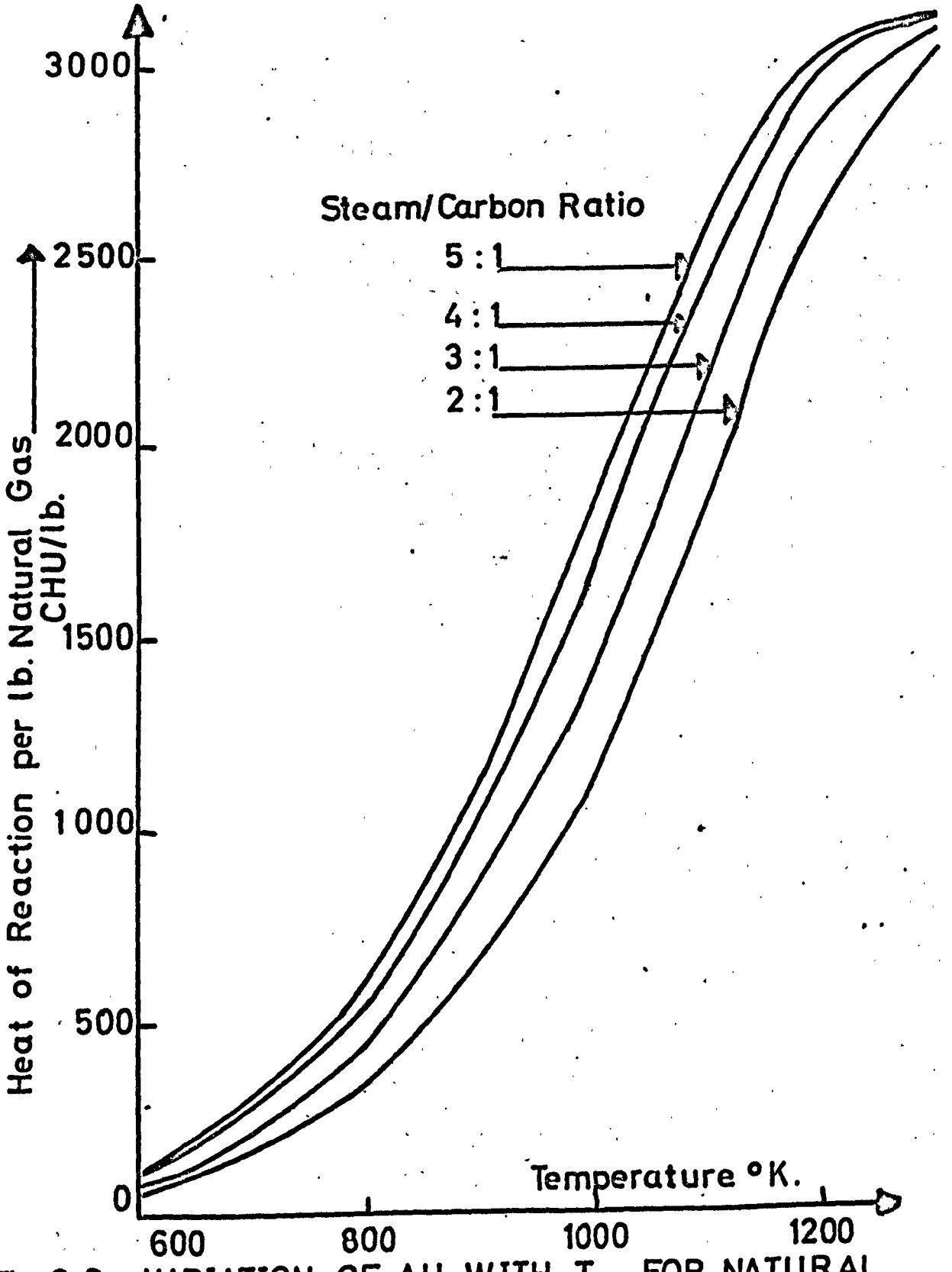

Fig 3.6 : VARIATION OF ΔH WITH T_p FOR NATURAL GAS REFORMING.

and their probable validity is set out below.

(a) In the radiation field the transfer of heat by conduction and convection is considered negligible compared with that transferred by radiation.

(b) Modification of the flue gas emissivity by the luminosity of the flames is neglected. The problem of flame luminosity has been studied extensively on an empirical basis and there is general agreement that the principal factor involved is the density of carbon particles in the flames (41). However, except when the burners are first ignited at plant start-up, the flames do not appear to be luminous and occupy only a small volume of the furnace enclosure. When parametric sensitivity tests were performed on the steady state model, an arbitrary change of the flue gas emissivity was made and no substantial changes in the heat flux and temperature profiles were apparent, so that no account will be taken of the flame luminosity.

(c) The tubes receive a constant radiation flux at all points on their circumferences at a given horizontal level, - that is, radial symmetry of heating about the central axes may be assumed. In fact, some shielding effects between adjacent tubes is inevitable, but any precise account of this would clearly be very difficult to formulate. The justification for neglecting asymmetric effects can only be, therefore, that the uncertainty of the flux distribution around the tubes is as large as the correction that would be made by accounting for it in the model.

(d) Chemical equilibrium exists at all positions inside the catalyst beds. This hypothesis was dealt with in the previous section and was considered at least as accurate as any kinetic data are likely to be.

(e) Implicit in the statements of Eqs. (3.1) and (3.23) is the one

dimensional treatment of the heat transfer processes occurring inside the furnace tubes. It has been shown by FROMENT (42) and CRESSWELL (43) amongst others, that a one-dimensional model for a tubular reactor is totally inadequate when highly exothermic reactions are involved mainly because of their inability to predict "hot spots" or instability problems. By contrast, the endothermic reforming processes do not give rise to these difficulties and so the only criterion of validity for the one-dimensional approach is whether its predicted temperature and composition profiles are in agreement with those from the two-dimensional model.

To verify this point, one - and two - dimensional models were set up for a particular heat input q (z). Constant pressure, physical properties and superficial mass flowrate were assumed. The mathematical details are given in Appendix C.

The comparison that must be made is between $Tp^{(1)}$, obtained from Eq. (3.24) and $Tp^{(2)}$ found by averaging Tp (r) over the cross sectional area of the tube, where the superscripts refer to the dimensionality. $Tp^{(2)}$ is given by:

$$Tp^{(2)} = \frac{2}{R^2} \int_{r_0}^{R} Tp\,(r).\ r.dr \qquad \text{------(3.25)}$$

The comparison was made for several different heat inputs and ΔH_{Tp} versus Tp functions and no significant discrepancies were revealed. Table 3.1 shows the results of such a computation using a constant heat input of 12000 CHU/hr.ft^2 and a cubic function for ΔH_{Tp} in terms of temperature.

AXIAL POSN (ft)	CENTRE TEMP(2) °C	TUBEWALL TEMP(2) °C	BULKMEAN TEMP(2) °C	$\bar{T}_p(1)$ °C
5	545.9	712.5	630.0	642.4
10	689.7	827.2	759.7	764.5
15	742.2	838.6	791.4	784.8
20	741.2	811.5	777.0	775.0
25	721.1	772.2	747.2	753.1

TABLE 3.1 Comparison between 1- and 2-dimensional tubular reactor models.

Comparison of the fourth and fifth columns reveals that little discrepancy is introduced by using a simplified, one-dimensional analysis. This is chiefly because the problem is only mildly non-linear, unlike the exponential dependence of the source term on temperature found in kinetically controlled reactions.

It should be mentioned that it is possible to apply model reduction techniques (44) to enable the essential features of the two-dimensional model to be retained whilst only having to be concerned with a one-dimensional computation procedure. However, an exercise of this kind will not be undertaken here.

CHAPTER IV. EVALUATION OF THE STEADY STATE MODEL PARAMETERS

When constructing a process model of a system it is desirable that all the data for the model be derived from fundamental examination of the physical and chemical mechanisms that operate. This is rarely possible, however, and so recourse is usually made to describing certain processes in terms of phenomenological parameters whose values can only be derived by empirical methods. In the present model, the number of such parameters necessary is limited to two; they are (i) the flue gas radiation absorption coefficient, and (ii) the overall coefficient of heat transfer between the tube skin and the process gas. To these may be added a third, (iii) the theoretical flame temperature which does correspond with a closely defined physical situation but the calculation of which requires slightly more amplification.

Physical property data and the geometrical quantities are all readily available.

4.1 The Theoretical Flame Temperature

One of the most important parameters in the model is the temperature that the burner flames would reach if the combustion of the hydrocarbon fuel were performed adiabatically - that is, with no heat radiated to the tubes or lost through the walls of the furnace.

In fact, of course, a substantial part of the heat released will be transferred to the tubes, thereby lowering the actual flame temperature by several hundred degrees. The theoretical flame temperature T^* is important however because it provides a direct measure of the total heat available to the furnace according to the relation

$$Hg^* = Gg\ Cg\ T^* \qquad \text{-------(4.1)}$$

Hg^* is essentially the initial condition for the set of state equations (3.5) to (3.10) with the radiation beams as intermediate

variables whose coupling equations predict how part of this heat input is distributed to the output stream Hp.

The value of T^* is calculated from a straightforward enthalpy balance. Taking a datum temperature of 298°K this gives:

$$\sum_{i = \text{all reactants}} N_i \left[(Hf_{298})_i + Cp_i (Ta-298) \right] \text{-------(4.2)}$$

$$= \sum_{j = \text{all products}} Nj \left[(Hf_{298})_j + Cp_j (T^* - 298) \right]$$

where Hf_{298} are the enthalpies of formation of the components in the gaseous phase at 298°K, Cp are their specific heats and N the molar flows. The temperature T_a is the temperature to which the fuel and combustion air have been preheated prior to the reaction.

The combustion equation may be written as:

$$CH_n + \left(\frac{n}{4} + 1 \right) O_2 \rightleftharpoons CO_2 + \frac{n}{2} H_2O \text{ ------- (4.3)}$$

where the hydrocarbon fuel may be either naphtha (as an atomised liquid) or natural gas. The value of n for naphtha is approximately 2.1, a reasonable stoichiometric formula being C_7H_{15}, whilst natural gas consists very largely of methane together with smaller amounts of ethane and propane. The value of n for this is taken as 3.7 .

Although Eq. (4.3) is written as a reversible reaction, the equilibrium is very far in the direction of complete combustion. If it is assumed that the reaction proceeds to completion, the molar quantities of reactants and products present can be obtained, and hence the value for T^*.

At 2000°C - a level to which T^* will rise under certain conditions - CO_2 is almost 5% dissociated to CO and O_2 (45). Heat is abstracted by these endothermic reactions, thus lowering the true theoretical flame temperature considerably. However, it is important that T^* should be estimated on the basis of the actual conditions existing in the furnace where the measured flame temperature would seldom rise above 1200°C, rather than on conditions that would exist

at the theoretical temperature of 2000°C. Hence no dissociation effects will be taken into account.

Table 4.1 gives calculated values for T^* for various air preheat temperatures Ta and excess air percentages when the fuel is naphtha.

Table 4.2 gives the equivalent value for burning natural gas.

		DEGREES OF AIR PREHEAT				
		0°C	100°C	200°C	300°C	400°C
Percentage Excess Air	0	1930	2048	2125	2221	2317
	10%	1764	1862	1959	2055	2151
	20%	1622	1721	1819	1916	2012
	30%	1502	1601	1699	1796	1893
	40%	1406	1506	1605	1703	1800
	50%	1315	1415	1515	1614	1712

TABLE 4.1 Theoretical flame temperatures for a naphtha fuel.

		DEGREES OF AIR PREHEAT				
		0°C	100°C	200°C	300°C	400°C
Percentage Excess Air	0	1870	1967	2065	2161	2256
	10%	1709	1807	1905	2002	2098
	20%	1576	1674	1772	1869	1965
	30%	1454	1553	1651	1748	1845
	40%	1351	1450	1549	1647	1745
	50%	1265	1365	1465	1564	1662

Table 4.2 Theoretical flame temperatures for natural gas fuel.

4.2 Furnace Gas Absorption and Emission Coefficients.

An assumption that is commonly made in radiative transfer problems involving a participating medium is that the absorbing power of the medium is independent of the spectral energy distribution of incident radiation; similarly, the radiant energy emitted is also of constant intensity over the entire spectrum. This is the so-called "grey" gas assumption and its usefulness lies in the fact that all radiation travelling a given distance through the gas is attenuated by a constant fraction, no matter where that radiation originated For a grey gas, therefore, all beams will ultimately be absorbed after passing through a sufficiently large quantity of gas, whereas a real gas has certain regions of transparency ("windows") in its spectrum, so that the absorptivity will never reach unity. If the medium is isothermal, the excess flux emission predicted for a grey gas will roughly compensate for insufficient interchange between the boundary surfaces, but when dealing with differential changes of flux intensity, the grey gas assumption is unlikely to prove very accurate.

Consider a monochromatic beam of intensity $I_\lambda(o)$ at one boundary of a gas mass and intensity $I_\lambda(\ell)$ after passing through a thickness ℓ of the gas. Taking an element of thickness dx at a distance x from the source, the change in intensity of the beam is described by the equation

$$\frac{d\,I_\lambda(x)}{dx} = -K_\lambda \rho_g I_\lambda(x) \qquad \text{-------(4.5)}$$

where K_λ is the mass absorption coefficient of the medium. Integration of Eq. (4.5) gives

$$I_\lambda(\ell) = I_\lambda(o) e^{-K_\lambda \rho \ell} \qquad \text{-------(4.6)}$$

The factor $e^{-K_\lambda \rho_g \ell}$ represents the fraction of the original beam which has penetrated as far as $x = \ell$, i.e. the "transmissivity" of the gas. Clearly, the remaining fraction has been absorbed, so

that

$$\alpha_\lambda = 1 - \exp^{-k_\lambda \rho_g \ell} \qquad \text{------- (4.7)}$$

It is impractical to consider radiation of every possible wavelength and then integrate over the entire spectrum to obtain the global quantities. Instead, the range of active frequencies is subdivided into finite "bands" within which the radiation properties are assumed constant. The band absorptivities are defined as :

$$A_i = \int_{\lambda_1}^{\lambda_2} \alpha_\lambda d\lambda \qquad \text{------- (4.8)}$$

where λ_1 and λ_2 are chosen such that the monochromatic absorptivity is zero for each value. The global absorptivity becomes:

$$\alpha = \sum_i W_i \left(1 - e^{-k_i \rho_g \ell}\right) \text{------- (4.9)}$$

where W_i are the fractions of the spectrum corresponding to the i'th absorption band. In the present circumstances, all absorbing frequencies are lumped into one band with the gas being considered transparent in the remainder of the spectrum.

Eq. (4.9) then takes the form,

$$\alpha = \psi \left(1 - e^{-k \rho_g \ell}\right) \qquad \text{------- (4.10)}$$

Turning now to the emission of radiation from the gas, the monochromatic emission per unit time and per unit volume may be expressed as (46):

$$E_\lambda = 4 k_\lambda \rho_g \sigma T_g^4 \qquad \text{------- (4.11)}$$

This assumes that the medium is in local thermodynamic equilibrium. As before, the band model is employed and emission in the i'th band will be

$$E_i = 4 \sum_i k_i W_i \rho_g \sigma T_g^4 \qquad \text{------- (4.12)}$$

or, using the two-band approximation,

$$E = 4 k \psi \rho_g \sigma T_g^4 \qquad \text{------- (4.13)}$$

The density of the participating gas is obtained from its equation of state. Assuming it obeys the ideal gas law at the low pressure and high temperature involved, this will give,

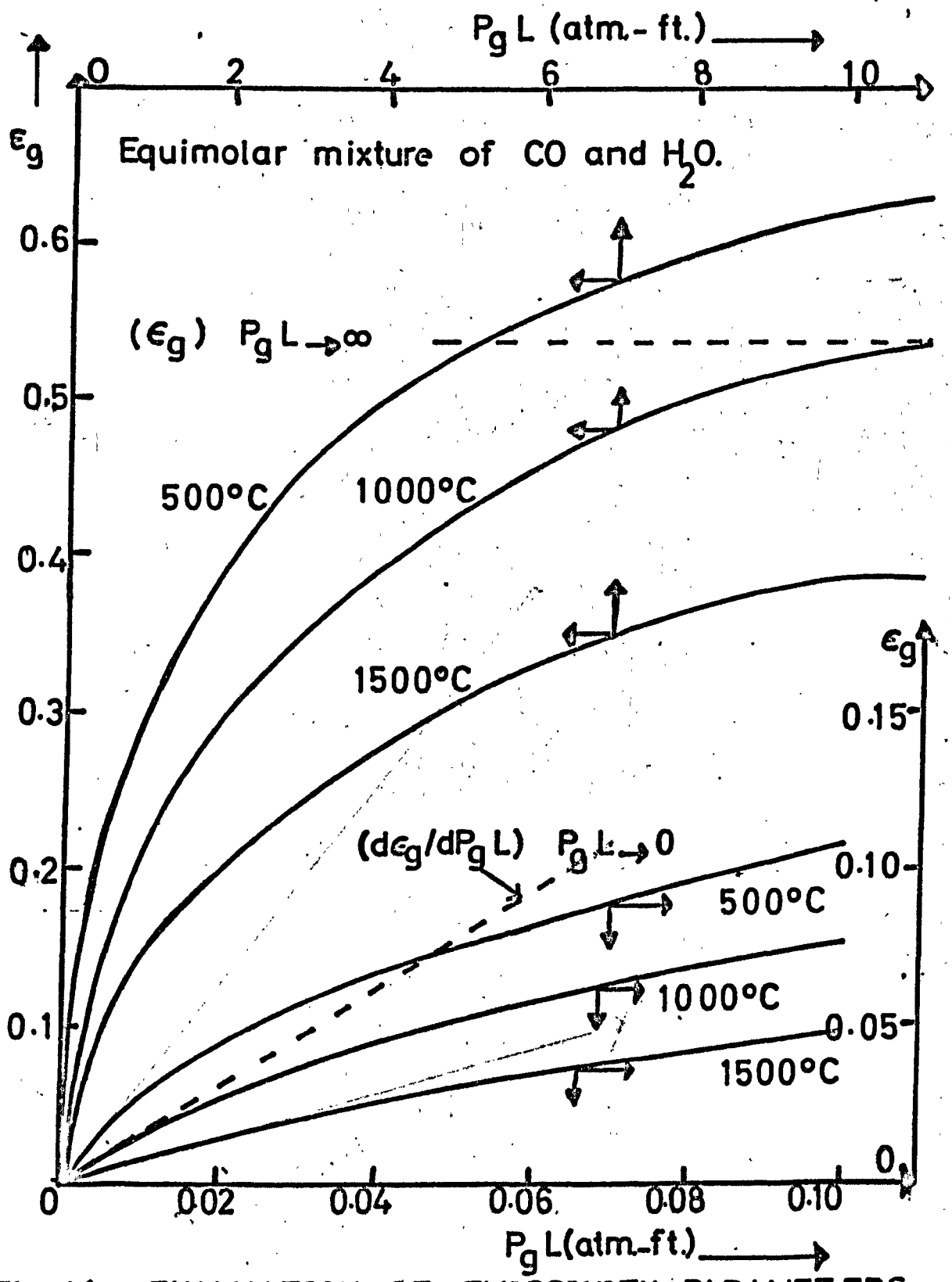

Fig. 4.1 : EVALUATION OF EMISSIVITY PARAMETERS

$$\rho_g = \frac{P_g M}{R T_g} \qquad \text{-------- (4.14)}$$

so that the emissivity and absorptivity finally become:

$$\varepsilon_g = \psi \left(1 - e^{-\frac{k P_g M \ell}{R T_g}} \right) \qquad \text{-------- (4.15)}$$

Charts of emissivities for various gases are normally given as plots of ε_g versus Tg with the product $P_g \ell$ as parameter. HOTTEL(47) gives a chart of ε_g for equimolar CO_2 and H_2O mixtures which is very useful, especially when the burner fuel is naphtha, because the flue gas then is very nearly equimolar in CO_2 and H_2O. If natural gas is the fuel, Eq. (4.4) shows that with n = 3.7 the flue gas will contain a substantially greater proportion of H_2O which may lead to some discrepancy if this chart is used. In this case, the sum of the separate emissivities must be found, and a small correction made to account for the mutual opaqueness of the two gases in certain spectral bands.

The unknown parameters k and ψ may thus be estimated from conventional emissivity charts by the equations:

$$\varepsilon_g \Big/ P_g \ell \longrightarrow \infty \quad = \psi \qquad \text{-------- (4.16)}$$

$$\frac{d\varepsilon_g}{d\, P_g \ell} \Big/ P_g \ell \longrightarrow 0 \quad = \frac{\psi k M}{R T_g} \qquad \text{-------- (4.17)}$$

Selecting a representative furnace temperature of 1000°C, a graph of ε_g versus Pg may be drawn as shown in Fig. 4.1. As a check on the values obtained for ψ and K, the curves are also drawn for two other temperatures 500°K and 1500°K. The results obtained are shown in Table 4.3, where the mean molecular weight, M is taken as 31.

	500 K	1000 K	1500 K
ψ	0.62	0.53	0.39
k	744	580	512

Table 4.3 Values of ψ and K

Hence the volumetric absorption coefficient, β becomes:

$$\beta = \rho_g K = \frac{P_g M}{R T_g} K \qquad \text{-------- (4.18)}$$

Pg will be taken as constant throughout the furnace volume for a particular fuel and air flowrates and must be estimated from the stoichiometric equation (4.3). Tg, of course, will vary down the length of the furnace.

4.3 The Overall Coefficient of Heat Transfer between the Tube Wall and Process Gas.

Radiant heat flux arriving on the outer skin of a furnace tube must be transferred to the process gas flowing through the catalyst bed inside the tube. There are numerous equations for the prediction of an overall heat transfer coefficient for packed-bed reactors. Most follow the example of LEVA (48) who correlates the data in terms of the modified Reynold's number and the ratio of tube to particle diameter. However, the great majority of these correlations deal with small, spherical particles through which air, at atmospheric pressure and moderate temperature, is being blown. This does not correspond at all closely with the situation existing in reformer tubes. Here, the pellets are porous cylinders with a hole bored through the axis, half an inch in length and outside diameter, packed in to a 5" bore tube through which high pressure steam and naphtha flow. The temperature ranges between about 400°C and 750°C.

Rather than using a straightforward correlation of the LEVA type, therefore, it is better to attempt to identify each of the heat transfer mechanisms separately. Coefficients are obtained for each process, then suitably combined into an overall heat transfer coefficient. In this way, extrapolation beyond the scope of the experimental data is only necessary for some of the less important mechanisms.

Apart from convection of heat by the bulk flow of gas along the tube axis, heat transfer processes inside the catalyst beds may be classified into three groups:

(i) conduction through the stainless steel tube wall, thermal conductivity K_w.

(ii) heat transferred through a thin film immediately adjacent to the inside tube wall surface, coefficient h_i.

(iii) heat transferred within the central core of the bed. The assembly of gas and catalyst pellets are considered as a quasi-homogeneous solid through which heat is transported by "effective" conduction. The effective thermal conductivity, K_e is thus a single parameter which enables all modes of heat transfer within the central core to be described by a simple conduction-type equation.

These three parameters may be combined to give the overall heat transfer coefficient by the relation

$$\frac{1}{h_{tc}} = \frac{1}{h_i} + \frac{t_w R_i}{K_w R_m} + \frac{R_i}{4 K_e} \qquad \text{-------- (4.19)}$$

where R_m is the logarithmic mean of the inner and outer radii of the tube.

The film coefficient h_i should contain terms for both the convective transfer of heat through the film of fluid adjacent to the tube wall and also radiative transfer from the wall to the inner core of the bed. Early correlations of the form $Nu = f(Re)$ neglected the radiation contribution. YAGI and WAKAO (49), for example, correlated their data with that of FELIX (50) and PLAUTZ and JOHNSTONE (51) by the equation

$$\frac{h_i d_s}{K_e} = 0.18 \left(\frac{d_s G_p}{\mu_p} \right)^{0.8} \qquad \text{-------- (4.20)}$$

Later work by YAGI and KUNII (52) do take the radiation contribution into account by defining a "static" heat transfer coefficient. Their relation is

$$\frac{h_i d_s}{K_s} = \frac{H_i^o d_s}{K_s} + 0.054 \left(\frac{d_s G_p}{\mu_p} \right) \left(\frac{C_p \mu_p}{K_p} \right) \qquad \text{-------- (4.21)}$$

The derivation of h_i^o is given in a previous paper by the same

authors (53). Two radiation transfer coefficients are required to describe radiant heat flows from the tube wall to the pellets and to gas voids near the wall.

These will take the form :

$$h_{rs} = \sigma \frac{\varepsilon_s}{2 - \varepsilon_s} T_{av}^3 \qquad \text{-------} \quad (4.22)$$

$$h_{rv} = \frac{\sigma}{1 + \frac{\delta}{2(1-\delta)} \frac{1 - \varepsilon_s}{\varepsilon_s}} T_{av}^3 \qquad \text{-------} \quad (4.23)$$

Clearly, the gas emissivity, ε_p will be very low because of the short path length for radiation within the bed. In addition to h_{rs} and h_{rv}, certain geometrical parameters are also required in the equation for h_i^o - these are supplied in the form of graphs obtained from experimental results for various packing arrangements. It is found that h_i^o increases rapidly with temperature and also with pellet diameter, since the increase in the mean volume of void spaces in the bed will increase thermal radiation. With a system such as that occurring in reformer tubes, static and dynamic components of the heat transfer coefficient should be of comparable magnitude.

Evaluation of the effective thermal conductivity, K_e may also be performed by Yagi and Kunii's method. A simpler one, however, is that due to ARGO and SMITH (54) who seek to define separate transfer mechanisms for the pellets and gas voids, i.e.

$$K_e = \delta \left(K_p + K_{td} + K_{rad} \right) + (1 - \delta) K_s \qquad \text{-------} \quad (4.24)$$

where the first term represents heat transferred through voids in the bed by molecular conduction, convective transport and radiation. The full equation for K_e is:

$$K_e = K_p + \frac{G_p C_p d_s}{P_{em}} + 4 \delta \frac{\varepsilon_s}{2 - \varepsilon_s} d_s \sigma T_{av}^3 + \frac{(1-\delta) h_s K_s d_s}{2K_s + o.7 h_s d_s} \qquad \text{----(4.25)}$$

The last term is the modified form proposed by BEEK (55) as a composite term for all fluid-to-particle heat transfer mechanisms. The Peclet number for mass transfer P_{e_m} occurs because convective transport is

more easily measured from mass transfer data where radiation and conduction effects are absent. $P_{\ell m}$ is obtained as a function of the Reynold's number from a graph by FAHIEN and SMITH (56) who used the relation $P_{\ell m} / \left(1 + 19.4 \left(\frac{d_s}{d_t}\right)^2\right)$ as ordinate and R_e as abscissa. In fact, $P_{\ell m}$ is substantially constant for Reynold's numbers in the turbulent region. This leaves only h_s, the particle-to-fluid heat transfer coefficient to be established. Here it is inevitable that a correlation is employed which is not strictly applicable to present conditions, but the discrepancy resulting in the overall coefficient should not be serious. For Reynolds numbers greater than 350, HOUGEN and co-workers (57) give the equation

$$\left(\frac{h_s}{C_p G_p}\right)\left(\frac{C_p \mu_p}{K_p}\right)^{2/3} = 1.06\, R_e^{-0.41} \qquad \text{-------- (4.26)}$$

For fluid properties such as C_p, μ_p and K_p it must be remembered that the process gas is a mixture of gases, so that the values used should be weighted accordingly. Another problem concerns the correct value to use for a characteristic dimension of the pellets, d_s. As previously stated, their shape is far from spherical so it is necessary to use a relation such as effective diameter = 6 x volume / Total surface area. For practical purposes, sufficient accuracy is achieved by using representative values for the fluid and tube wall temperatures in Eqs. (4.22) and (4.23). A rigorous use of varying temperatures would require additional iteration in the solution of the model - something to be avoided if at all possible, and because of the approximations, is not really justified.

Table 4.4 gives typical values for all physical properties employed in deriving the overall heat transfer coefficient, h_{tc}. In view of the empirical nature of the derivation the accuracy of values obtained must be doubtful; nevertheless, it is probably adequate because the radiation field equations are insensitive to changes in the process gas temperature.

Table 4.5 is a summary of the parameters calculated.

SYMBOL	QUANTITY	VALUE	UNITS
R_i	inside tube radius	0.208	ft.
R_m	log. mean of inner and outer radii	0.023	ft.
K_w	tube metal thermal conductivity	12.0	CHU/hr ft^2 ^oC
d_t	tube inside diameter	0.416	ft.
t_w	wall thickness	0.0313	ft.
d_s	mean particle diameter	0.027	ft.
K_s	particle thermal conductivity	0.3	CHU/hr ft^2 ^oC
ε_s	particle emissivity	0.9	-
T_{av}	average bed temperature	1000	^oK
δ	void fraction of bed	0.4	-
Pe_m	Peclet N^o for mass transfer	11	-
G_{pt}	Gas mass velocity (referred to tube cross sectional area)	0.65	CHU/lb ^oC
Kp	gas thermal conductivity	0.06	CHU/hr ft ^oC
μ_p	gas viscosity	0.25	lb/ft hr
$h_i{}^o$	see Ref (53)	40	CHU/hr ft^2 ^oC
Re	Modified Reynolds number	650	-
h_s	see Eq. (4.26)	148	CHU/hr ft^2 ^oC
Ke	see Eq. (4.25)	11.2	CHU/hr ft ^oC
h_i	see Eq. (4.21)	1110	CHU/hr ft^2 ^oC
h_{tc}	see Eq. (4.19)	74.5	CHU/hr ft^2 ^oC

TABLE 4.4 Parameter values required to evaluate heat transfer coefficient.

SYMBOL	QUANTITY	VALUE	UNITS
Gg	Superficial mass flow of flue gas	91.6	lb/hr ft^2
Gp	Superficial mass flow of process gas	73.7	lb/hr ft^2
Cg	Specific heat of flue gas	0.32	CHU/lb°C
Cp	Specific heat of process gas	0.65	CHU/lb°C
T^*	theoretical flame temperature	2220	°K
ψ	fraction of absorbing wavelengths	0.53	-
Pg	partial pressure of $CO_2 + H_2O$	0.25	atm.
$\mathcal{K}$	radiation absorption coefficient	580	$ft^2\ lb^{-1}$
htc	overall heat transfer coefficient	74.5	CHU/hr ft^2 °C
ε_t	tube emissivity	0.93	-
ε_r	refractory wall emissivity	0.80	-
a_t	half effective tube surface p.u. volume	0.056	ft^{-1}
a_r	half refractory tube surface p.u. volume	0.106	ft^{-1}
L	height of furnace	26.5	ft
ℓ^1	penetration depth of flames	8.0	ft

TABLE 4.5 Summary of Parameter Values for design flowsheet case.

CHAPTER V. SOLUTION OF THE STEADY STATE MODEL (1).

5.1 Consideration of Numerical Methods of Solution.

It is important that the solution algorithm for the steady state model should be as efficient as possible because when the solution of the dynamic model is undertaken it becomes necessary to evaluate the pseudo-steady state profiles at each finite increment in the time domain.

The steady state system of equations to be solved is :

$$\frac{d\underline{x}}{dz} = f(\underline{x}, Tg, Tt, Tp) \qquad \text{-------- (5.1)}$$

where $\underline{x} = (Hg, Hp, Ia^+, Ia^-, Ib^+, Ib^-)$ -------- (5.2)

In addition there are subsidiary equations relating Tg, Tt and Tp to the components of $\underline{x}$. These may be written as:

$$Tg = \frac{Hg}{Gg\ Cg} \qquad \text{-------- (5.3)}$$

$$h_{tc}\ (Tt - Tp) = \frac{\Sigma t}{2}\ (Ia^+ + Ia^- + Ib^+ + Ib^- - 2\sigma\ Tt^{\,4}) \qquad \text{------(5.4)}$$

$$Hp = Gp\ Cp\ (Tp - Tp^{o}) + \Delta H_{Tp} \qquad \text{-------- (5.5)}$$

where the last term in Eq.5.5 is the cubic equation in temperature representing the heat of reaction function.

Before solution of the radiation equations is possible, the process gas temperature profile, Tp and hence the heat sink within the furnace (Eq. 5.5) must be specified. The strategy then is, first of all, to assume values for Tp at all positions z down the furnace so that the tube skin temperature profile can be computed from Eq. (5.4) Next, the radiation equations (5.1) are solved and the profile for Hp obtained. This is a measure of the distribution of heat flux received by the tubes. Eq.(5.5) is then used to determine how accurately this profile fits in with the profile of heat consumption that was predicted by the initial assumption of Tp. Finally, Tp is adjusted and the radiation equations (including that for Hp) are

integrated again. The whole scheme is then repeated a sufficient number of times until the profile for T_p has converged.

Considering first the radiation system alone, it is seen that the fourth-power dependency of the radiant intensity on T_g and T_t make the system non-linear. Furthermore, Eq.(5.4), the local flux balance condition on the furnace tubes is a non-linear algebraic equation which has to be solved many times during the integration of the differential equations. Clearly this algorithm should be as efficient as possible.

Probably the best method of solution for non-linear unimodal algebraic equations is the Fibonacci sequential search method. A fine illustration of the technique and relevant theory is given by WILDE (58). A series of "experiments" or evaluations of the square of the function $f(T_t) = 0$ are performed until the value of T_t that gives a minimum is found. KEIFER (59) shows that the special usefulness of the Fibonacci method is that the interval in which the minimum is assumed to lie is subdivided in an optimum manner for all search-type methods. In other words, the minimum is found to a given accuracy by the fewest possible experiments.

Since boundary conditions for the beams are prescribed at both ends of the domain of integration, the system becomes a two-point boundary value problem. The two general methods of solving problems of this kind are, (a) iteration on the boundary conditions at one end, and (b) matrix methods. The latter are well suited to linear equations but with non-linear systems their attractiveness rapidly diminishes as the number of equations increases. The basis of the boundary iteration approach is to assume additional conditions for those variables whose correct values are not specified at one boundary, use an initial-value integration routine to proceed to the other boundary, then check whether the requirements at this boundary are in

fact satisfied to within some required tolerance. This will not be the case generally so some logical means of adjusting the assumed conditions must be made until ultimate agreement is reached.

There are many elegant methods of doing this but they are only useful if the variables at both boundaries either have specified values, or are given as explicit functions. In the present case this is not so; inspection of Eqs. (3.11) to (3.14) reveals that at the roof of the furnace the downward travelling beams I_a^+ and I_b^+ are given in terms of those beams travelling upward and conversely at the furnace floor. This implicit arrangement does inhibit the formulation of rapid convergence techniques for the problem and so rather simple iteration procedures have to suffice.

With regard to the computational efficiency of boundary iteration methods, much depends on the inherent stability of the set of equations. This is a point that has to be considered most carefully here because of the nature of the general solutions for each beam. Remembering that the radiant beam equations consist essentially of an attenuation term plus an emission term, it is clear that the solution takes the following general form:

$$I_z = I_0 e^{-kz} + f(T_z) \qquad \text{-------- (5.6)}$$

If a co-ordinate system is taken with the origin fixed at the roof of the furnace and all the equations integrated in the downward direction then those beams that do in fact travel upwards will contain the factor e^{+Kz} in their solution. Therefore small rounding errors in the evaluation of these beams in the upper part of the furnace will very rapidly lead to much larger errors further down. To avoid this each beam must be integrated along the direction of its propagation so that the exponential terms are all decaying with increasing values of the independent distance variable.

The need to do this prevents the six equations being solved simultaneously in one march down the length of the furnace. Instead a cycle of operations is set up whereby the equations are solved sequentially, keeping those quantities not immediately affected in a particular integration phase as constant profiles stored as discrete functions in the computer memory. Table 5.1 shows the phases of integration in the full cycle of operations.

Phase Number	Variables	Direction
1	Hg	down
2	Ia^+ , Ib^+	down
3	Ia^- , Ib^-	up
4	Hp	down

Table 5.1 Phases of Integration Cycle.

To start the series of calculations, the entire profiles of the beams Ia^+, Ia^-, Ib^+ and Ib^- must be given assumed values and stored in the computer. Since there is little guidance available on the likely shapes of these profiles, convergence could be slow. With more experience, the starting values can be chosen more accurately and the convergence process speeded up to some extent.

As soon as a new profile has been found in any phase of the computational cycle it is immediately incorporated into subsequent phases in the cycle. Thus, for example, the new profile for Hg which is obtained in the first phase is used in place of the flue gas temperature, Eq. (5.3) in the subsequent phases 2, 3 and 4. This is obviously desirable so that the computation is always making use of the most recent information available.

Any one of several initial-value "marching" methods, could be used for the solution of the differential equations. A convenient one

with regard to automatic computation is the fourth-order Runge-Kutta process. This has low truncation error and requires no special starting algorithm. Changes of step length to accommodate various degrees of non-linearity and to check for stability of the solutions are possible and these were made automatic in the adaptation by GILL (60) of the basic Runge-Kutta method.

Evaluation of the tube wall temperature profile from Eq.(5.4) is performed once per cycle, not in every phase. As indicated earlier the Fibonacci search technique was used in order to keep the computing time to a minimum.

The problem has been changed from that of solving a set of differential equations simultaneously with boundary conditions specified at each end of the domain of integration into essentially an iterative initial value problem whereby integration proceeds in each co-ordinate direction in turn. The initial values of each variable are then compared and suitably adjusted.

Boundary conditions for the beams $1a^+$, $1a^-$ and $1b^+$ and $1b^-$ are not available as explicit values but rather as implicit functions. Therefore it is arbitrary which values at $z = 0$ are changed for the next iteration cycle, (apart from H_p at $z = 0$ which is defined by the condition of the process feed), so long as ultimately the profiles are all stable and the boundary conditions satisfied.

The interaction by the beams in the boundary equations can lead to oscillations in the solution. Some form of damping between successive iteration cycles is advisable at least during the initial stages of the integration process. A simple means of doing this is the use of a weighted mean of the current and previous values calculated. A few trial runs to discover an optimum value for this weighting parameter are well worthwhile.

The program to solve the steady state model was written for the ICL KDF9 Digital Computer.

5.2 Results from the Steady State Model (1)

The purpose of this section is to discuss the profiles that emerge from various runs of the model and to examine the sensitivity of the model to changes in some of the defined parameters.

As a first example the data presented at the end of the preceding chapter will be used. These are figures obtained from the design flowsheet for the Dewsbury No. 1 Reformer and should be typical of those found in practice. (In fact the plant was normally run at considerably lower throughputs). The second set of data is for the maximum possible level of operation for peak load circumstances, and finally, results are given for the reformer operating at 40% of the design rate - the so-called "minimum make" condition. In all of these three examples the air to fuel ratio is fixed at approximately 17 to 1 and the steam to carbon ratio at 3 to 1. This enables all the parameters with the exception of the heat transfer coefficient, h_{tc} to remain almost constant. For instance, the air to fuel ratio principally determines the theoretical flame temperature and flue gas specific heat; the steam to carbon ratio determines the process gas specific heat and the quantity of heat consumed by the chemical reaction on a per unit mass basis. The geometrical and optical parameters are, of course, unique for a particular furnace.

In addition, the inlet temperatures are constant at their values given in the flowsheet. Hence only three quantities remain to be varied for these three runs - Gg, Gp and, by virtue of its dependency on the rate of flow of process gas, the coefficient h_{tc}. The appropriate value for this is acquired from the procedures described in Chapter IV. Table 5.2 shows the actual figures employed.

Quantity	Units	Minimum	Design	Maximum
G_g	$lb/ft^2\ hr$	36.5	91.6	100.8
G_p	$lb/ft^2\ hr$	29.3	73.7	80.6
ht_c	$CHU/hr\ ft^2\ ^oC$	58.6	74.5	82.9

Table 5.2 Input data for the Steady State Model (1) for changing total throughputs.

Fig 5.1 depicts the profiles predicted for the state variables for the flowsheet input data. The most interesting is that for Hp, the heat demand curve for the reaction. It is clear that the major portion of the heat is consumed in the upper section of the furnace, whilst further down, the curve becomes much flatter, indicating a diminishing heat requirement. This is a feature of top-fired reforming furnaces which do provide a heat input configuration that fits in well with the requirements of the process.

To some extent, this is in contrast to furnaces which are fired from the side by burners placed along the length of the tubes, such as those described, for example, by HACKETT, et al (61). These are designed to give a substantially constant heat flux profile along the tube length rather than the rapid preheating of the steam-hydrocarbon mixture that is required.

Fig. 5.2 shows the steady state heat flux and temperature profiles for the flowsheet design case. The flux profiles represent, respectively, the nett amount of radiant flux travelling downward through the furnace at given horizontal planes, and the flux transferred to the furnace tubes at particular points down the length of the reformer. Their equations may be written as:

$$\Delta I^+ = Ia^+ + Ib^+ - Ia^- - Ib^- \qquad \text{-------- (5.7)}$$

$$\Delta I_t = \frac{\varepsilon_t}{2} (Ia^+ + Ib^+ + Ia^- + Ib^- - 2\sigma T_t^{\,4}) \qquad \text{--------(5.8)}$$

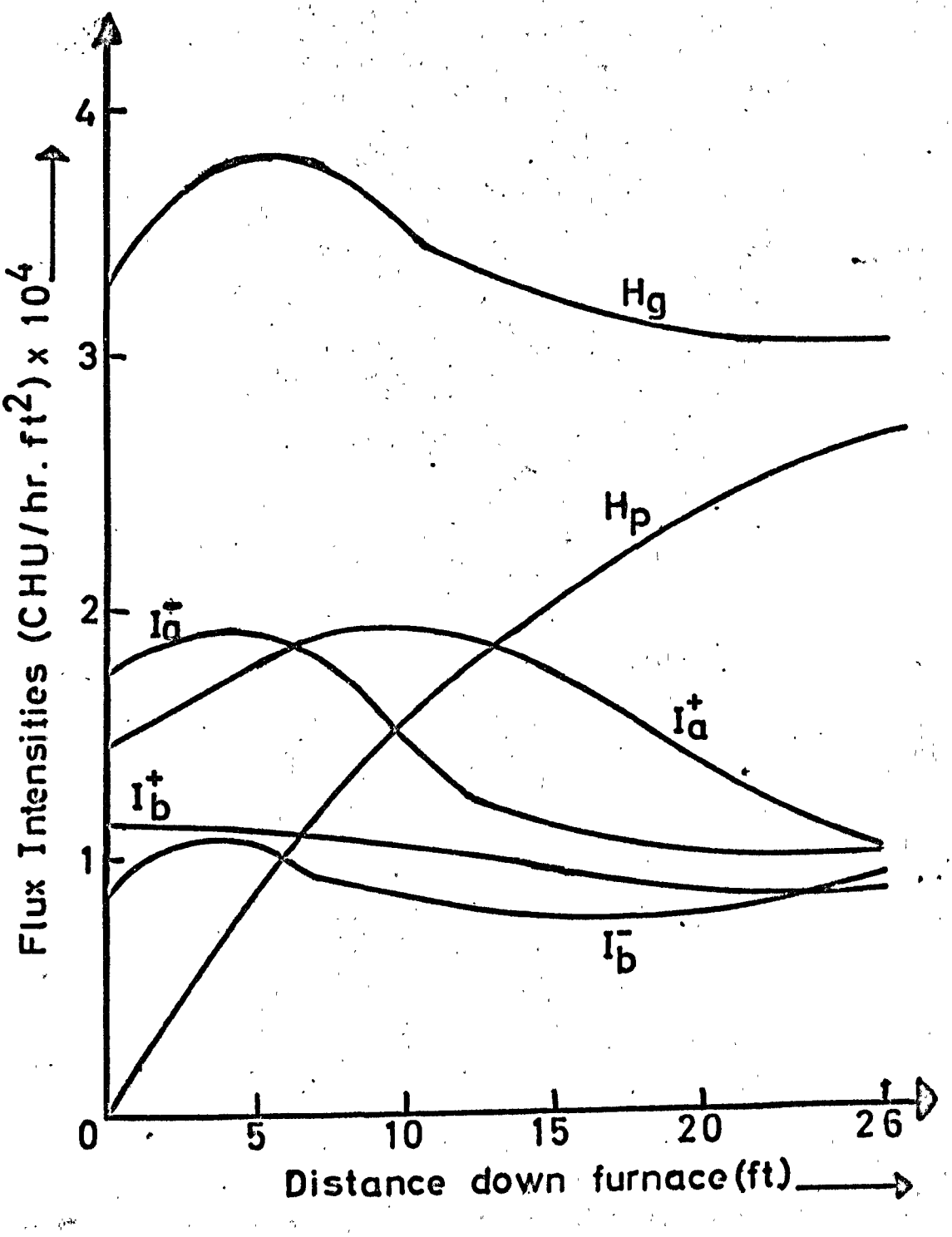

Fig 5.1 : STATE VARIABLE PROFILES.

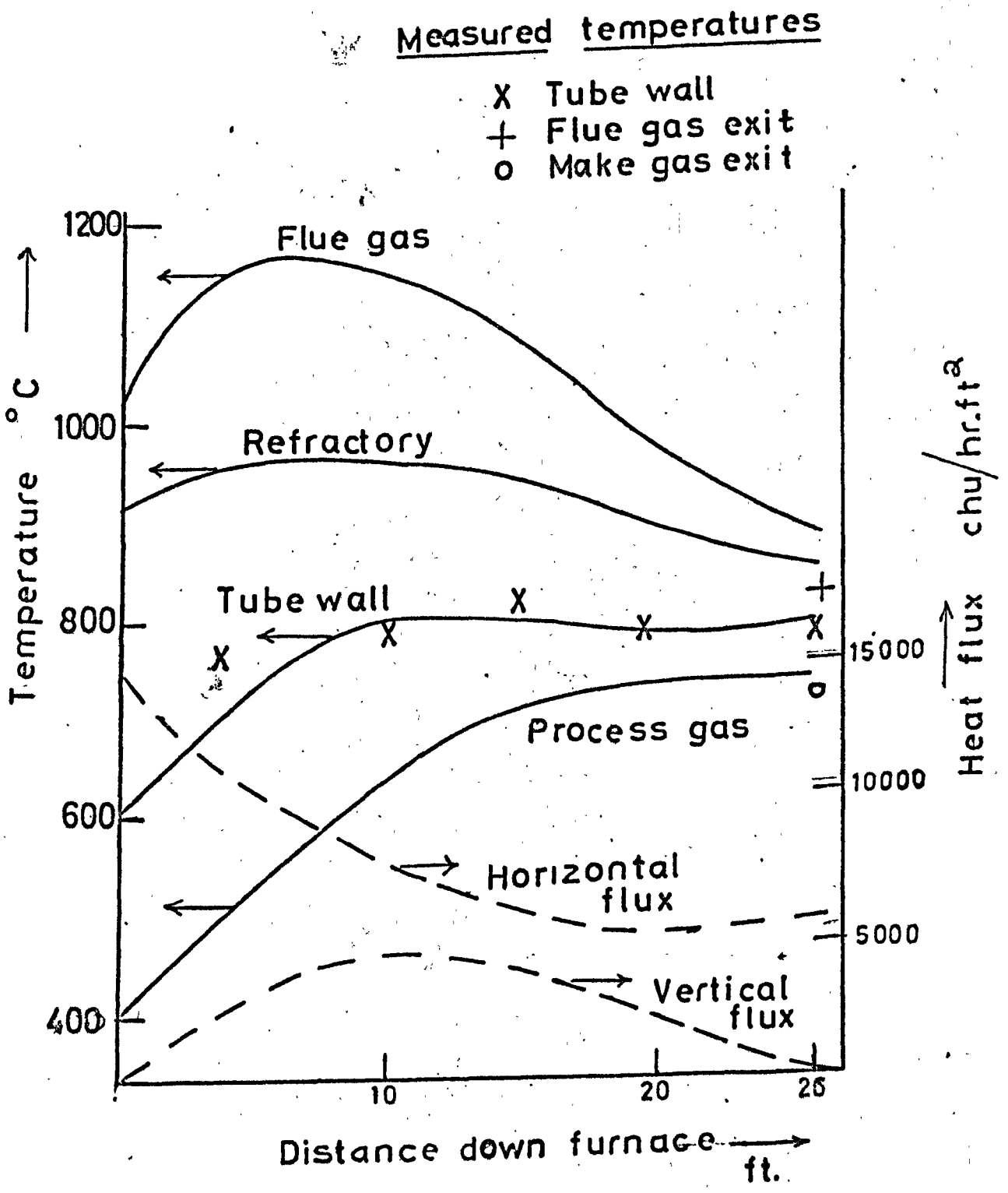

Fig 5·2 STEADY STATE HEAT FLUX AND TEMPERATURE PROFILES

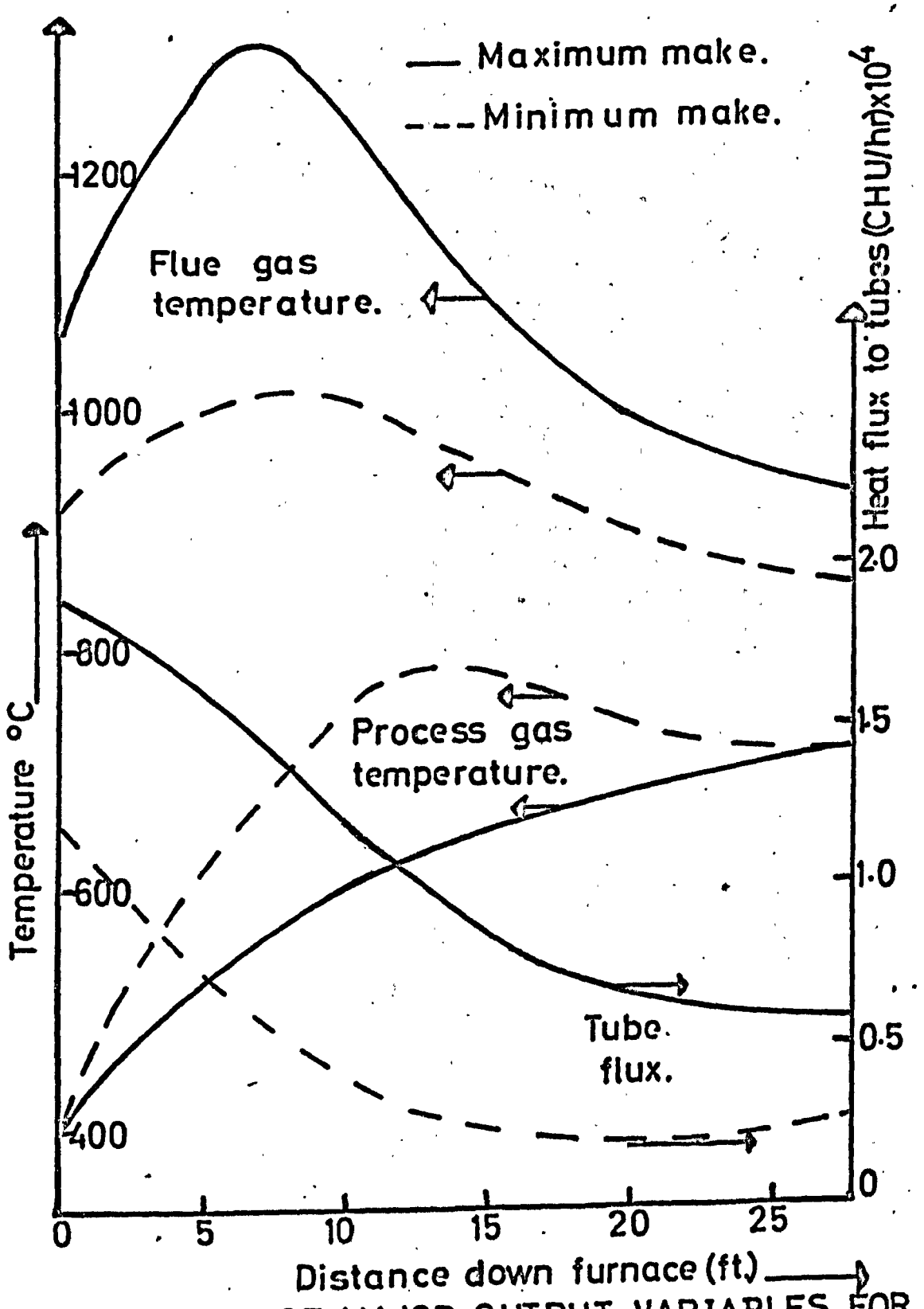

Fig. 5.3: RANGE OF MAJOR OUTPUT VARIABLES FOR MAXIMUM AND MINIMUM THROUGHPUTS.

In the upper zone of the furnace where the gas is being recirculated, the values of ΔI^+ are not very meaningful. Below this zone, the temperature is stable and there is a nett downward flux with a maximum value roughly halfway down the furnace, then diminishing to zero at the furnace floor.

The refractory temperature profile T_r is obtained from a local flux balance on the refractory wall, assuming this to be adiabatic at steady state :-

$$\frac{\varepsilon_r}{2} \quad (Ia^+ + Ia^- + Ib^+ + Ib^-) \quad = 2 \varepsilon_r \sigma \quad T_r{}^4 \quad \text{-------} \quad (5.9)$$

Examination of the profiles shown by Fig.5.2 reveals that although the gas temperatures undergo large variations on passing through the furnace, the temperatures of the tube walls and refractory linings are far more nearly constant. This is important from the mechanical aspects of reformer design, particularly regarding the furnace tubes. Fairly high stresses are unavoidable in reformer engineering and at the temperature level involved, the metal creeps. Clearly the metal will be working most efficiently if the amount of creep is constant over the entire tube length. The curve for Tt in Fig. 5.2 shows that this condition is adequately met in top-fired furnaces. In side-fired ones there is generally a definite peak in tube temperature toward the bottom of the furnace, assuming that the process gas passes downward through the catalyst filled tubes.

The computer print-out for the flowsheet case from which Fig.5.2 is drawn are contained in Appendix D. Run 1.

In Fig.5.3 profiles are given for two extreme cases of total gas throughput. Several interesting points emerge . Firstly, the temperature profiles of the process gas and tube wall (not shown) have definite maxima about halfway down the furnace at low flowrates, whereas no such peaks are apparent at high flowrate. As stated earlier, the life of the tubes is enhanced if their temperature

profiles are substantially flat. A second point is that the make gas composition is primarily determined by the outlet temperature, clearly, therefore, it is wasteful to heat the make gas to a high temperature in the upper part of the furnace and then let it fall to the correct exit value. However, this is precisely what happens at very low flowrates and a look at the profiles for radiant heat flux input to the tubes (Fig.5.3) shows why. The ratio between the heat flux at the top of the furnace to that at the floor is approximately 6 to 1 for the lowest flowrates, but only 3 to 1 at the highest. In the former case, then, too much heat is concentrated in the upper parts of the tubes.

The conclusion is therefore, that the furnace operates more efficiently at high rather than low throughputs, as indeed it was designed to do. However, a substantial part of the time is spent working at the lower makes.

The effects on performance of varying the operating conditions in the furnace will now be considered. Computer print-outs for all these runs are collected in Appendix D; only the temperature profiles are normally shown.

5.2.1 Feedstock

The alternative to naphtha as the reforming feedstock is natural gas. A comparison is made between the two feedstocks for identical total throughputs, heat inputs and steam to carbon ratios. Comparing runs 4 and 5, it is evident that much higher temperatures are achieved when using naphtha as the feed. This is to be expected since the endothermic heat of reaction per unit mass of hydrocarbon is higher for natural gas reforming (compare Figs. 3.5 and 3.6) and there is the same quantity of heat input available in both cases.

At first sight it may appear that there is no drawback to reforming natural gas at low temperatures since the unreacted methane can still remain as a constituent of the final product. However the

equilibrium is such that below about 740°C the total amount of steam remaining unconverted rises very rapidly. Thus at 670°C, the outlet temperatures of the process gas for these conditions predicted by Run 5, there would be so much steam to condense out of the system, re-vaporise and superheat that the whole process would be quite uneconomic. Hence to achieve the desired outlet temperature of 740°C to 750°C for natural gas reforming it is necessary to use higher fuel/process feed ratios than for the equivalent conditions using naphtha.

5.2.2 Steam/ Carbon Ratio

Runs 5 and 6 illustrate the effects of varying the steam to carbon ratio between values of 2: 1 and 4 : 1. The feedstock and burner fuel are both natural gas. The parameters which are varied are the coefficients for the equation of heat of reaction as a cubic function of process gas temperature, representing the relevant curves in Fig. 3.6.

It is seen from the print-outs for the two cases that the variations in heat flux and temperature profiles are not very great - a fact which the process operators take advantage of in "trimming" the plant in terms of total lean gas make. That is, the quantity of gas made can be changed within certain limits by altering only the steam to carbon ratio, keeping the burner fuel and air flow settings unchanged and using the same amount of feedstock, without upsetting the furnace temperatures very much.

The lower limiting value of the steam to carbon ratio is about 2 : 1 because below this the risk of depositing carbon on the catalyst becomes too great. The upper limit is determined simply by the availability of steam which in turn is dependent on the waste heat recovered from the flue gas and process gas streams. If the exit temperatures are too low the process may "run out of heat" and hence of steam raising capacity. This is most likely to occur when reforming naphtha at low throughputs.

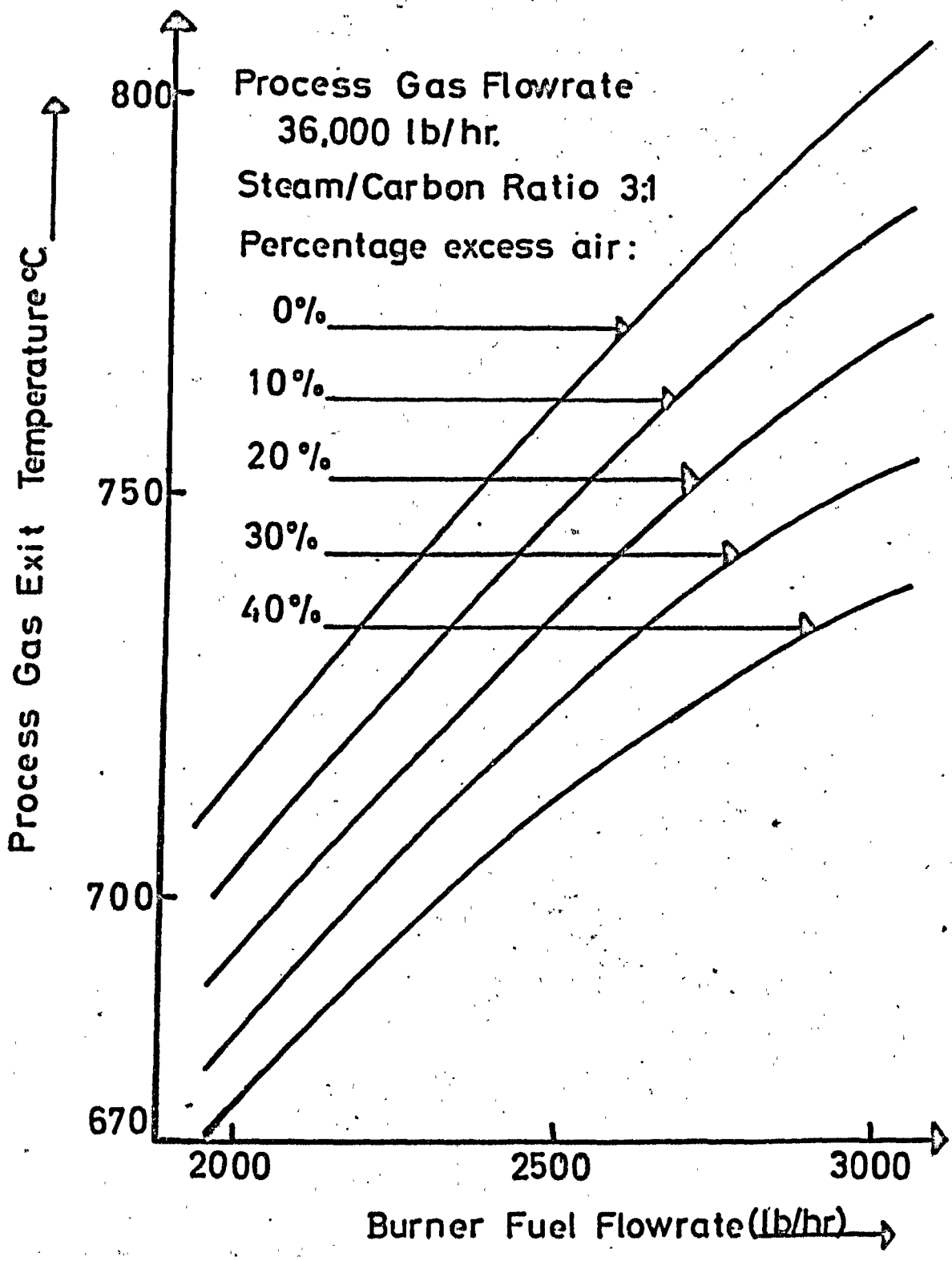

Fig 5.4 : EFFECT OF USING EXCESS COMBUSTION AIR ON FURNACE OUTLET TEMPERATURE.

5.2.3 Air/ fuel ratio

A series of runs were made to determine the process gas exit temperature achieved by burning a given quantity of fuel but varying the amount of excess combustion air employed. The process gas feed conditions were constant.

Fig.5.4 shows the results of these runs. Clearly the burner fuel consumed to achieve a desired outlet temperature of say 750°C varies markedly, from 2400 lb/hr at the stoichiometric quantity of air to 3000 lb/hr at 30% excess. The zero excess curve is slightly unrealistic since it is unreasonable to expect perfect mixing of fuel and air and so in practice a certain amount of fuel would be unburnt. However, it would seem that more careful control over the air flow used, with the aim of staying around the 10% mark, would be beneficial. Frequently the plant works in the region of 30% excess, without counting stray leakages into the furnace.

Complete results for two cases are shown in runs 7 and 8. These are for air to fuel ratios of 16.5 and 19.5 respectively, corresponding to combustion air excesses of 10% and 30%. There is a large difference in the theoretical flame temperatures calculated; 2225°K against 1945°K which illustrates clearly how excess air "dilutes" the heat input. The tube flux profiles are interesting also; the differences between maximum and minimum fluxes for the 10% excess case are distinctly higher than for the 30% excess case. This is due to the extra flow of flue gas in the second case (Run 8) pushing heat further down the furnace. This could be useful at low throughputs because it would flatten out the sharp peaks in temperature experienced by the reactor tubes. However, there would still be a penalty to pay in terms of the extra fuel consumption necessary.

5.2.4. Combustion Air Preheat

It was remarked in Sec. 5.2.3 that the theoretical flame temperature had a most important bearing on the make gas outlet

temperature and hence on fuel consumption. Obviously, it is advantageous to increase the flame temperature without increasing the fuel flow or reducing the air excess to unmanageable margins. This can be done by increasing the temperature to which the combustion air is preheated prior to entry into the furnace.

Runs 9 and 10 illustrate the difference this can make using air preheat temperatures of 300°C and 400°C respectively. It is seen that there is more than a 20°C increase in the make gas outlet temperature in the second run - a most useful increase in the thermal duty of the furnace has thus been achieved.

When reforming natural gas no vaporisation or superheating is required and it is usual to work at somewhat lower steam to carbon ratios than with naphtha. This means that less waste heat is required for process feed heating and for steam raising. Since the make gas exit temperature is fixed by the required gas composition, any modifications to the existing waste heat utilisation must be made on the flue gas side. It does not seem possible to lower the flue gas exit temperature whilst keeping the same make gas exit temperature without a major re-design of the furnace geometry.

However, there remains the possibility of taking more heat out of the flue gas train in the air preheater and less in the waste heat boiler. The extra air preheat temperature raises the theoretical flame temperature as stated. Basically, heat is re-cycled around the furnace instead of being lost through the flue gas stack.

Further runs on the model indicate that every additional 10°C rise in the preheat temperature at normal throughputs saves approximately 0.8% in fuel usage.

CHAPTER VI STEADY STATE MODEL (2) FORMULATION AND SOLUTION.

6.1 Formulation of a model based on the actual geometry of the furnace.

In the formulation of the generalised model in Chapter II, use was made of the so-called Schuster-Schwarzchild approximation to resolve the angular distribution of flux intensity into two beams travelling in opposing vertical directions through the furnace. In order that these beams might intercept the furnace tubes and refractory walls, it was considered that the solid surface areas were uniformly distributed throughout the volume of the enclosure. It was as though the beams were being propagated through an interacting medium whose absorbing and emitting power was due not only to the furnace gases but also to the solid surfaces. Clearly, this model reduces the description of the reformer geometry to ratios of tube skin and refractory wall surface areas per unit volume of furnace, whereas it may well be supposed that the detailed layout of the tubes and burners has an important bearing on the ultimate performance achieved.

The purpose of developing a second model then, is two-fold. Firstly, some means of assessing the validity of neglecting the detailed geometry of the furnace is desirable; obviously this is something that is not immediately apparent. Secondly, the analysis used in model 2 is more closely akin to that normally employed in engineering radiative transfer problems, and will this serve as a valuable check on the first model.

The starting point for the present treatment is the close analogy that can be drawn between a reforming furnace and a co-current heat exchanger. Basically, the process gas flows downwards through the tubes and receives heat from the flue gas flowing through the "shell", also in the downward direction. The coupling equations between the two streams are given by radiation flux balances inside the furnace enclosure, rather than by using a composite heat transfer coefficient which is generally the case in heat-exchanger calculations.

Reformers are fired by gaseous or atomised hydrocarbon fuel so that combustion occurs very rapidly and the temperature initially attained approaches the theoretical flame temperature in the vicinity of the furnace roof. The flue gases cool continuously as they flow from burners to outlet. Recirculation of the gas in the upper compartment due to the jetting action of the burners destroys the stable temperature pattern there, but the principle is still valid. However, it is not possible to use the profile of gas temperature falling monotonically from theoretical flame temperature to its exit value as the basis on which to calculate the heat flux to the tubes. This is because although the furnace is long compared to the distance of the path from source to sink, it is not permissable to neglect radiation in the direction of the gas flow as being of minor importance.

The effect of this on the analysis of the problem is analogous to a situation in which the tubes of a heat exchanger are made of very thick copper, so that a large amount of heat is conducted along the length of the exchanger instead of just through the walls. In this case the quantity of heat conducted would clearly depend on the temperature gradient along the length of metal, which would not be available until the coupling equations had been solved. In short, it is necessary to adopt an iterative means of solution. Similarly with reformers, the downward radiant flux depends principally on the flue gas temperature gradient, but this is not known until the flux balances have been evaluated.

The total heat input to the furnace per unit cross sectional area of roof, per unit time is described by the term $G_g C_g T^*$. If T_g^L is the exit flue gas temperature at the furnace floor, the amount of heat leaving via this stream is $G_g C_g T_g^L$. In the intervening space, the resulting difference of heat $G_g C_g (T^* - T_g^L)$ has been distributed to the tubes, thereby raising the enthalpy of the process gas by an equal amount. This is shown diagramatically in Fig. 6.3. The top curve

represents the heat input function and the bottom one the temperature of the process gas. The initial values for these (at the furnace roof) are the theoretical flame temperature T* and the inlet feed temperature Tp^{o} respectively.

Taking a point in the lower region of the furnace where the gases are in plug flow, it can be seen that the heat flowing down through the furnace consists of the sensible heat of the bulk flow of flue gas together with the downward radiant heat flux. If the heat input at any one point is characterised by the temperature Ti this equation may be written:

$$Gg\ Cg\ \frac{d\ Ti}{dz} = Gg\ Cg\ \frac{d\ Tg}{dz} + \frac{dq_V}{dz} \qquad \text{-------- (6.1)}$$

where q_V is the downward radiation flux component. Integration with respect to z gives

$$Gg\ Cg\ Ti = Gg\ Cg\ Tg + q_V + K \qquad \text{-------- (6.2)}$$

At the furnace floor, radiant energy is conserved, so that $q_V = 0$ and Ti = Tg. Hence in equation 6.2 K = 0 so that

$$Ti = Tg + \frac{q_V}{GgCg} \qquad \text{-------- (6.3)}$$

This relationship is only true of the plug flow region; in the upper zone, where mixing of the gases occurs, the temperature is fairly uniform. Evaluation of the net downward radiant flux requires a knowledge of the average distance travelled by beams of radiation, i.e. the mean beam length of the gas body. The shape of the gas body may be taken as a rectangular parallelpiped with dimensions 1 : L : L, $L \longrightarrow \infty$. PORT (64) gives the correct value of beam length B, for very low partial pressures of absorbing gas, as twice the shortest dimension, this factor diminishing as Pg is increased. Thus q_V is found by considering that, on average, a given point receives flux from half a beam length above it, and radiates to an equal distance below.

The equation for the downward flux becomes

$$q_V(z) = \sigma \varepsilon_g\ Tg^4\ (z + B/2) - \sigma \varepsilon_g\ Tg^4\ (z - B/2) \qquad \text{-------- (6.4)}$$

Near the top and bottom of the furnace, the equation for q_v requires flue gas temperatures at points beyond the roof and floor. However, radiant energy must be conserved at both ends of the furnace, so the roof and floor act as perfect mirrors or planes of symmetry with regard to the vertically travelling fluxes. The flue gas temperature profile is therefore extended symmetrically by the relations

$$T_g(-z) = T_g(z); \quad -B/2 \leqslant z < 0 \qquad \text{---- (6.5)}$$

$$T_g(L+z) = T_g(z); \quad L < z \leqslant L + B/2$$

and equation 6.4 is then valid for all z.

6.2 Heat flux received by the Tubes

The next factor to be considered is the heat flux to the tubes. This is not an easy problem because each part of the surface of a tube interchanges heat flux with every other part of the furnace, rather than being solely dependent on the temperature of the flue gas in the immediate vicinity. Nor, of course, does each tube "see" the same surroundings, because the centre row of tubes is flanked by the outer lanes, whereas the latter face a refractory wall on one side.

Mutual shielding of tubes in the same row is a further complication. It is clearly impractical to deal with each tube individually because of this shielding effect; instead each row of tubes has to be considered as a plane wall whose effective surface area is reduced by a suitable "shape factor" depending on the ratio:

Outside tube diameter / centre to centre distance between adjacent tubes. A method of evaluation of such factors for a bank of tubes with a refractory wall behind was devised by CHAO (65), and a later more accurate method by ROSS (66). The factor is defined as that fraction of the radiation incident on a bank of tubes which is intercepted by unit area of a plane passing through the tube axes.

The centre row of tubes is obviously a plane of symmetry, and all three planes are of infinite extent in the sense that the flux pattern of the tubes at the ends of the rows is not altered by the proximity

of the refractory walls. It is also assumed that each element of tube surface "sees" the same proportion of refractory surface as any other element; this is reasonable because the refractory surface temperature is fairly uniform throughout. However, the flue gas temperature varies more widely, and some averaging of the heat fluxes received from a hemi-spherical shell centering at a given point, with radius of half the beam length is required. As an approximation, therefore, an effective flue gas temperature, Te, is defined by taking the mean value of the flue gas temperatures half a beam length away in either direction.

$$T_e(z) = \frac{1}{2}\left(T_g(z + B/2) + T_g(z - B/2)\right) \qquad \text{-------} \quad (6.6)$$

Fig. 6.4 shows the method of computing the radiation fluxes in the furnace. The outer tube planes are assumed to receive identical fluxes, but the centre plane is considered separately. Taking the outer plane first the sketch shows that it "sees" a refractory wall on one side and a mirror image of itself on the other; the "mirror" being situated halfway between the outer and centre planes. Flux arriving at the tube plane from the refractory walls is labelled q_r, that from the mirror q_m.

In the present analysis, the gas is taken to be grey. It is easily shown that the radiant flux falling on unit area of tube plane on one side is given by $\varepsilon_g \sigma T_e^4$, where Te (z) represents the appropriate gas temperature at that point down the furnace. Thus the total flux R' to the refractory wall is

$$R' = F_r\left(x_t \varepsilon_t \sigma T_t^4 + q_m(1 - x_t)\right)(1 - \varepsilon_g^r) + F_r \varepsilon_g^r \sigma T_e^4 \quad \text{--(6.7)}$$

where F_r is the amount of refractory surface area associated with unit area of the plane. The first term denotes the emission of flux from the tubes, and the second term the flux from the mirror side which has passed through the gaps between the tubes; both fluxes being partially attenuated on subsequent passage through the gas. The

fractions x_t, $(1 - x_t)$ to be used are obtained from Hottel's chart for radiation falling directly on one face of the leading row of a bank of tubes.

In the steady state case, the refractory wall is not a net absorber or emitter of flux; therefore the expression for q_r becomes

$$q_r = \varepsilon g^r \sigma T_e^4 + w F_r (1 - \varepsilon g^r) R^1 \qquad \text{-------- (6.8)}$$

where w is the fraction of flux originally emitted by the refractory that eventually arrives at the tube planes - either directly or by reflection. It may be shown that it is equal to $1/(1 + \varepsilon g^r)$.

On the other side of the tube plane, the flux M^1 striking the mirror is composed of the emission from the tubes together with the fraction of q_r that has passed through the gaps between the tubes, i.e.

$$M' = \varepsilon g^m \sigma T_e^4 + (x_t \varepsilon_t \sigma T_t^4 + q_r (1 - x_t)) (1 - \varepsilon g^m)^2 \qquad \text{----- (6.10)}$$

Beam lengths required in the evaluation of εg^r and εg^m are taken as 1.7 times the distances between the appropriate parallel planes (64) - in the first case these are the refractory wall and the tube plane; in the second case, the tube plane and the mirror. The tubes themselves can only absorb a fraction x_t of the flux coming from both sides $(q_m + q_r)$ and emit an amount $x_t \varepsilon_t \sigma T_t^4$ to both sides. Therefore, the net flux absorbed by either of the outer rows of tubes is given by

$$q_t = x (q_r + q_m - 2 \varepsilon_t \sigma T_t^4) \qquad \text{------- (6.11)}$$

For the centre tube plane, the effect of the refractory walls is far less. To a good approximation, the flux arriving at this plane from both sides is q_m, and so the net heat flux to the tubes is given by

$$q_t = 2 x (q_m - \varepsilon_t \sigma T_t^4) \qquad \text{------- (6.12)}$$

Since equation 6.11 describes the net heat flux to two rows of tubes, and equation 6.12 the flux to one only, an average value of the heat flux is obtained by taking a weighted mean of these expressions, giving

$$q_t = \frac{x}{3} (q_r + 2q_m - 3 \varepsilon_t \sigma T_t^4) \qquad \text{------- (6.13)}$$

6.3 Equations for Heat Transfer inside the Tubes

The development of equations for heat transfer mechanisms within the tube is similar to the procedure adopted for model 1. The enthalpy of the process gas is the sum of two components - the sensible heat and the heat consumed by the endothermic chemical reaction. Using the same nomenclature as section 3.3, the process gas enthalpy becomes

$$Gp \frac{dU}{dz} = Gp\ Cp \frac{d\ Tp}{dz} + Gp\ \psi \frac{\Delta H_{Tp}}{L} \qquad \text{-------- (6.14)}$$

This may be integrated with respect to z to give

$$U = Cp\ (Tp - Tpo) + \psi \int_0^L \frac{\Delta H_{Tp}}{L}\ dz \qquad \text{-------- (6.15)}$$

which is identical with equation (3.27).

Clearly the increase in process gas enthalpy is equal to the net rate at which heat is applied to the tubes, since in the steady state there can be no accumulation of heat within the system. If W is the total length of the three tube planes in the horizontal direction the equality may be written

$$Gp \frac{dU}{dz} = W.qt\ (z) \qquad \text{-------- (6.16)}$$

The final equation is derived from the original co-current heat exchanger analogy. The rate at which the process gas enthalpy increases must be equated not only to the net flux absorbed by the tubes, but also to the rate at which the heat input function decreases. This gives

$$Gg\ Cg \frac{d\ Ti}{d\ z} = Gp \frac{d\ U}{d\ z} \qquad \text{-------- (6.17)}$$

and integrating with respect to z gives

$$\frac{Gg\ Cg}{Gp} (\ T_i - T^*) = U \qquad \text{-------- (6.18)}$$

which is valid for any position z down the length of the furnace. The tube wall temperature profile is related to Tp via the overall heat transfer coefficient (h_{tc}) by the equation

$$qt = h_{tc}\ (Tt - Tp) \qquad \text{-------- (6.19)}$$

6.4 Solution of Model (2).

Although graphical solution of the equations would be feasible, it is quite impractical in view of the large number of runs that are required to test the model adequately. Therefore, as before, a numerical method is sought which is suitable for programming on a computer.

It is immediately apparent from the foregoing sections that the equations themselves are fairly simple. The difficulties that are likely to arise are concerned with matching various profiles to the requirements of different equations. For example the process gas enthalpy curve must agree with equations (6.16) and (6.17) whilst the flue gas temperature profile has to satisfy (6.3) and (6.4). Iterations such as these are likely to give rise to oscillations in the profiles obtained in successive solutions. An attempt may be made to dampen these oscillations using a method based upon a low degree polynomial spline technique (67).

The steps used to obtain correct profiles for the model are summarised below:

(i) An initial estimate of the profile of the heat input curve Ti is made. The value at z = o is the theoretical flame temperature T* and the curve falls monotonically from this value to the flue gas exit temperature, Tg^{L} (as yet unknown) at the floor of the furnace.

(ii) Now a flue gas temperature profile Tg that is compatible with the Ti curve is sought. First, a shape must be assumed for this curve such that in the top recirculation zone the temperature is constant and in the lower plug flow regime falls linearly to the exit valve. The nett downward heat flux is evaluated from Eq (6.4), then Eq. (6.3) is used to check if the resulting curve for Ti agrees with the assumed profile for Tg. If not, the latter must be altered until acceptable agreement is reached.

(iii) The next step involves calculating the radiation heat flux

absorbed by the tubes, using the equations developed in Sec. 6.2. This procedure requires values for the tube wall temperature profile which as a starting guess can be taken as constant.

(iv) Equating the right hand sides of Eqs. (6.14) and (6.16) enables the process gas temperature profile Tp to be calculated . Again, however, it is necessary to iterate since a profile for Tp must be known before the term ΔH_{Tp} can be calculated and hence the equation integrated.

(v) The tube wall temperature profile and the process gas temperature profile are linked by Eq. (6.19). A revised curve for Tt is now provided and the heat flux to the tubes re-evaluated. The sequence of operations to calculate qt, Tt and Tp is therefore repeated until all are in agreement.

(vi) Finally Eq. (6.17) is used to check whether the assumed profile for Ti is correct or not. In general it will not be, so steps (i) to (vi) must be repeated until the correct profile for Ti is obtained.

The only input values known are the theoretical flame temperature and the process feed temperature; the complete set of profiles have to be generated by a process of repeated iteration. In addition to the overall iterative loop for the heat input curve, there are two major loops within it for the flue gas and tube wall temperature profiles. The second of these includes another iteration loop to deal with the process gas temperatures. Both the Tg and Tp curves require the local smoothing technique indicated earlier.

Computer run times for model 2 were considerably higher than those for model 1 - by a factor of 5 usually. It proves difficult to obtain a profile for Tg which enables Eq.(6.3) to be satisfied at every point in the plug flow regime of the furnace. As many as 30 iterations on Tg may be needed before successive profiles differ nowhere by less than 0.1% (about $1^{\circ}C$). Similarly the "loop within a loop"

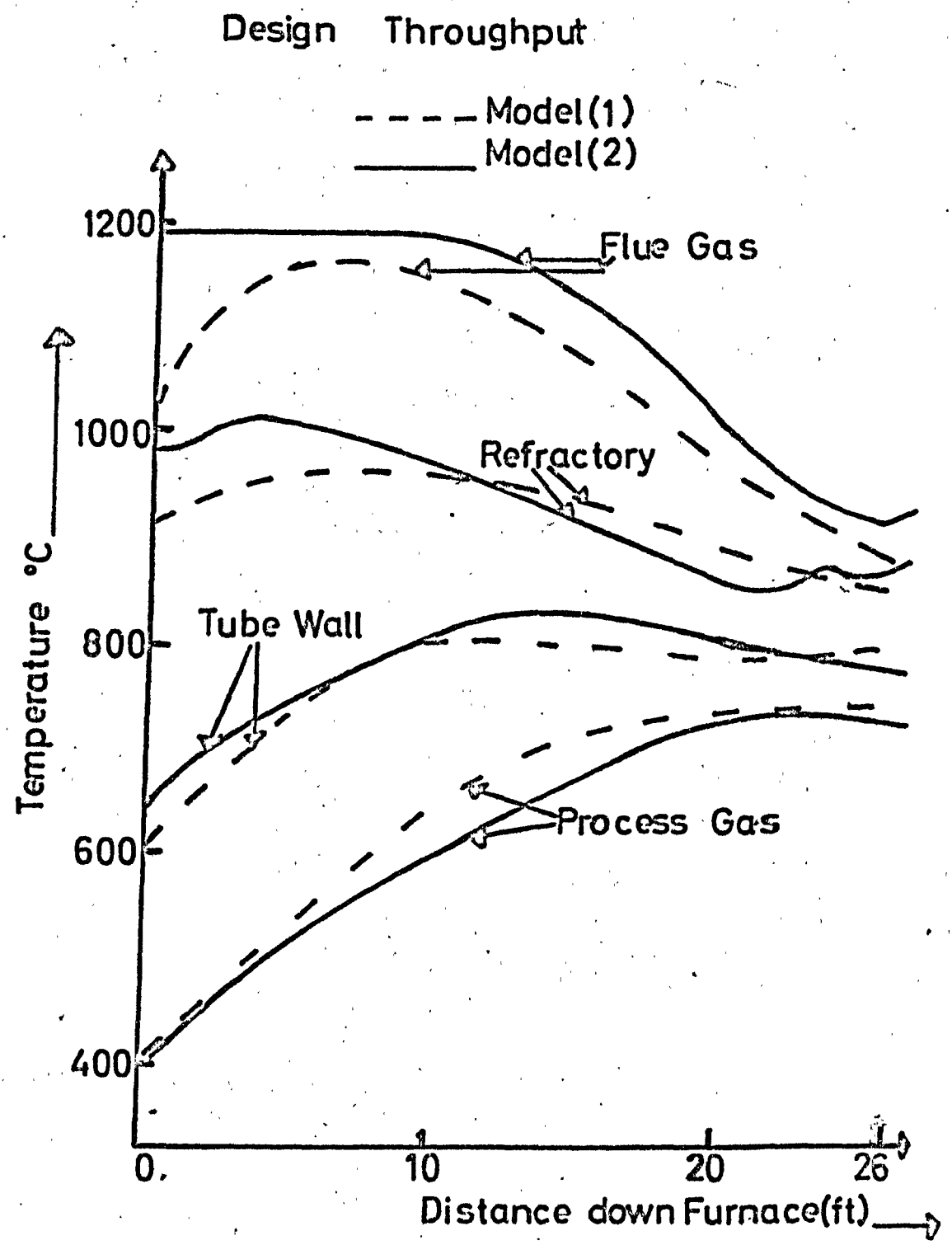

Fig.6.1: COMPARISON OF TEMPERATURE PROFILES FROM MODELS (1) AND (2).

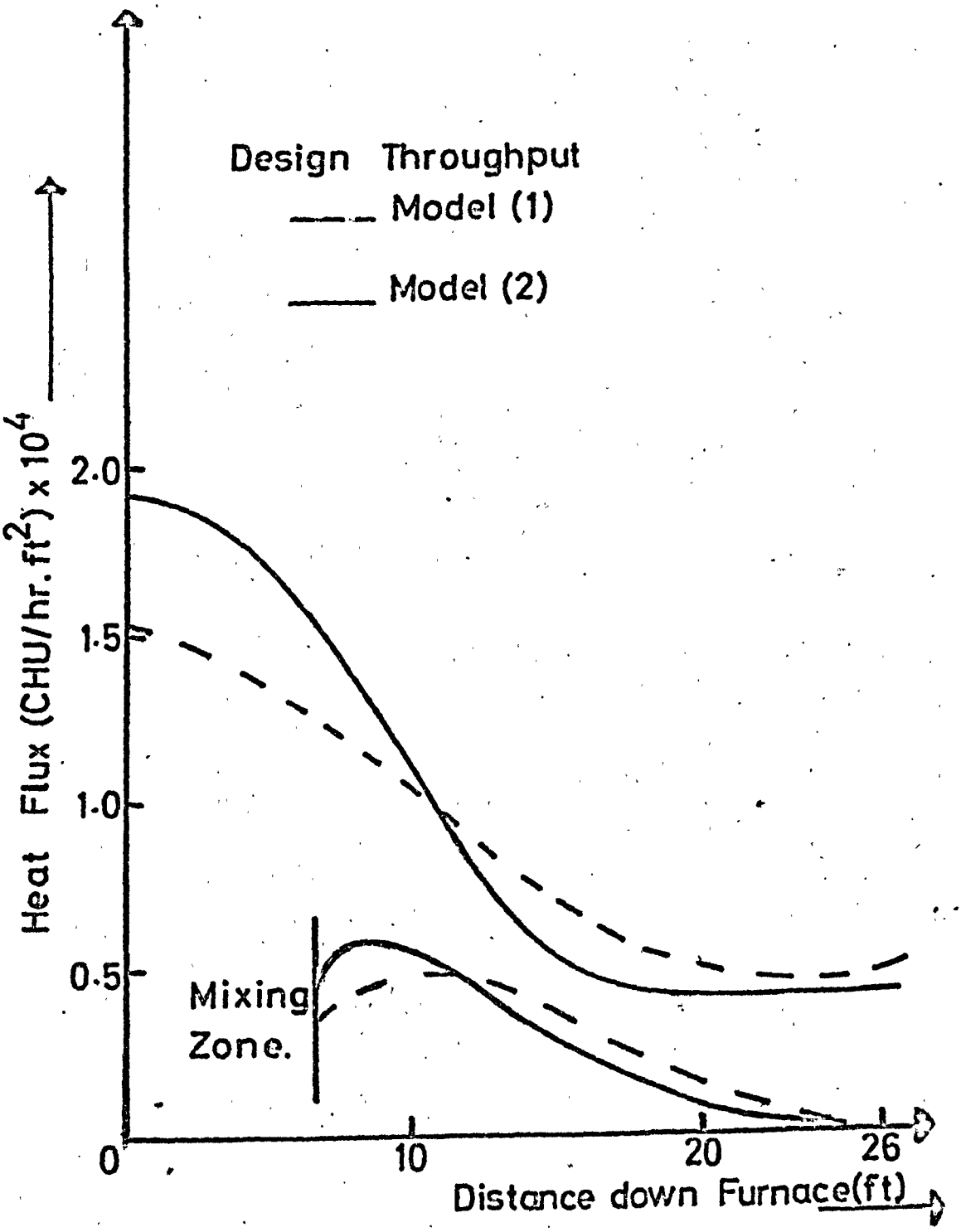

Fig. 62 : COMPARISON OF HEAT FLUX PROFILES FROM MODELS (1) AND (2).

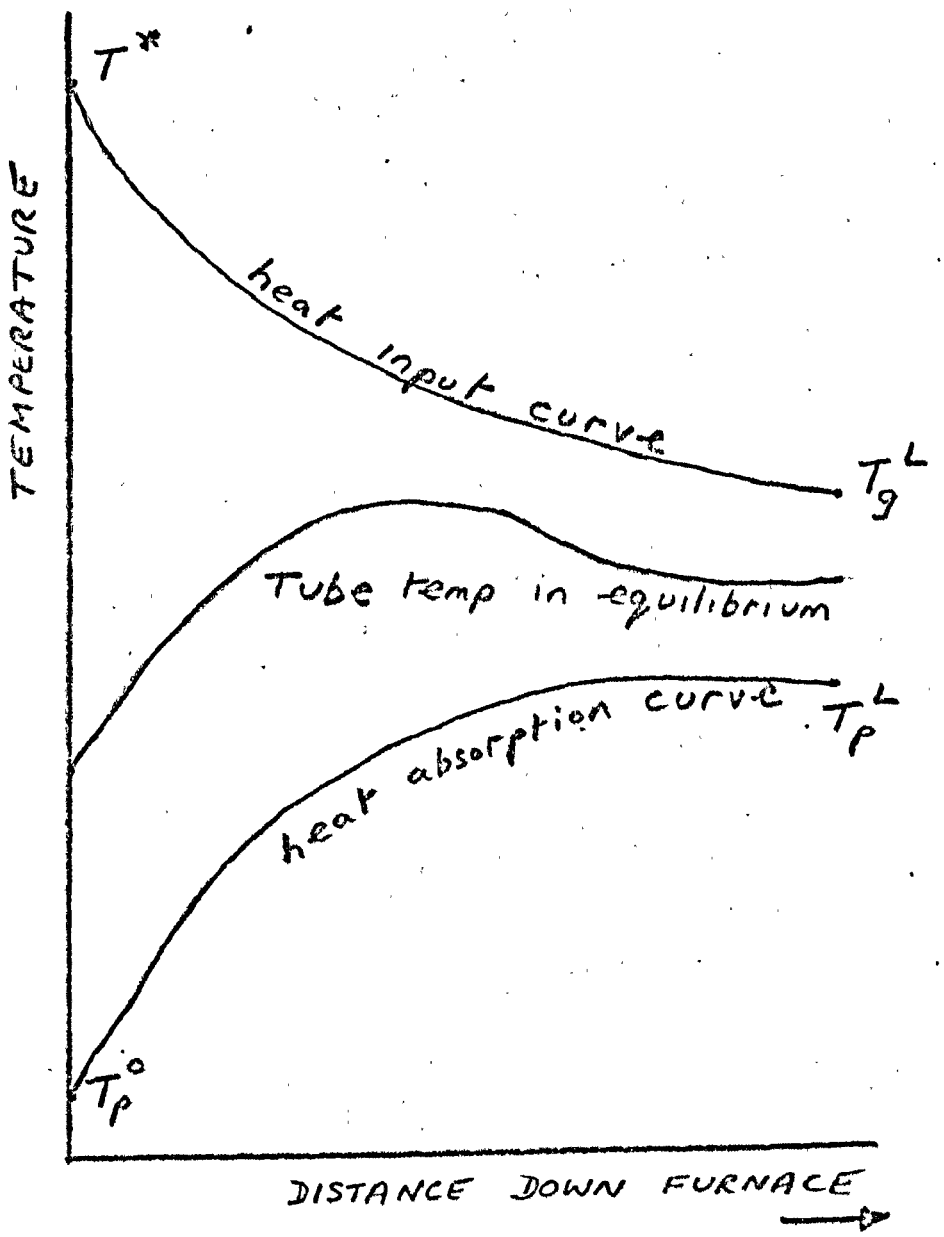

Fig. 6·3 : General shape of furnace temperature profiles showing model analogy of co-current heat exchanger

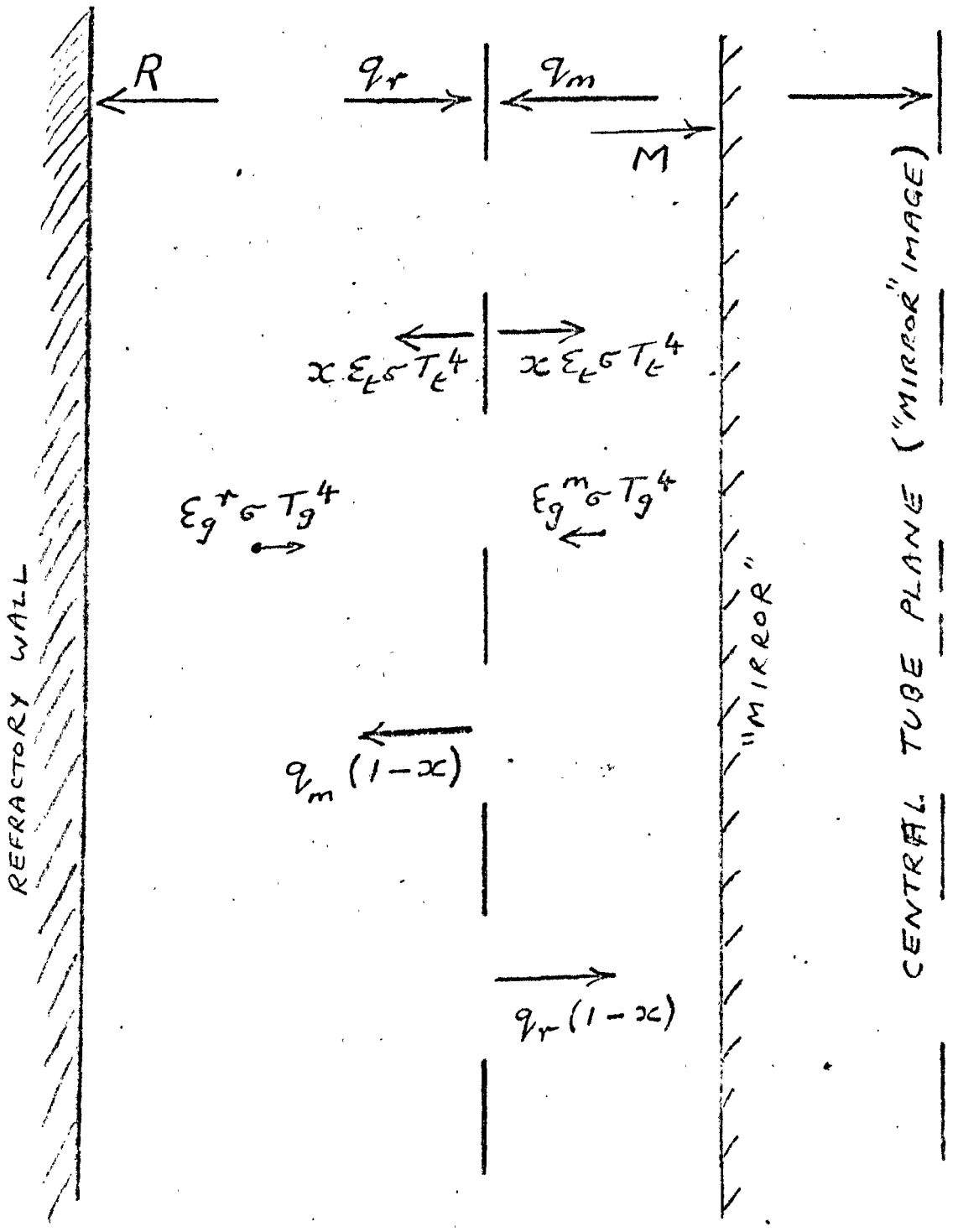

Fig 6·4 : Terms in heat flux balance equations for Model 2

arrangement described in steps (iii), (iv), and (v) is inherently time consuming. Considering that perhaps 0 to 10 iterations are necessary before Ti converges via the outermost loop, it is clear that some of the sub-routines are employed several hundred times and the computing time required inevitably reflects this.

6.5 Comparison of results obtained with those from Model 1.

To make a valid comparison between results obtained from the two models the same basic input data must be used. The first run performed was for the design flowsheet data whose values are tabulated in Table 4.5 Certain parameters which have no direct counterparts in model 1 must also be evaluated. Table 6.1 is a list of the operating conditions and parameter values for the design flowsheet case.

Fig. 6.1 shows a comparison between the temperature profiles obtained from the two models for the flowsheet data. The corresponding radiant heat flux profiles are given in Fig. 6.2 Some significant differences are observed. The flue gas temperature profile for model 2 is considerably above that for model 1, whereas the reverse is true for the process gas temperatures. Moreover, the shapes of the flue gas temperature profiles are quite different, a distinct peak predicted by model 1 is not revealed in the output from model 2. It appears that model 1 predicts that more heat is extracted from the flue gas and transferred to the process gas. But not only is the total quantity of heat transferred more, the distribution of the heat input profiles are different. The profiles for q_t, shown in Fig.6.2, demonstrates that model 2 calculates a greater difference between the heat flux to the tubes at the top of the furnace and that to the tubes lower down. This gives rise to more rapid heating of the process gas and tubes at the top of the furnace than lower down resulting in a definite peak in the T_t curve for model 2; model 1 predicts a flatter tube wall temperature over most of the tube length. Similarly the peak in the refractory wall temperature profile is more pronounced in the model 2

run and is pushed further to the top of the furnace.

Symbol	Quantity	Value	Units
Gg	Superficial mass flow of flue gas	91.6	lb/hr ft^2
Gp	Superficial mass flow of process gas	73.7	lb/hr ft^2
Cg	Specific heat of flue gas	0.32	CHU/lb ^oC
Cp	Specific heat of process gas	0.65	CHU/lb ^oC
T*	theoretical flame temp.	2220	^oK
εg^m	"mirror" side gas emissivity	0.31	-
εg^r	refractory side gas emissivity	0.34	-
εr	refractory wall emissivity	0.80	-
h_{tc}	overall heat transfer coeff.	74.5	CHU/hr $ft^2 {}^oC$
L	height of furnace	26.5	ft.
ℓ^1	penetration depth of flames	0.0	ft.
F_r	amount of refractory surface per unit area of tube skin surface	1.73	-
α	fraction of tube skin equivalent to plane surface	0.43	-
εt	tube skin emissivity	0.93	-
W	total length of tube planes	72.0	ft.

TABLE 6.1 Operating conditions and parameter values for Model 2 - Design flowsheet case.

A second run at a lower throughput - about 60% of the design make- is considered. The relevant operating conditions are:

Burner fuel flowrate	1840	lb/hr.
Air to fuel ratio	16.9	
Process Gas flowrate	26400	lb/hr.
Steam to Carbon ratio	3.0	
Theoretical flame temperature	2180 ^oK	

The resulting profiles from models 1 and 2 are set out in Tables (6.2) and (6.3) respectively. On comparing these it is seen that the same discrepancies between the two models are observed at low throughput as at high, and it must therefore be concluded that there are inherent differences in the two analyses which will not be resolved

by fitting certain parameters. For instance, the emissivity parameters Eg^m and Eg^r can be adjusted until the outlet stream temperatures are identical for the two models. However, this distorts the tube wall and refractory temperature profiles such that quite unrealistic values are predicted in the upper zone of the reformer.

When the models are compared against in-plant data it is found that the exit flue gas, and make gas temperatures predicted by model 1 are far nearer the observed values. Also no sharp peak in the tube wall temperature profile is measured. Add to this the much lower computing time required for model 1 and clearly this model is the one to adopt, particularly for extension to the dynamic case.

However, the development of model 2 has been worthwhile, because it provides a useful physical insight into the problem and helps clarify the abstract formulation associated with model 1.

DISTANCE DOWN FURNACE	FLUE GAS TEMP.	REFRACTORY TEMP.	FLUX TO TUBES	TUBE SKIN TEMP.	PROCESS GAS TEMP.
0.0	1005.6°C	972.7°C	16,224.0 CHU/hrft.^{2}	615.5°C	399.0°C
1.1	1025.2	976.5	15,369.0	656.6	451.8
2.1	1088.5	981.9	14,615.0	693.3	500.3
3.2	1151.8	987.6	13,838.0	727.8	544.5
4.2	1196.4	991.9	13,040.0	757.1	584.3
5.3	1215.4	993.5	12,183.0	780.7	619.8
6.4	1207.0	991.7	11,212.0	799.9	650.8
7.4	1170.3	986.6	10,248.0	812.8	677.0
8.5	1103.9	979.2	9,289.1	821.8	698.7
9.5	1057.9	969.7	8,321.0	828.0	716.2
10.6	1031.1	959.5	7,486.5	830.8	729.7
11.7	1011.5	949.8	6,822.5	830.9	739.9
12.7	995.1	940.6	6,223.2	830.8	747.4
13.8	980.7	932.0	5,750.6	829.2	752.6
14.8	967.7	924.1	5,309.8	828.0	756.1
15.9	955.8	916.8	5,018.0	824.7	758.0
17.0	944.9	910.0	4,744.8	821.8	758.9
18.0	934.9	903.9	4,512.3	819.0	758.9
19.1	925.8	898.4	4,318.6	816.2	758.3
20.1	917.5	893.4	4,191.8	812.8	757.1
21.2	910.0	889.1	4,049.8	810.5	755.6
22.3	903.3	885.4	3,991.9	807.2	753.7
23.3	897.5	882.4	3,949.7	804.4	751.9
24.4	892.5	880.1	3,948.4	801.6	750.0
25.4	888.4	878.6	3,941.0	799.9	748.2
26.5	885.2	877.9	3,981.5	798.2	746.5

TABLE 6.2 Steady State Profiles from model 1.

DISTANCE DOWN FURNACE	FLUE GAS TEMP.	REFRACTORY TEMP.	FLUX TO TUBES	TUBE SKIN TEMP.	PROCESS GAS TEMP.
0.0(ft)	1169.3°C	987.4°C	20,247 CHU/ hr/ft^2	669.0°C	399°C
1.1	1169.3	993.5	19,415.0	707.2	448.3
2.1	1169.3	999.6	18,575.0	741.8	494.1
3.2	1169.3	1005.6	17,744.0	772.8	536.2
4.2	1169.3	993.4	15,956.0	786.7	574.0
5.3	1169.3	981.9	14,379.0	797.7	606.0
6.4	1169.3	968.4	12,865.0	804.3	632.7
7.4	1169.3	955.3	11,542.0	808.6	654.7
8.9	1169.3	945.3	10,512.0	812.5	672.4
9.5	1128.4	949.5	10,251.0	823.9	687.2
10.6	1090.1	953.1	9,998.9	834.0	700.7
11.7	1048.1	954.6	9,680.3	841.9	712.8
12.7	1008.2	956.2	9,410.3	848.9	723.5
13.8	976.7	958.7	9,214.1	855.8	732.9
14.8	980.3	938.8	8,039.1	847.9	740.8
15.9	903.1	919.0	7,009.7	838.9	745.5
17.0	981.2	891.9	5,801.5	824.7	747.3
18.0	980.2	865.9	4,792.3	810.2	746.3
19.1	981.2	848.7	4,225.6	799.4	743.1
20.1	970.2	853.3	4,512.2	799.4	739.3
21.2	957.2	859.1	4,818.0	800.7	736.5
22.3	930.1	852.5	4,629.3	796.0	734.3
23.3	904.4	847.5	4,512.7	791.9	731.7
24.4	893.2	852.0	4,751.6	792.7	729.3
25.4	903.6	857.1	4,997.6	794.3	727.6
26.5	917.3	862.4	5,231.1	796.4	726.7

TABLE 6.3 Steady State Profiles from model 2.

CHAPTER VII. PLANT DATE ACQUISITION: COMPARISON OF RECORDED DATA WITH STEADY STATE MODEL PREDICTIONS.

Mathematical models of chemical plants or items of plant equipment fall into two main categories. The first of these uses the inputs to the system and attempts to predict the resulting outputs by identifying the physical and chemical processes occurring within that system. The second type of model differs from this because it employs the observed relationship between the inputs and outputs to infer which mechanisms are most important and to fit numerical values to the parameters thus defined. Alternatively a relationship is assumed that is merely convenient from statistical or computational aspects, such as the use of multiple linear regression analysis. Here the physical basis of the model is lost and it may not be possible to determine other internal variables of the system which cannot be measured directly.

In the case of inferential models, the necessity of obtaining accurate data from the system is obvious. A little consideration, however, will show that a predictive model, such as that developed in this work, has an equal dependence on correctly measured inputs and outputs. The reason is that except in very simple cases it is impossible to describe a physical process precisely in mathematical terms even if the mechanisms of the process are all apparent. In the complex situations that arise in industrial plant many interacting phenomena occur, some of which may affect the system in a random fashion. The need is, therefore, for a feedback of information from the measured plant outputs via the model builder to update the basis of the model predictions.

7.1 The Data Logging System

It is possible to obtain the general operating characteristics of a steam reformer by reference to the existing plant instruments. These do, after all, provide the operators with sufficient information

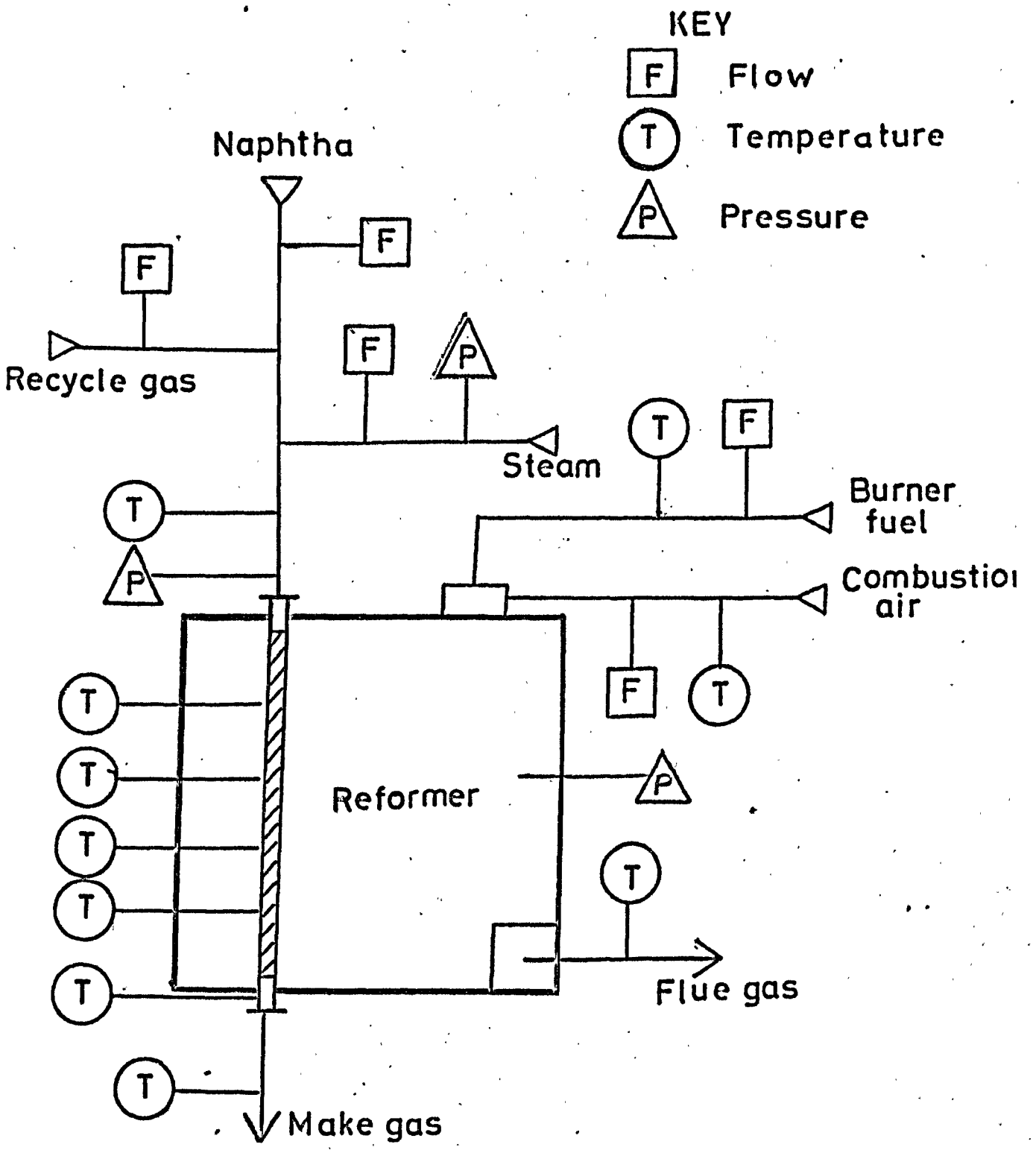

Fig 7·1

MEASUREMENTS TAKEN AROUND REFORMER

to control the plant and meet required product specifications. However, the disadvantages of using plant operating records are considerable. Recorded variables are displayed by ink traces over scaled charts. Some of these are paper strips with linear scales, others have square root calibrations and still others are circular in shape and are replaced every 24 hours.

Apart from the tedium of obtaining plant data from these charts the accuracy achieved is likely to be low. Other important variables are only indicated by the instruments and usually recorded once per shift by the operating personnel. The validity of these figures is even more doubtful. These comments are true for essentially steady state operation; for dynamic studies, some form of digital data acquisition is indispensible, and this was the scheme adopted.

A Dynamco Data Logger linked to an Ohrtronics paper tape punch was installed for this purpose. Up to 60 channels were available for the input data each of which may be scanned in turn and visually displayed on the digital voltmeter panel. The same values, together with the appropriate channel numbers are simultaneously recorded on 8-hole punched tape, the format being compatible with the ICL KDF9 computer. A complete scan of the inputs can be initialised at pre-set intervals, ranging from one minute to two hours, by means of an automatic timer device. Other features of the system include an internal calibration voltage source and facilities for obtaining repeated scans of a single channel or continuous scanning of a selected group of channels.

The quantities to be measured are shown diagrammatically in Fig.7.1. They are listed in Table 7.1 together with the channel numbers and plant instrument reference numbers (where applicable).

All temperature measurements are made using chromel-alumel thermocouples which generate electrical voltages in the 0 - 100 millivolt range and thus provide direct inputs to the data logger. The relation

CHANNEL NUMBER	PLANT INSTRUMENT	VARIABLE MEASURED
00	-	Tube Skin temperature 1
01	-	Tube Skin temperature 2
02	-	Tube Skin temperature 3
03	-	Tube Skin temperature 4
04	-	Tube Skin temperature 5
10	TR 1112	Inlet Combustion Air temperature
13	TI 1103	Process feed temperature
14	TI 1104	Make gas exit temperature
16	TI 1110	Flue gas exit temperature
25	FRRC 1101	Steam flow to reformer
26	PIC 1103	Furnace Box pressure
27	FR 1103	Burner fuel flowrate
28	FI 1101	Combustion air flowrate
38	FR 1101	Hydrocarbon process feed flowrate
45	FRC 1001	Recycle gas flowrate
29	PRC 1103	Superheated steam pressure
37	PI 1003	Process feed pressure at inlet

TABLE 7.1 Plant data recorded by logger.

between voltage output and temperature is well-defined but slightly non-linear. Transducers convert the instrument air signals to the diaphragm valves controlling the principal pressures and flows into electrical voltages which the logger can handle.

The thermocouple and transducer leads are connected to terminals in a common junction box. Multi-cored cables then link these terminals with special plugs for the input gates of the logger. The thermocouple signals are calibrated by disconnecting each circuit from the plant and switching an accurately measured voltage corresponding to the voltage that would be generated on to the appropriate channel. For the transducers, the element is shunted with standard resistors which change the overall circuit resistance

in exactly the same way as the transducer resistance changes over its full range.

Care must be taken to ensure that the signal input lines are shielded and that so far as possible, common-mode voltages are eliminated.(68) These arise when the two transducer leads are earthed at different locations due to the remoteness of sensor and receiver (69). Otherwise they are picked up on the transducer lines with consequent degrading of the valid signals. In addition, the logger incorporates an analogue filter as an option to limit the frequency bandpass of the channel. This cuts down normal mode noise, but sufficient bandwidth must be retained to reveal the genuine process dynamics.

Despite these precautions it is still probable that fluctuating responses will be obtained because of short-term fluctuations in the measured variables themselves. Therefore digital filtering is performed on the logger output values to acquire both steady state levels and transient movements of the system. For steady state values this means, in practice, scanning the whole set of channels repeatedly and taking a mean value for each variable, neglecting any points that are clearly spurious. The smoothed data is then converted into corresponding temperatures, pressures and flowrates using the appropriate calibration curve.

One final manipulation is necessary for the temperature readings - the so-called "radiation correction". A thermocouple probe located in a strong radiation field establishes an equilibrium temperature between those of gas and the immediate surroundings. It is this steady state temperature rather than the true gas temperature which is recorded on the logger. A correction should also be applied to the tube skin temperature measurements although the magnitude of these corrections will be smaller than those for the gas streams. The method of estimating the radiation correction is supplied in the book by ECKERT and DRAKE (70).

7.2 Comparison between logged data and values predicted by model 1

Industrial plants never completely achieve steady state operation because random fluctuations of the system parameters prevent it. It will be arbitrarily assumed, however, that the reformer is at steady state if none of the measured quantities has altered by more than 1% either side of its mean value in any four hour period. During the 20-month period when the data was recorded, such occasions were comparatively uncommon.

In that time, certain parameters of the system inevitably change - the catalyst activity declines, the emissivity of the tubes and refractory walls changes and the heat transfer coefficient between tube skin and process gas will be reduced. Nor, of course, are the data logger and punch immune from such effects; in the dusty conditions of the control room damage can easily occur to the input-gate contacts. Hence differences in the model accuracy are to be expected because these long-term changes cannot be included in the model in any systematic fashion.

Six cases are set out below to demonstrate the ability of model 1 to predict the output temperatures correctly for various load levels and with either naphtha or natural gas as the feedstock and burner fuel. A broad consideration of Tables 7.2 to 7.7 shows that the input quantities recorded on the data logger are in substantial agreement with the plant instrument readings, although the pen-and-ink flowmeter charts could not be read with very great precision. After the radiation correction had been applied to the output temperatures, the logged values were consistently above those indicated by the plant instrument, probably indicating this correction was not allowed for in its calibration.

The logged furnace tube temperatures are in close agreement with values predicted by the model, especially at high levels of throughput. Only the flue gas exit temperature is markedly lower than the model

VARIABLE MEASURED	PLANT INSTRUMENT	LOGGER	MODEL (1)
Burner fuel flow (Naphtha) lb/hr	2960	2902..	
Combustion air flow lb/hr	48000	50980	
Process naphtha flow "	8900	8850	
Superheated steam flow "	34600	34420	
Recycle gas flow "	290	260.1	
Combustion air inlet temp. °C	330	333.5	
Inlet process gas temp. "	400	402.5	
Exit flue gas temp. "	885	900.2	904.6
Exit process gas temp. "	752	749.9	746.8
Tube temperature 1 "		740.7	738.0
Tube temperature 2 "		828.6	833.8
Tube temperature 3 "		835.0	832.5
Tube temperature 4 "		822.3	814.7
Tube temperature 5 "	806	817.3	805.1

TABLE 7.2

VARIABLE MEASURED	PLANT INSTRUMENT	LOGGER	MODEL (1)
Burner fuel flow (Naphtha) lb/hr	2530	2506	
Combustion air flow lb/hr	42900	43300	
Process naphtha flow "	7610	7495	
Superheated steam flow "	30200	29640	
Recycle gas flow "	340	269.2	
Combustion air inlet temp. °C	330	336.2	
Inlet process gas temp. "	398	401.8	
Exit flue gas temp. "	878	873.5	887.3
Exit process gas temp. "	750	754.1	747.0
Tube temperature 1 "		749.8	737.6
Tube temperature 2 "		826.0	828.7
Tube temperature 3 "		835.9	832.4
Tube temperature 4 "		818.6	810.4
Tube temperature 5 "	803	813.7	800.2

TABLE 7.3

VARIABLE MEASURED	PLANT INSTRUMENT	LOGGER	MODEL (1)
Burner fuel flow (naphtha) lb/hr	1450	1389	
Combustion air flow lb/hr	28700	27910	
Process naphtha flow "	4080	4023	
Superheated steam flow "	19700	19530	
Recycle gas flow "	290	201.8	
Combustion air inlet temp. °C	330	333.9	
Inlet process gas temp. "	400	392.6	
Exit flue gas temp. "	805	824.7	836.8
Exit process gas temp. "	745	747.2	737.1
Tube temperature 1 "		715.2	699.7
Tube temperature 2 "		784.5	794.3
Tube temperature 3 "		807.0	801.7
Tube temperature 4 "		792.1	794.6
Tube temperature 5 "	763	772.5	782.5

TABLE 7.4

VARIABLE MEASURED	PLANT INSTRUMENT	LOGGER	MODEL (1)
Burner fuel flow (natural gas) lb/hr	2350	2431	
Combustion air flow lb/hr	49000	48200	
Process natural gas flow "	6250	6380	
Superheated steam flow "	29100	28700	
Combustion air inlet temp. °C	331	339.8	
Inlet process gas temp. "	400	396.0	
Exit flue gas temp. "	872	886.4	902.9
Exit process gas temp. "	750	754.9	752.5
Tube temperature 1 "		748.6	720.0
Tube temperature 2 "		819.8	821.6
Tube temperature 3 "		837.5	840.6
Tube temperature 4 "		822.7	829.3
Tube temperature 5 "	792	816.0	804.4

TABLE 7.5

VARIABLE MEASURED	PLANT INSTRUMENT	LOGGER	MODEL (1)
Burner fuel flow (natural gas) lb/hr	3020	3036	
Combustion air flow lb/hr	57500	58630	
Process natural gas flow "	8440	8382	
Superheated steam flow "	31400	30670	
Combustion air inlet temp. °C	324	320.8	
Inlet process gas temp. "	396	401.3	
Exit flue gas temp. "	886	929.7	941.8
Exit process gas temp. "	748	753.2	746.5
Tube temperature 1 "		780.5	774.4
Tube temperature 2 "		832.8	846.0
Tube temperature 3 "		839.1	867.3
Tube temperature 4 "		836.4	841.6
Tube temperature 5 "	813	828.9	825.7

TABLE 7.6

VARIABLE MEASURED	PLANT INSTRUMENT	LOGGER	MODEL (1)
Burner fuel flow (natural gas) lb/hr	1500	1437	
Combustion air flow "	32500	30090	
Process natural gas flow "	3820	3892	
Superheated steam flow "	15900	15400	
Combustion air inlet temp. °C	315	322.1	
Inlet process gas temp. "	402	400.8	
Exit flue gas temp. "	814	841.8	847.2
Exit process gas temp. "	754	752.4	761.5
Tube temperature 1 "		698.7	693.3
Tube temperature 2 "		783.5	798.9
Tube temperature 3 "		829.1	820.2
Tube temperature 4 "		801.9	807.4
Tube temperature 5 "	773	779.6	789.3

TABLE 7.7

prediction. This may be due to poor positioning of the thermocouple probe or possibly air leakage into the furnace flues. An overall heat balance on the furnace shows that the values predicted by the model are more likely to be correct.

When the furnace is operated at well below its design level, the fit of the model to the data is less satisfactory. The reaction zone recedes to a relatively short region near the top of the tubes whereas the model assumes that the heat sink is apportioned down the whole length of the tubes. Also the estimate of the heat transfer coefficient is uncertain at low flowrates of process gas.

In general then, the steady state model proves an adequate representation of the reforming furnace both both naphtha and natural gas feedstocks. The furnace tube skin temperatures are easily the most sensistive variables to use for testing the model because they are in thermal equilibrium between the radiation field and the consumption of heat by the endothermic chemical reactions on the process gas side. The other major variables of the model are the mass flowrates, which are determined by differential pressure measurements. Bearing in mind the well-known difficulties of obtaining these values accurately (71) the performance of the model in the steady state case is acceptable.

CHAPTER VIII THE DYNAMIC MODEL

8.1 Object of a Dynamic Model

Industrial processes in which the rate of throughput of material is frequently changed must operate under transient conditions for a substantial part of the time. A town gas manufacturing plant is one such process, and so there may be much to be gained by considering the plant dynamics in some detail.

There are two main areas of investigation in which knowledge of the transient behaviour of a system is necessary. The first is dynamic optimisation and control studies which attempt to establish a time-dependent criterion of performance as the system is brought from one level of operation to another. Clearly, the model must predict the consequences of a given control action in terms of the transient response of the system, in order that an optimal control policy based on this criterion may be formulated. A useful,indication of whether the dynamics of a process are important in control studies is obtained by comparing the average time between significant disturbances with the time taken for the process to settle down to a new steady state after a disturbance has occurred. If the two periods are of similar magnitude then the system dynamics should be considered in any attempt at genuine optimal control.

The second reason for studying the dynamic characteristics of a system is to determine whether important constraints are violated during transient operation. Virtually every practical process is subject to constraints. These take many forms, but may be broadly categorised as either physical limitations of the processing equipment or restrictions on the product specification. Physical constraints arise on both the control and the process variables of the system: there is a maximum temperature that the furnace can attain; the flow rate of process gas through the tubes is restricted by the pressure drop

through the catalyst bed; if the steam pressure is to be raised it has to be done slowly because of the finite capacity of the boilers. The last problem is a dynamic constraint - a maximum rate of change of a quantity is stipulated within an overall limiting range of values.

Constraints imposed on the dependent process variables are generally due to the mechanical strength of the equipment materials. The maximum pressure that the tubes can withstand is one obvious example. Dynamic constraints are particularly important here, because they reflect the danger of thermal shock effects in the furnace refractories and tubes when the burners are turned up or down. It is this aspect that will be of primary interest in the present work.

Dynamic models are obtained from theoretical analysis, experimental data, or some combination of the two.

As shown in Chapter II, the theoretical treatment gives rise to state variable equations of a distributed parameter nature in the general formulation. In practical control studies, the system of equations are often reduced to a lumped parameter representation, so as to reduce the mathematics of the problem to manageable terms. Usually some of the state variables chosen to characterise the process will not be directly measurable, although it is clearly desirable that some quantities are capable of being checked against experimental values.

If the model is to be derived solely from experimental data, the resulting model will be of the input-output-type, that is, the dependent variables of the model must be the measurable output variables of the system related in some way to the input control variables. Often this relationship will be derived from empirical, rather than fundamental considerations, because the system is regarded essentially as a "black box" and the internal features are ignored; only the change in output corresponding to a given change in input is required. This forms the basis of many statistical modelling techniques to which a useful introduction is given by SAVAS (72).

8.2 The Dynamic Model equations for the furnace

The complete set of state variable equations were derived in Sec.2.3 For convenience they will be restated here:

$$\frac{G_g C_g \partial T_g}{V_g \partial \theta} + G_g C_g \frac{\partial T_g}{\partial z} = -2\beta\sigma\psi T_g^4 + \beta I_a^+ + \beta I_a^- \quad \text{------- (8.1)}$$

$$\frac{\partial I_a^+}{\partial z} = (-\beta - \varepsilon_r a_r - \varepsilon_t a_t) I_a^+ + \beta\sigma\psi T_g^4 + \varepsilon_t a_t \sigma\psi T_t^4 + \varepsilon_r a_r \sigma\psi T_r^4 \quad \text{------- (8.2)}$$

$$-\frac{\partial I_a^-}{\partial z} = (-\beta - \varepsilon_r a_r - \varepsilon_t a_t) I_a^- + \beta\sigma\psi T_g^4 + \varepsilon_t a_t \sigma\psi T_t^4 + \varepsilon_r a_r \sigma\psi T_r^4 \quad \text{------- (8.3)}$$

$$\frac{\partial I_b^+}{\partial z} = (-\varepsilon_r a_r - \varepsilon_t a_t) I_b^+ + \varepsilon_t a_t (1-\psi)\sigma T_t^4 + \varepsilon_r a_r (1-\psi)\sigma T_r^4 \quad \text{------- (8.4)}$$

$$-\frac{\partial I_b^-}{\partial z} = (-\varepsilon_r a_r - \varepsilon_t a_t) I_b^- + \varepsilon_t a_t (1-\psi)\sigma T_t^4 + \varepsilon_r a_r (1-\psi)\sigma T_r^4 \quad \text{------- (8.5)}$$

$$\frac{1}{V_p}\frac{\partial H_p}{\partial \theta} + \frac{\partial H_p}{\partial z} = \varepsilon_t a_t (I_a^+ + I_a^- + I_b^+ + I_b^- - 2\sigma T_t^4) \quad \text{------- (8.6)}$$

From the above set of equations, the only state variables which are considered to have time dependencies on the enthalpies of the flue and process gas streams. Clearly, however, the major lags in the system are due to the heat capacities of the solid components of the furnace - in particular, the influence of the refractory walls.

If the furnace burners are turned up the new flame temperature consistent with the changed air-to-fuel ratio will be attained almost immediately. Likewise, the whole volume of flue gas will undergo a sudden temperature jump because the high flow rate causes the increased heat content of the gas in the vicinity of the flame to be rapidly carried to the lower section of the furnace. This will produce an instantaneous increase in the radiation heat flux emitted by the gas and falling on the refractory and tube surfaces; the rise

in radiant flux, of course, being proportionally greater than the flue gas temperature increase.

Since the surface temperatures of the refractory and tubes do not change immediately, the flux they emit will likewise be initially unaltered. Hence the surfaces absorb more radiant flux than they emit, with a consequent gradual increase in temperature until a new equilibrium position is attained. The excess heat will gradually be conducted through the thicknesses of the refractory slab and tube walls, thereby bringing the interior temperatures (including that of the process gas and catalyst pellets), up to their new steady state values.

Basically, therefore, the thermal lags in the system are the result of the material components acting as additional heat sinks, so that the full increase of available radiant heat cannot be realised immediately. Conversely, when the burners are turned down, the various component heat capacities act as additional heat sources, which prevent the radiant flux from falling immediately to its new steady state level of intensity.

8.3 Process Gas Side Lags

The subsidiary partial differential equations describing the imbalance of heat in different parts of the furnace are derived by methods identical to those used for the original state equations. That is, the substantial derivative of the enthalpy of a component, which represents the accumulation of heat within unit volume during unit time, is equated to an energy balance between itself and other external components. The equation for the flue gas (8.1) is already in this form, although, as stated above, its capacity term is negligible, and may be safely ignored.

Inside the furnace tubes, the process gas, catalyst pellets, and alloy steel tube walls all have finite thermal capacities, and should therefore be taken into account. An energy balance on the tube walls

gives:

$$a_w \rho_t C_t \frac{\partial T_t}{\partial \Theta} = 2\, a_t\, h_{FW} \quad (T_p - T_t) \qquad \text{-------- (8.7)}$$

$$+ E_t\, a_t \quad (Ia^+ + Ia^- + Ib^+ + Ib^- - 2\, \sigma \quad T_t^4)$$

For the fluid phase (process gas) the energy balance is :

$$\delta \rho_p C_p \frac{\partial T_p}{\partial \Theta} + \rho_p C_p V_p \frac{\partial T_p}{\partial \Theta} = 2\, a_t h_{FW} \quad (T_t - T_p)$$

$$+ a_s \; h_{FC} \quad (T_s - T_p) - G_p \Delta H/L \qquad \text{-------- (8.8)}$$

Finally, the equation for the catalyst packing is:

$$(1 - \delta) \rho_s \; C_s \frac{\partial T_s}{\partial \Theta} = a_s \; h_{FC} \quad (T_s - T_p) \qquad \text{-------- (8.9)}$$

In developing the above equations for thermal lags on the process gas side of the reformer, it has been assumed that gradients of temperature and fluid momentum in a horizontal direction are absent. Axial diffusion of heat in the fluid is disregarded; so also is conduction along the tube length, or between vertically adjacent pellets. The net result of these simplifying assumptions is that the only spatial temperature distribution needing consideration is that of the process gas down the length of the tubes. This gives rise to the term for the bulk flow of process gas, and represents the only important mode of heat transfer in the vertical direction.

Convection and radiation of heat horizontally through the tubes is defined by the various heat transfer coefficients which provide lumped parameter approximations to very complex situations. The quantity h_{FW} is equivalent to the overall heat transfer coefficient h_{tc} developed in Chapter IV; the fluid-to-particle coefficient h_{FC} is determined from j - factor correlations such as those given by CARBERRY (73) and HOUGEN (57). The various areas for heat transfer corresponding to these coefficients are based on unit volume of the reformer. Thus:

$$a_w = \frac{A_w}{L.A_f} \qquad \text{-------- (8.10)}$$

$$a_s = \frac{6}{d_s} \quad (1 - \delta) \quad \frac{A_t}{A_f} \qquad \text{-------- (8.11)}$$

Where A_w is the cross-sectional area of all the metal walls of the furnace tubes, and A_t the sum of the cross-sectional areas of the empty tubes.

Examination of equations (8.7) - (8.9) reveals that they are coupled together and must be solved simultaneously. Furthermore, the system is non-linear because of the inclusion of the terms for endothermic reaction heat and tube-skin radiant emission. In principle equation (8.7) shows that the process gas side equations should also be solved in conjunction with those of the radiation field; but the latter are insensitive to changes in tube-skin temperature, so this coupling may safely be disregarded.

To complete the system description, the initial peturbations that give rise to subsequent dynamic operation must be specified. Usually, this takes the form of stating new values for the dependent variables at the origins of both distance and time coordinates. In this case, however, it is the radiant flux intensity and process gas flow rate that change, whereas the inlet temperatures remain constant. Also, the peturbations are distributed along the z - dimension, and do not both occur simultaneously.

When the furnace throughput is to be increased the burners are first turned up, this quickly increases the flue gas exit temperature, and, after a short delay, the amount of steam produced in the flue gas waste heat boilers. After the pressure in the drum has built up sufficiently, the steam flow rate to the furnace can be increased. The naphtha flow rate is linked to this by an automatic ratio controller. Thus, with regard to equations (8.7) - (8.9), the initial disturbance is due to step-changes in the beam intensities I_a + etc. Then, after a certain time-lag, the process gas flow rate parameters Gp and Vp are increased. It is assumed that the change of flow rate is also a step function, and that the gas is incompressible; which means that an alteration in V_p at the inlet ($z = o$) is instantly propagated to the

lower regions ($z > 0$) of the reactor tubes.

The non-linear interactive nature of the process gas equations, together with the separate peturbation conditions, precludes solution by analytical methods. However, numerical solution by finite differences is not difficult. The new profiles for tube-skin temperatures can therefore be substituted back into the radiation equations to update the beam intensities.

8.4 Conduction within the Refractory Wall

When considering the refractory wall, it is apparent that neglecting temperature gradients in the horizontal direction - i.e. through the slab thickness - is a gross assumption to make. The inside face temperature is in excess of 900°C, falling to ambient temperature through a thickness of about 0.75 ft., moreover, the thermal conductivity of the refractory material is low, so that the chief resistance to heat transfer occurs within the solid itself, rather than at the two faces. A realistic treatment must, therefore, take account of the lateral temperature distribution through the wall.

The equations governing the transient state of the refractory wall are the well-known, one-dimensional heat conduction equations, together with a flux boundary condition on the inside face to couple it with the radiation field:

$$\rho_r \quad C_r \quad \frac{\partial v}{\partial \Theta} \quad = K_r \quad \frac{\partial^2 v}{\partial s^2} \qquad \text{-------- (8.13)}$$

$$Q_r = K_r \left(\frac{\partial T_r}{\partial s} \right)_{s = l_r} = h_{ri} \ (T_g - T_r) + \frac{\varepsilon_r}{2} \left(I_a^+ + I_a^- + I_b^+ + I_b^- - 2\sigma T_r^4 \right) \qquad \text{-------- (8.14)}$$

where $v(s, \Theta)$ is the temperature distribution through the slab thickness, and T_r the value of v at the inside face ($s = l_r$). In equation (8.14), the term $(T_g - T_r)$ represents the flow of heat into the hot face by convection, which maintains the steady state temperature gradient. This amount of heat is eventually lost to the atmosphere from the outer face; thus the second boundary condition should be of the form:

$$K_r \left(\frac{\partial v}{\partial s} \right)_{s = 0} = h_{ro} (v - T_A)$$

However, in practice, the flux at the outer refractory surface is negligible in the dynamic analysis of the furnace, hence, putting $h_{ro} = \infty$ this boundary condition becomes a prescribed surface temperature

$$(v)_{s = 0} = T_A \qquad \text{-------} \quad (8.15)$$

The appropriate initial condition for the equations is the original steady-state temperature profile through the slab, given by:

$$v(s,0) = (T_F - T_A) \frac{s}{\ell} + T_A \qquad \text{-------} \quad (8.16)$$

There is a set of equations (8.13) - (8.16) applicable to each horizontal increment of the furnace. In the boundary condition at the inside face, the radiation beams and surface temperature are functions of z, the distance down the furnace, thus giving rise to varying amounts of radiant flux to be absorbed by the refractory. However, vertically adjacent sets of equations are not coupled because conduction of heat along the length of the refractory wall is neglected, hence they may all be solved independently.

The radiant flux to the refractory is not only a function of z; it is also strongly time-dependent. Immediately after the burners have been turned up, there is a large net flow of heat to the refractory, but as the surface temperature gradually rises, more flux is emitted and the amount potentially available to raise the temperature further, is reduced. Eventually, the radiation field and refractory surface will once again be in thermal equilibrium. When this occurs, the furnace has, for most practical purposes, reached its new steady state. The conduction equation will show that the interior of the refractory slab is still in a transient state, but this is of minor importance. Clearly, the major interest is in the initial stages of the dynamic response of the furnace.

Since the furnace radiation beams and temperature profiles are

normally resolved into 50 discrete increments, it is necessary to solve 50 sets of equations for each time-step in the transient analysis of the radiation field, that is, for each occasion in which a new surface refractory temperature profile, T_r , is sought for substitution into equations (8.2) - (8.5). A rapid computational procedure must therefore be developed in order that the reformer dynamics can be adequately established within the total computing time available.

If, in the evaluation of new refractory temperature profiles, the values inserted into the right-hand side of equation (8.14) are those calculated in the preceding time-step, the radiation and conduction equations are effectively de-coupled. Of the two boundary conditions to the equation, one remains linear, while the other is now a prescribed flux condition, since equation (8.14) can now be found explicitly. By letting the flux term lag in this way, a little accuracy is lost, but the problem is greatly simplified. Solution of the equations may be performed using either analytical or numerical methods.

In CARSLAW and JAEGER (92), the original functions v (s,) is found. In its final form this is:

$$v = 2\sqrt{\alpha_r \theta}\left(\frac{q_r}{k_r} - \frac{T_r}{l_r} + \frac{T_A}{l_r}\right)\sum_{n=0}^{\infty}(-1)^n\left\{i\,\mathrm{erfc}\,x_1 + i\,\mathrm{erfc}\,x_2\right\} + \frac{(T_r - T_A)}{l_r}s + T_A \qquad \text{----(8.22)}$$

where $$x_1 = \frac{(2n+1)l_r + s}{2\sqrt{\alpha_r \theta}} \qquad \text{-------- (8.23)}$$

and $$x_2 = \frac{(2n+1)\,l_r - s}{2\sqrt{\alpha_r \theta}} \qquad \text{-------- (8.24)}$$

The integrals of the complimentary error function for arguments x_1, x_2 is available from standard mathematical tables, but for machine computation, it is more convenient to expand the function in an infinite series, and truncate after a suitable number of terms.

8.5 Strategy of the complete solution

Solutions for the various component equations of the model have been discussed in the foregoing sections; here, the steps required in the overall model solution are set out.

(i) Initially the reformer is at steady state conditions, and the heat flux and temperature profiles are evaluated as in Chapter V.

(ii) The system now undergoes a peturbation. In practical terms, the fuel flowrate to the burners is increased, resulting firstly in more heat being pumped through the furnace, and secondly, in a higher theoretical flame temperature being reached, since the combustion air flow is not normally increased proportionally. To idealise the situation, it is assumed that the new initial flue gas temperature is reached immediately, whilst the tube skin and refractory temperatures remain at their original steady state values. Hence a new set of profiles can be made at the instant of peturbation.

(iii) Clearly, there is now more heat flux irradiating the refractory and tube surfaces than is emitted from them, so the next step is to find the response to this excess of flux after a predetermined interval. In other words, the sets of equations for heat transfer within the refractory slab and furnace tubes are solved. During this period of time, the beam intensities are assumed to remain constant - this effectively decouples the radiation equations from those for the tubes and refractory.

(iv) Revised profiles for T_r and T_t obtained in step (iii) are fed into the radiation equations (8.1) - (8.5), and new values formed for the beam intensities. These in turn cause the refractory surface and tube skin temperature profiles to be updated. This procedure of working alternately within the furnace volume, then in the solid components, using the radiant beam intensities in the boundary conditions of the unsteady state equations enables the complete transient response of the reformer to be evaluated.

8.6 Comparison between logged data and values predicted by the dynamic model.

The dynamic effects of the furnace that were considered were limited to those resulting from deliberate changes in load level made on the plant. Apart from short term fluctuations, the output temperatures would drift upwards or downwards over a period of several hours even though the inputs were ostensibly steady. This was presumably due to external disturbances influencing the system, such as changes in the moisture content of the combustion air which can affect the flame temperature quite markedly. However, no attempt was made to model these stochastic variations because it was considered that they pose no real problems to the operating personnel.

It is more difficult to establish the validity of the dynamic model by comparison with logged data than it was for the steady state case. In the first place, unlike steady state values which can be obtained by averaging a large number of scans over an almost indefinite period, dynamic data must, in principle, be obtained instantaneously. and definite trends discerned from these over a fixed time period. In practice it was necessary to limit the number of points being logged in the dynamic runs to three - the exit temperatures of the flue gas and process gas and the tube skin temperature at the spproximate centre of the heated length. At pre-set times each variable in turn was sampled repeatedly for several seconds using the manual scanning mode on the logger and averages then taken for each variable. In this way the scanning of each variable was not strictly simultaneous but it was found to be too dangerous to rely on single scans so this discrepancy had to be accepted.

Another difficulty in establishing satisfactory model discrimination was that fairly small perturbations in the feedrate variables must suffice to determine the furnace response characteristics. Instead of raising the input quantities to their new throughput levels in a single step change, the operators normally make three or four

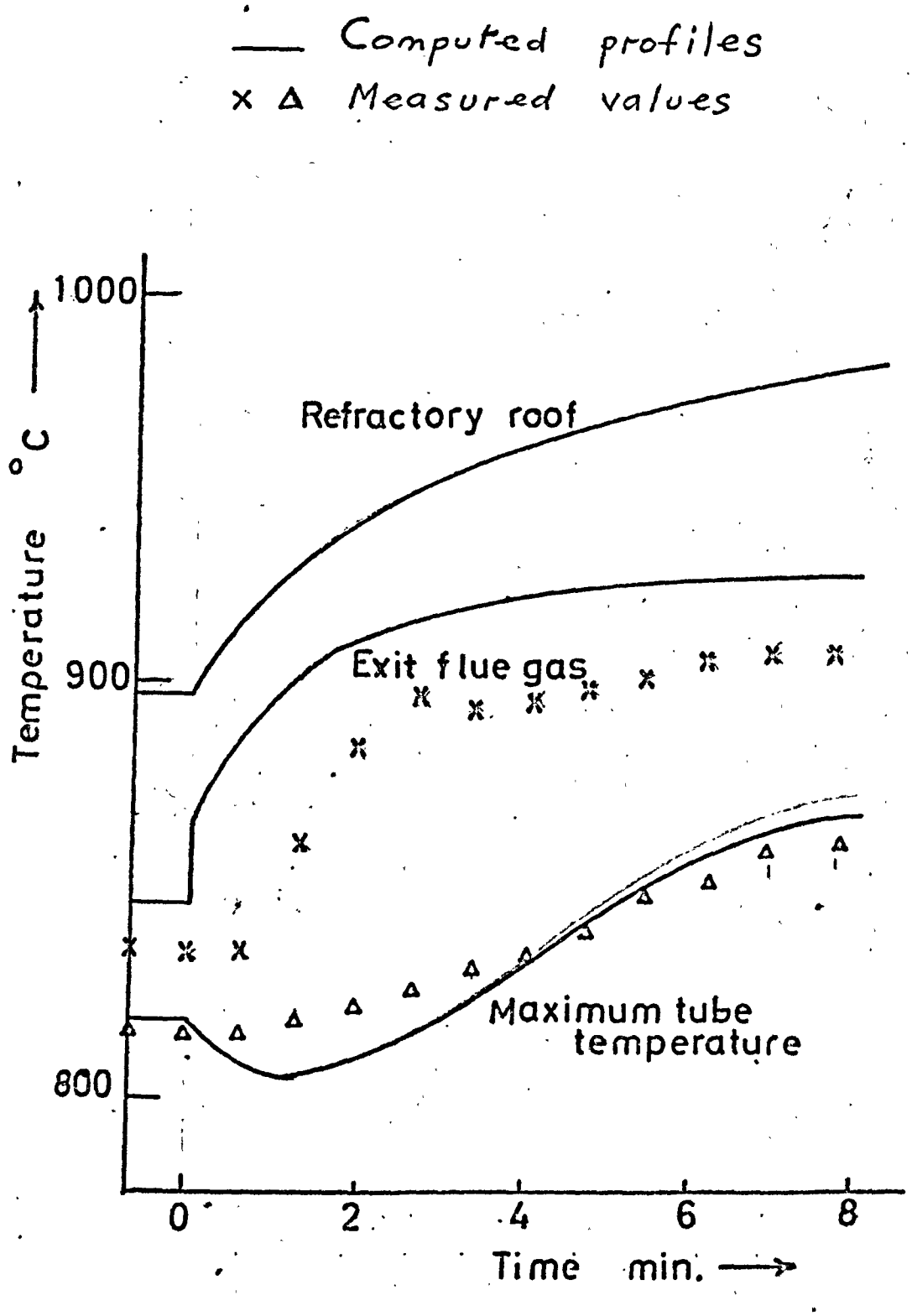

Fig 8·1 FURNACE TEMPERATURE RESPONSES IN UNSTEADY STATE

smaller increases, allowing the furnace to settle down to a quasi-steady state after each change. The smaller increments themselves are not particularly good approximations to step-changes, especially when the automatic control loop between the fuel and process feed flows via the make gas exit temperature is being used.

Hence it is impossible to test the model properly direct from genuine plant load changes; instead certain manipulations were performed on the furnace specifically for testing the model, These involved changing only the burner fuel flowrate, keeping the other inputs constant, by overriding the automatic loop scheme. However, the magnitude of the changes were limited to approximately 6% of the original steady state values.

In order to compare more easily the response predicted by the dynamic model with the observed plant behaviour, the model parameters were adjusted so that the relevant initial steady state outputs agreed exactly with the logged data. This was done by altering the coefficient for heat transfer between furnace tubes and process gas and also the optical parameters of the flue gas.

The results of four runs are set out in Tables 8.1 to 8.4. In addition, Fig. 8.1 illustrates a run where the predicted and measured initial steady state outputs were not made equal. At first sight, the closeness of fit between the model and data for the test runs seems excellent, but it must be remembered that the perturbations are small and well within the linear region of the system. Considerable care must be exercised in extrapolating these results to cases in which the perturbation is of the order of 20 or 25% of the steady state figures. Nevertheless, the general features predicted by the model should correspond with reality even for these larger disturbances.

The response to a step increase in the burner fuel flowrate is a delay followed by first order type increases in the output temperatures to the new steady state levels. There are thus three criteria which

can conveniently be used to assess the goodness of fit of the model in the dynamic test runs. These are: i) the initial time lags, (ii) the final steady-state temperatures, and (iii) the time constants of the furnace. Equivalent comparisons would be very difficult to make for furnace perturbations made by the operators because it is not possible to identify separately the responses to each small perturbation.

The model assumes that the time lag experienced by the flue gas temperature is equal to the residence time of the flue gas in the furnace enclosure. On the process gas side, the delay time is defined as the time elapsed before the mean process gas temperature has risen by $1^{o}C$. (From the mathematical analysis, the process gas "knows" that a rise in heat flux input at the bounding tube walls occurs at the same moment that the flame temperature increases so that in this sense the temperature begins to rise immediately. However, the practical purposes, the increased flux must penetrate the thermal resistance of the catalyst particles before any temperature change is manifest.)

An attempt was made to fit each set of temperature-time readings to a simple function consisting of a delay followed by a first-order rise to the new steady state temperature level. However, the degree of correlation was not high even with the theoretical model values. This is not unexpected because the analysis is complex and only obeys the first order response curve very approximately.

The four runs selected cover a wide range of operating conditions The first two have naphtha as fuel, and feedstock; the last two use natural gas for both functions. Run 3 is for a reduction in heat input whilst the others consider increases.

Table 8.5 shows the mean differences in temperature between the values predicted by the model and those recorded on the logger. It is seen that the model consistently predicts higher flue gas temperatures than those recorded and gives a faster response for both increases and decreases in heat input. On the other hand, for heat increases, the

Inputs

Initial Burner fuel flowrate (naphtha) = 1862 lb/hr

Final " " " " = 1990 lb/hr

Initial theoretical flame temperature = 2084°K

Final " " " = 2195°K

Process gas flow (naphtha + steam + recycle gas) = 27070 lb/hr

Outputs

	LOGGER			MODEL		
Time	$T_p(L)$	$T_t(3)$	$T_g(L)$	$T_p(L)$	$T_t(3)$	$T_g(L)$
0	746.3	820.5	854.1	746.3	820.5	854.1
1	749.5	820.6	859.6	746.3	820.8	866.7
2	751.3	823.7	869.4	746.9	822.1	872.4
4	752.9	825.5	875.1	749.2	825.7	878.5
6	756.0	826.9	878.2	751.8	830.7	881.9
8	758.4	831.4	877.6	755.0	835.2	884.9
10	758.1	837.2	878.8	756.8	838.8	887.1
20	758.9	839.6	883.0	757.4	841.5	888.3
30	759.3	843.8	883.9	757.8	842.0	888.6
40	759.6	845.1	886.4	758.0	842.2	888.6
50	760.7	846.3	885.6	758.1	842.3	888.6

TABLE 8.1 Measured and predicted temperature responses for Run 1.

(All temperatures in °C and times in minutes)

Inputs

Initial Burner fuel flowrate (naphtha) = 2420 lb/hr

Final " " " " = 2604 "

Initial theoretical flame temperature = 2156 ^{o}K

Final " " " = 2261 ^{o}K

Process gas flow (naphtha + steam + recycle gas) = 34360 lb/hr.

Outputs

	LOGGER			MODEL		
Time	$T_p^{(L)}$	$T_t^{(3)}$	$T_g^{(L)}$	$T_p^{(L)}$	$T_t^{(3)}$	$T_g^{(L)}$
0	744.9	815.2	879.7	744.9	815.2	879.7
1	746.1	812.6	884.3	744.9	815.6	888.6
2	746.1	811.4	891.6	745.3	816.8	893.1
4	747.8	815.2	895.2	746.2	820.5	898.2
6	752.7	824.0	900.1	751.3	825.8	901.9
8	756.0	827.3	903.9	754.4	828.1	905.0
10	756.5	830.1	906.7	756.7	829.6	908.5
20	758.2	830.5	908.3	757.9	830.9	910.7
30	757.3	829.2	912.1	758.6	831.5	911.0
40	757.9	834.9	908.4	759.0	832.2	911.1
50	758.8	835.7	906.7	759.3	832.7	911.2

TABLE 8.2 Measured and predicted temperature responses for Run 2.

Inputs

Initial Burner fuel flow (natural gas) = 3083 lb/hr

Final " " " " " = 2879 lb/hr

Initial theoretical flame temperature = 2218 ^{o}K

Final " " " = 2294 ^{o}K

Process gas flowrate (natural gas + steam) = 44800 lb/hr

Outputs

	LOGGER			MODEL		
TIME	$T_p^{(L)}$	$T_t^{(3)}$	$T_g^{(L)}$	$T_p^{(L)}$	$T_t^{(3)}$	$T_g^{(L)}$
0	757.6	866.4	943.8	757.6	866.4	943.8
1	756.3	864.1	937.6	757.5	865.5	931.1
2	749.2	863.7	930.7	754.7	863.5	925.3
4	744.7	861.9	922.4	750.8	858.3	920.7
6	739.5	855.6	915.1	746.0	850.8	916.4
8	736.0	851.8	912.3	742.6	846.6	913.0
10	730.1	847.2	907.8	739.3	843.9	910.2
20	733.4	848.5	903.4	736.1	839.2	907.2
30	732.1	842.3	900.6	733.1	837.0	904.9
40	732.8	839.9	895.9	730.8	836.4	903.0
50	723.7	837.8	895.2	729.4	835.8	902.6

TABLE 8.3 Measured and predicted temperature responses for Run 3.

Inputs

Initial Burner fuel flow (natural gas) = 2085 lb/hr

Final " " " " " = 2209 lb/hr

Initial theoretical flame temperature = 1938^{o}K

Final " " " = 1996^{o}K

Process gas flow (natural gas + steam) = 34570 lb/hr

Outputs

	LOGGER			MODEL		
Time	$T_p^{(L)}$	$T_t^{(3)}$	$T_g^{(L)}$	$T_p^{(L)}$	$T_t^{(3)}$	$T_g^{(L)}$
0	728.4	790.1	860.8	728.4	790.1	860.8
1	732.8	786.7	862.5	728.4	790.1	870.0
2	729.1	790.4	871.4	728.4	790.3	876.2
4	731.5	791.8	875.9	729.6	792.5	879.8
6	734.7	795.0	878.6	733.2	797.7	882.7
8	738.2	799.0	880.0	737.0	803.2	884.6
10	740.4	804.3	881.4	738.6	807.6	886.1
20	742.3	808.8	880.6	739.1	809.9	887.0
30	738.6	814.6	884.1	739.4	811.9	887.2
40	740.6	816.1	883.3	739.5	812.4	887.3
50	744.9	811.8	887.2	739.6	812.7	887.3

TABLE 8.4 Measured and predicted temperature responses for Run 4.

process gas exit temperature is found to increase faster than the model predicts although the final steady state temperatures are in fair agreement in Runs 1 and 2. When the burner fuel flow is reduced, the $T_p^{(L)}$ curve shows a slower than expected response.

TABLE	T_p	T_t	T_g
8.1	- 2.74	0.12	4.90
8.2	- 0.39	1.27	2.21
8.3	3.29	-3.38	1.39
8.4	- 2.03	1.04	4.30

TABLE 8.5 Mean differences between predicted and recorded temperatures (^oC).

The recorded tube skin temperatures, $T_t^{(3)}$ indicate a slower than predicted initial response but later the rate of change tends to increase and overtake the model values. Again Run 3 is an exception; here the lagged values are consistently higher.

Taking the test results overall it would appear that the thermal damping effect of the refractories has not been fully accounted for whereas the process gas side lags are somewhat overstressed. The model does provide a reasonable approximation to the non-steady state behaviour of the furnace over a wide range of operating conditions. However, it must be emphasised that the perturbations made are small so that the tests are not very stringent ones. Moreover the initial steady state values of the relevant variables are compelled to be consistent by suitable parameter estimation and the final steady states should be estimated accurately because the method of calculation employed ensures the computation of a correct heat balance. Hence the recorded responses in Tables 8.1 to 8.4 should be regarded more as an indication of the state of the system than as true quantitative values.

Results from the dynamic model indicate that reformers are usually

stable systems with fairly rapid response to load changes. Before full advantage can be taken of this for control purposes, particularly during start-up and shutdown, it is necessary to check that excessive thermal stresses are not developed in the refractory wall and tube metal. This problem is considered in the next chapter.

CHAPTER IX CONSIDERATION OF THE REFRACTORY SPALLING PROBLEM

The most important constraint imposed on the furnace during non-steady state operation is concerned with the maximum thermal stresses that the refractory walls and furnace tubes can withstand. A theoretical treatment of the mechanical failure of the tubes would be mathematically prohibitive. At the high working temperature of the metal, the calculated thermal stresses are indeed high if no allowance is made for stress relaxation induced by creep deformation of the material. In practice, however, the effects of creep are all-important. Because creep rate is strongly temperature dependent, and also varies non-linearly with the imposed stresses, the resulting strain rates in different parts of the tube are complex functions of the heat flux variation.

Moreover, it appears that creep rate depends in some manner on the past history of the metal and this is very difficult to explain in physical terms. All that can be stated with confidence about the potential tube failure problem is that it is of a long-term nature. For an immediate alteration in the load level or other operating conditions of the furnace, the refractory linings are far more susceptible to damage.

The problem of refractory spalling arises because of the non-uniformity of temperature within the slab. Under such conditions, free expansion of each volume element cannot occur because the elements are constrained to remain in the same body. The result is that stresses within the body are induced and these may eventually exceed the inherent mechanical strength of the material.

A linear temperature gradient does not give rise to thermal stresses because the body is able to expand without producing incompatible strains. A slab subjected to a linear temperature gradient will, if free to expand, form the arc of a circle in which each element

of the slab has expanded by an amount proportional to its temperature increase. If the temperature gradient is other than linear, however, there is no shape which the body can take up such that the expansion of each element is exactly satisfied. Instead, the body will assume a mean position such that some parts are in tension and the remainder in compression. Clearly the tensile and compressive stresses must balance one another.

In addition to these stresses there will be those due to the bending of the slab. If the temperature distribution were symmetrical about a plane through the mid-point of the slab thickness, the tensile and compressive stresses would likewise be symmetrical and so no bending stresses could arise. In this case, however, the fact that one face is exposed to the hot furnace gases and the other to the external environment, gives rise to a mechanical couple about the mid-plane. They are balanced by bending stresses distributed over the cross section such that the algebraic sum of the moments of all bending forces is zero.

As a starting point for the present analysis, the refractory walls and roof are considered to be infinite, homogeneous, flat plates. Now the slab thickness is indeed small compared with the overall dimensions of the furnace box so that stresses perpendicular to the planes of the walls can safely be neglected. It is in the requirement of homogeneity of the slab that the doubt arises. The walls consist of many individual firebricks, approximately cubic in shape and covered with a layer of heat-resistant ceramic on the inside and insulating material on the outside. The justification for assuming a homogeneous slab is that it gives rise to a conservative estimate of the ability of the refractories to withstand thermal shock.

This idealisation of the situation will therefore be adopted at least as a preliminary analysis. It is hoped that the framework of the model will lend itself to a more refined treatment of the stress

analysis at some future date.

Variations in temperature along the vertical length of the refractory slab are neglected in this treatment. At a particular horizontal level z, the temperature profile through the slab thickness may be denoted by $T_z\ (y, \theta)$. From these considerations it can be easily shown that the thermal stresses at any point y within the slab is given by the expression

$$\sigma_x(y, \theta) = \frac{\alpha E}{1-\nu}\left[\frac{1}{\ell_r}\int_0^b T_z\ (y, \theta)\, dy + \frac{12y}{\ell_r^3}\int_0^b T_z\ (y,\theta)\, y dy - T_z\right] \qquad \text{-------- (9.1)}$$

This is derived rigorously in the book by BOLEY and WEINER (83). Thus to calculate the thermal stresses in the refractory at any time it is necessary to find the temperature profile T_z, perform the quadrature indicated and the stress components follow immediately. Since the heat flux to the refractory is time-dependent, an analytical solution is not feasible.

The case of a suddenly applied constant heat flux has been investigated by HASSELMAN (84) where general analytical solutions were derived. However, the calculated stresses for this treatment approach constant values as time approaches infinity and this is at variance with actual conditions where the stresses achieve maximum values then fall to zero when the slab temperature reaches a new steady state.

From the solution of the dynamic model there exists a series of refractory temperature profiles for each time step taken in the model. These may be substituted into Eq. (9.1) and the stresses evaluated but it was found that in the initial unsteady state phase, the numerical procedure used to calculate stress values was subject to numerical instability. It was concluded that the assumption of constant heat flux input over a full time step in the overall solution of the model could not be used successfully to predict the refractory stresses.

Instead, the boundary conditions must be considered as time-dependent in order that the stresses are obtained as smooth functions of both slab thickness and time.

For an arbirary time variation of heat flux input, the temperature or stress profiles at time θ may be obtained by the application of Duhamel's Theorem. It can be stated thus:

$$T_z(y,\theta) = \int_0^t \frac{q(\tau)}{q^0} \frac{\partial T(y,\theta-\tau)}{\partial \theta} \, d\tau \qquad \text{-----(9.2)}$$

In this and subsequent equations, the superscript zero refers to the values applicable to a constant heat flux q^0 maintained over a time interval (H). The variable τ can be regarded as a subdivision of (H); i.e. $q(\tau)$ refers to the instantaneous value of heat input at time τ where $0 \leq \tau < (H)$

Integrating Eq. (9.2) by parts gives:

$$T_z(y,\theta) = \frac{q(o)}{q^0} T^0(y,\theta) + \frac{1}{q^0}\int_0^t \frac{dq(\tau)}{d\tau} T^0(y,\theta-\tau)\, d\tau \qquad \text{-------- (9.3)}$$

The stress due to time-varying heat inputs can be obtained from σ_{xx}^0 (that due to constant q^0) by direct application of Duhamel's Theorem without first determining the temperature profile for the varying case. The equivalent equation for the stress is:

$$\sigma_{xx}(y,\theta) = \frac{q(o)}{q^0} \sigma_{xx}^0(y,\theta) + \frac{1}{q^0}\int_0^t \frac{dq(\tau)}{d\tau} \sigma_{xx}^0(y,\theta-\tau)\, d\tau \qquad \text{-------- (9.4)}$$

This equation shows clearly how the "history" of the thermal inputs experienced by the refractory slab influences the resultant stress. It is not sufficient merely to know the instantaneous distributions of q and T because the rates of change of these quantities have a vital bearing on the stress levels attained. In Chapter 8, analytical solutions were developed for obtaining the temperature distribution through the slab as a function of the heat input and time. The heat input is available only at specific times (H), 2 (H), 3 (H) .....

corresponding to the times at which the radiation equations are solved so that some approximation must be assumed for the derivative of q with respect to time. A negative exponential curve fits the variation of q with time and thus its derivative also.

The complete method of solution is as follows:

(i) Evaluate the dynamic model as before and obtain the heat input to the refractory wall at each horizontal increment down the furnace at specific time intervals: Ⓗ, 2 Ⓗ, 3 Ⓗ, etc.....

(ii) Find an analytical expression for the heat input function in the form:

$$q = q(o)\,e^{-ct} \qquad \text{-------- (9.5)}$$

where the coefficient c in the exponent is fitted by a least squares method.

(iii) Choose a suitably short time interval τ having regard to the conflicting requirements of high numerical precision and moderate computation times. In fact, τ was chosen as Ⓗ /10.

(iv) Put t = Ⓗ initially. Then for a series of time steps of length τ, calculate the slab temperature distributions at times $t - \tau$ for corresponding heat inputs $q(t - \tau)$ obtained from the equation given in (ii). The error function expression, Eq. (8.22) is used with a constant heat input $q(t - \tau)$ from time zero to time $t - \tau$.

(v) The corresponding stresses $\sigma_{xx}^{o}(y, t - \tau)$ at each time step τ are then found using Eq. (9.1).

(vi) Equation (9.4) is now employed which calculates the desired stress levels at time Ⓗ. The integrals in both Eqs. (9.1) and (9.4) must be evaluated by numerical quadrature.

(vii) The whole process is repeated from step (iv) with t = 2 Ⓗ, 3 Ⓗ, etc. until such time that the stresses have clearly passed their maxima and are declining towards zero again.

With a little extra effort the temperature distributions at times Ⓗ, 2 Ⓗ, 3 Ⓗ ..... can be found and compared with those obtained

without recourse to Duhamel's theorem. In fact, there are small discrepancies but these are not important in evaluating the other temperatures in the furnace.

In principle, the stress analysis should be done at each horizontal increment down the furnace, but a major limitation here is the amount of computer time required. The complete dynamic model must be evaluated before steps (i) to (vii) can be performed to obtain the refractory stresses. Therefore, the slab stresses are only calculated for two horizontal levels - at the furnace roof and at the place in the wall opposite the burner flames, i.e. facing the hottest gas temperature.

Some of the inherent complexities of the problem and the simplifying assumptions made have been mentioned already. There are though several others in addition, and these are set out below.

The maximum stresses calculated will be those necessary to initiate a fracture; whether or not propagation of the crack with consequent spalling will occur is another problem. GRIFFITH (85) describes a criterion for crack propagation based on the strain energy in unit volume of the material. However KINGERY (86) considers the value of these quantitative predictions questionable and they are not included here.

A further important assumption concerns the omission of mechanical traction or body forces superimposed on the thermal stresses that arise. In this case the most important body force is the weight of the bricks and any loads that they bear. These induce compressive forces in the slab which, as shown later, are less important than tensile stresses.

Other assumptions include neglecting the effect of creep deformation, taking constant mechanical and thermal properties for all temperatures and neglecting "end effects" at the corners of the slab. Regarding creep, a paper by HASSELMAN (87) defines a relaxation time

for the stresses to decay by creep mechanisms. Based on typical grain sizes and other material properties for firebrick, it is found that, at the temperature levels involved, the relaxation time calculated is very long compared with the time during which the furnace undergoes state operation.

The material property values required for firebrick are set out in Table 9.1. The slab thickness indicated is for the roof and that part of the wall opposite the burner flames; further down the wall is thicker. An average temperature of 500°C was chosen at which to estimate the material properties.

Several runs were made on the computer using the dynamic model in conjunction with a subprogram incorporating steps (i) to (vii). Four cases are considered here. They all involve step changes in both burner fuel flow and make gas throughput of some 20% or more from the original steady state levels. The important input variables are summarised in Table 9.2. It is seen that Case 1 involves a step increase from minimum make; Case 2 is a step increase from normal make to essentially the maximum load; Case 3 is a step reduction from normal make and Case 4 a step reduction from maximum to roughly normal make. The dynamic conditions for all these cases are substantially more severe than would arise in practice.

The general shape of the stress profiles for heating the slab is shown in Fig. 9.1 (a). During the initial stages, the outer surfaces are under compressive stresses whilst the bulk of the inner core is in slight tension. The compressive stresses then reach their maxima on the wall surfaces (greatest on the hot face where the flux change is made) and the flat tensile stress curve becomes more peaked. Then the tensile stress achieves its maximum in the interior of the slab and the curve assumes the shape of a skewed parabola as shown in Fig.9.1 (a). The compressive stresses have diminished. Finally, all the stresses will become zero again, although the computations are not pursued to

(a) Heating

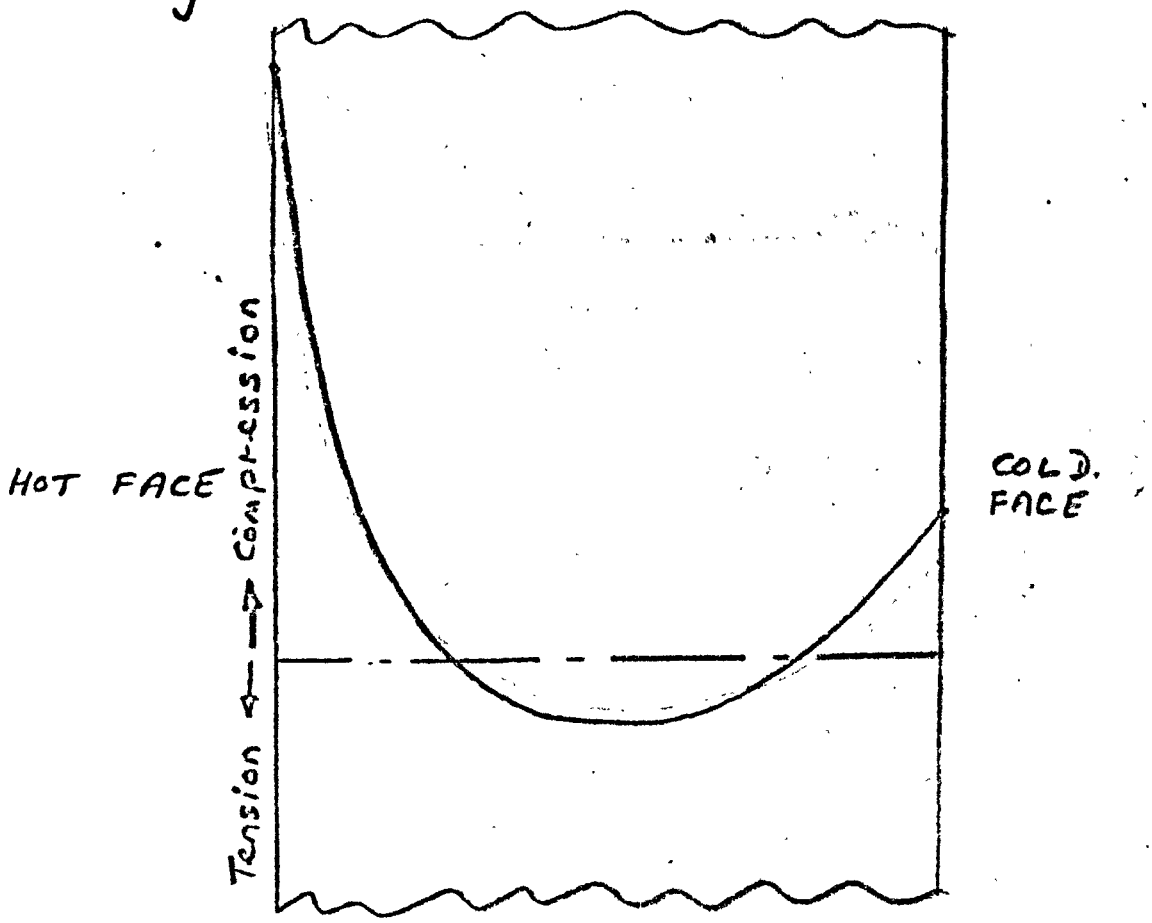

(b) Cooling

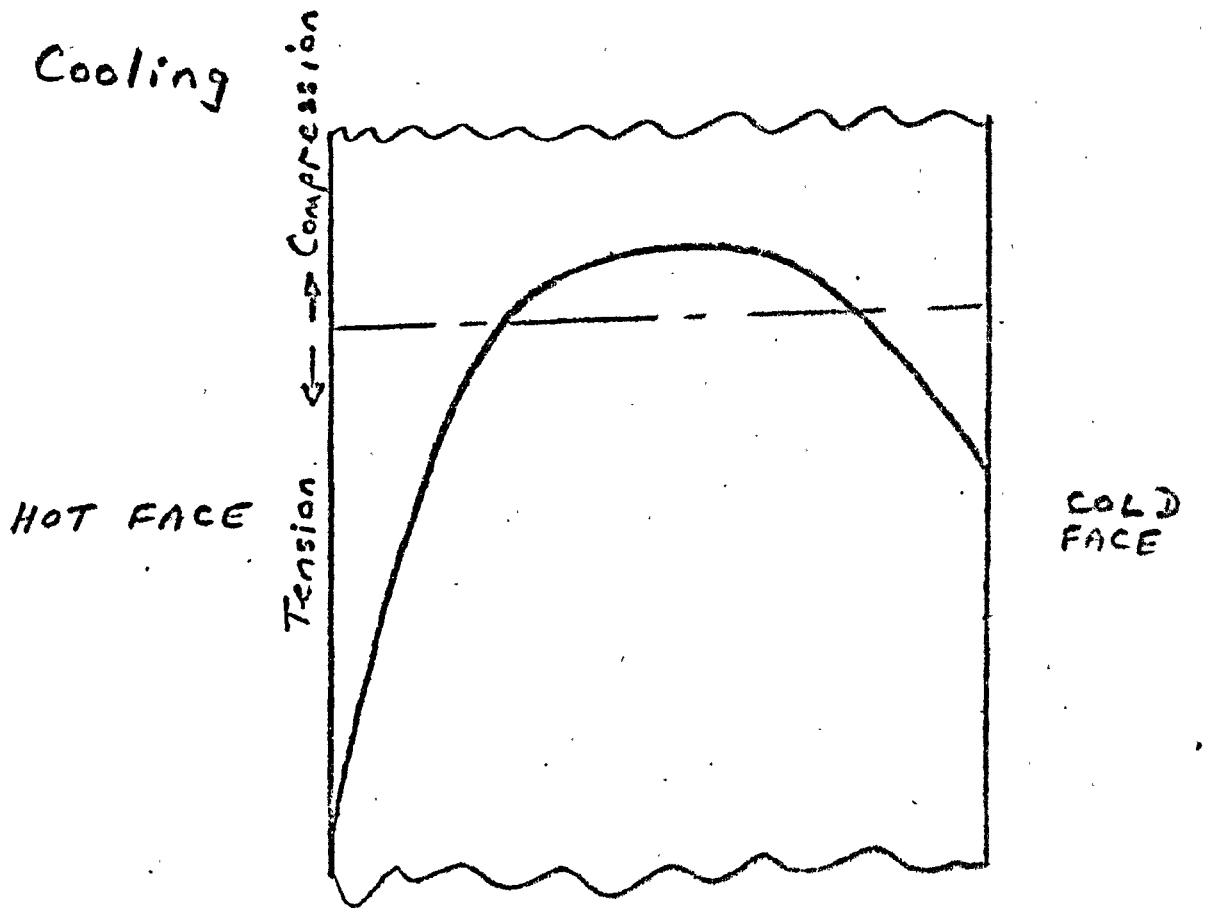

Fig 9·1 : General shape of stress profiles through refractory slab

this point.

When the refractory walls are cooled by reducing the load, the corresponding stress profiles are shown in Fig. 9.1 (b). The pattern is similar to the heating case except that the tensile and compressive parts of the curve are interchanged. Also the profile is less skewed. Here the compressive stresses are of no interest because long before their maxima are reached the slab would have failed in tension.

The salient features of the results obtained from the four computer runs are presented in Tables 9.3 to 9.6. At each time step the values of the following variables are given:

(a) Inside wall temperature T_r

(b) Heat flux to wall q_r

(c) Maximum tensile stress σ^-_{max}

(d) Maximum compressive stress σ^+_{max}

The plant process operators are not allowed to raise the load level at such a rate that the rise in flue gas exit temperature exceeds 50°C per hour. This is equivalent to a rise of about 38°C per hour for the refractory temperature. The changes resulting from Cases 1 and 2 are equivalent to changes of 42°C and 61°C per hour respectively in the maximum hot face refractory wall temperature, but the maximum tensile stresses induced never exceed 40% of the failure level. The compressive stresses are less than 20% of the maximum, even though the calculated compressive stresses are six times the tensile stresses. It would, therefore, appear that the safety margin is ample and the furnace load level could be increased more rapidly if the need arose. It might be truer to say that the problem of refractory spalling is not the limiting constraint when the load level is being increased.

When reducing the load the program calculates that the ultimate tensile strength is exceeded when the rate of change of temperature is of the order of 65°C per hour. Thus when reducing the throughput, considerably more care must be taken because the margin of safety

is so much loss. It should be emphasised, however, that the analysis is certainly conservative.

TABLE 9.1 Properties of the Refractory Walls

Slab thickness	6 0	in.
Young's Modulus	4 0 X 10^6	psi
Poisson's Ratio	0 27	
Thermal Conductivity	840	CHU/hr ft^{o}C
Density	124	lb/ft^3
Specific Heat	0 24	CHU/lb^{o}C
Emissivity	0 80	
Thermal expansion coefficient	4 5 X 10^{-6}	^{o}C $^{-1}$
Ultimate tensile strength	500	psi
Crushing (compressive) strength	4400	psi

TABLE 9.2 Input flowrates for stress analysis runs

Case No.	Flow (lb/hr)	Initial Value	Final Value
1	Burner fuel	1500	1800
	Combustion air	32000	32000
	Process gas	22000	26400
2	Burner fuel	2600	3100
	Combustion air	54000	54000
	Process gas	39000	47000
3	Burner fuel	2600	2100
	Combustion air	45000	45000
	Process gas	39000	31000
4	Burner fuel	3200	2500
	Combustion air	57000	57000
	Process gas	48000	38000

Case 1 : Increase from minimum make

Time (min)	T_r	q_r	σ^+_{max}	σ^-_{max}
Initial steady state	925.6	6945	0	0
0	925.6	7108	0	0
1	934.9	7162	84.2	12.8
2	942.1	7185	161.8	24.3
4	949.4	7209	252.8	38.9
6	953.8	7226	274.1	42.7
8	956.6	7240	298.5	48.2
10	958.2	7251	315.0	50.3
20	960.5	7265	306.2	52.4
30	963.2	7272	293.7	53.9
40	965.0	7276	280.9	55.1
50	966.5	7277	262.6	48.5
60	967.3	7280	234.2	39.4

Time (min)	$T_r(^oC)$	q_r(CHU/hr/ft^2	σ^+max(psi)	σ^-max(psi)
Initial steady state	1005.4	12420	0	0
0	1005.4	12597	0	0
1	1017.6	12670	156.4	22.3
2	1027.1	12705	304.9	43.7
4	1034.7	12736	397.4	70.2
6	1040.3	12761	475.6	84.3
8	1046.2	12777	559.1	91.1
10	1051.3	12789	532.0	97.6
20	1056.8	12808	493.3	100.9
30	1059.9	12817	451.5	102.0
40	1062.5	12823	380.8	103.3
50	1063.8	12828	297.8	92.5
60	1064.9	12831	188.7	74.6

Case 2 : Increase from normal make

Time (min)	T_r (°C)	q_r (CHU/hr/ft^2)	σ^+_{max} (psi)	σ^-_{max} (psi)
Initial steady state	1032.6	10150	0	0
0	1032.6	10008	0	0
1	1022.9	9943	16.2	125.8
2	1014.2	9916	30.4	245.2
4	1007.9	9894	56.5	299.5
6	1001.2	9877	63.8	342.6
8	996.5	9865	69.0	377.1
10	992.0	9855	73.7	368.2
20	985.8	9840	78.4	330.2
30	981.3	9832	80.0	284.4
40	979.6	9826	75.3	229.0
50	978.3	9819	62.7	158.6
60	977.4	9817	48.1	95.9

Case 3 : Reduction from normal make

Time (min)	T_r (°C)	q_r (CHU/hr/ft^2)	σ^+_{max} (psi)	σ^-_{max} (psi)
Initial steady state	1070.2	13008	0	0
0	1070.2	12774	0	0
1	1056.0	12681	34.2	189.4
2	1046.7	12646	61.3	319.9
4	1038.1	12612	85.6	404.6
6	1031.4	12583	104.1	472.0
8	1025.6	12562	118.5	521.4
10	1020.3	12547	128.5	549.7
20	1011.8	12530	135.9	496.3
30	1006.3	12525	138.2	421.8
40	1003.0	12521	125.8	330.2
50	1000.2	12518	109.5	204.7
60	998.5	12516	87.6	128.5

Case 4 : Reduction from maximum make.

CHAPTER X CONCLUSIONS

10.1 Conclusions resulting from this work

The principal aims of this work have been as follows:

(i) To produce a detailed mathematical model of a reforming furnace in terms of fundamental radiation transfer concepts.

(ii) To check this model for the steady state case using more traditional furnace modelling methods.

(iii) To confront the steady state models with data logged from a full-scale plant in actual operation.

(iv) To develop a dynamic model of the furnace and appropriate algorithms for solving it.

(v) To verify this model, so far as possible, with plant data logged during special tests.

(vi) To consider the problem of refractory spalling and its implications for rapid load changes to meet varying consumer demand.

It is evident from the description of the process given in Chapter I that the furnace is only one of many items of equipment on the plant. Moreover, due to the endothermic nature of reforming reactions, the economic viability of the process depends to a large extent on the efficient recovery of waste heat; the aim being to ensure that the plant is self sufficient in heat apart from that supplied to the furnace itself. Still, it is the successful operation of the reformer that determines how effectively this can be done, especially during load level changes or other disturbances. Also, the furnace represents the major commitment of capital expenditure and is subject to the greatest technical uncertainty (except possibly the hydrogenator which is rapidly declining in importance). It is therefore justifiable to concentrate effort in a thorough analysis of the reformer.

Another major decision taken was to develop both the steady state and dynamic models from theoretical principles, employing the minimum

number of empirical parameters possible. With the facilities available for acquiring almost unlimited in-plant data, the incentive for using some kind of curve fitting technique seems strong. This was resisted for two reasons. Firstly, it is essential that the model be used to examine regions outside the normal operating conditions so that if the model was fitted to data over a comparatively narrow range, the confidence in its predictions outside this range would be low. The second reason is that the expected quality of the data to be received is not particularly high. Despite the precautions discussed in Chapter 7, the difficulties encountered in establishing the true state of the system in quantitative terms are such that satisfactory model discrimination on a completely empirical basis is most unlikely.

The steady state model 1 uses Roesler's treatment of the radiation fluxes (31) on the flue gas side of the furnace, but extends the problem to consider the thermal effects occurring within the furnace tubes which Roesler assumes are fully defined a priori. Local thermodynamic equilibrium is assumed in order to compute the temperature and composition of the process gas. Engineering correlations are used for the coefficient of heat transfer between the tube walls and process gas. An iterative procedure is necessary to obtain a solution of the complete model because of the thermal interactions of the flue gas, tube wall and process gas temperatures and the radiation fluxes.

Equilibrium compositions of the process gas for various temperatures, pressures and steam/carbon ratios are given and the results found to agree with published data. A series of runs of the complete steady state model are made for specific plant studied in this work. The results acquired illustrate several interesting points. These are:
(i) At low makes a sharp peak in the tube skin temperature profile is indicated which could lead to a shortened life for the tube metal. Also, a substantial portion of the furnace height is wasted because the shape of the heat input profile determines that the process gas has to

be overheated in the upper section of the furnace, then allowed to cool to the desired exit temperature.

(ii) Natural gas reforming demands a higher fuel usage than naphtha under equivalent process operating conditions. This is, (a) because the endothermic heat of reaction is greater, and (b) as the temperature falls the amount of steam not converted to combustible products increases very rapidly.

(iii) It is seen that the use of a large amount of excess air reduces the heat radiated from the flames and hence reduces the thermal efficiency of the furnace. A more careful control over the combustion air input is called for.

(iv) A scheme for utilising a large excess of waste heat on the flue gas side that arises when reforming natural gas is discussed. This would involve recycling the heat around the reformer by increasing the air preheat temperature. From the model runs it would appear that a worthwhile saving in fuel costs could be made.

The formulation of model 2 is based on a physical analogy of the reformer with a co-current heat exchanger. The non-uniform flue gas temperature and consequent transfer of radiant heat in the direction of gas flow is accounted for by assuming that for a given vertical position in the furnace the source and sink of the vertical heat flux component are, respectively, half a beam length upward and downward from that point. The roof and floor of the furnace are assumed to act as mirrors to the radiation beams. Similar averaging procedures are made for the horizontal flux from the flue gas to the tubes. To simplify calculation of this flux, balances are written on a single tube plane and the adjacent plane is considered as a mirror image of the first.

In this way the boundary-value nature of the radiation flux equations is circumvented. However, although this model is conceptually far simpler than model 1, the actual computational effort

required to solve it is in fact higher. Also, the program is less robust and requires reasonably accurate starting values. Presumably, this is due to the numerical instability that arises during iterations on the various furnace profiles. Therefore, the usefulness of this model was limited essentially to checking the results from the first model. It was found that the technologically important variables, such as tube skin temperature, process gas temperature and the radiation fluxes did agree fairly well; others, in particular the flue gas temperature profile, did reveal certain discrepancies.

The validity of the model can only be properly established by comparing its predicted values with those measured directly on the plant. Some of the state variables in the model are radiation fluxes, and it would be preferable to measure these directly. Although in principle this technique is possible it is far easier to convert these to process temperatures in the model and measure the latter.

Although the plant studied was extensively instrumented, the appropriate temperatures were not always measured and so for acceptable model verification the probes had to be re-located. Also in the strong thermal radiation field, all the readings had to be corrected before comparison with predicted values, otherwise they are merely an indication of the state of the system and are of no quantitative value. The measure of agreement achieved when comparing the model predictions against in-plant data is satisfactory and gives reason to believe that the model may be used to simulate the performance of the furnace in operating regions outside the present limits.

The major original contribution of this work lies in the development of a dynamic model of the furnace from fundamental theoretical principles. In most industrial applications of dynamic modelling, all physical concepts of the system are jettisoned and the transient response patterns simulated by statistical correlation

techniques. Although this method has met with success in numerous cases, it is only suitable generally when the integrity of the data is high. Furthermore, a soundly based theoretical treatment can be used to study the transient responses of variables which are not easy to measure directly, such as radiation flux, refractory temperature and gas composition. Extrapolation to cases outside the linear region is also more justifiable with a physical model even though the model verification has been done within the linear region. Finally, most successful "black box" applications have been concerned with lumped parameter systems. Very often this assumption is quite unwarranted and this is certainly true in the case of a reformer where strong gradients in the radiation field compel any realistic model to become a distributed parameter one.

Model runs for the dynamic case indicate that each of the transient profiles of the furnace temperatures comprise a time delay followed by an approximately first-order response curve to a new steady state level. As expected, the refractory walls act as the most important buffer to changes in the radiant flux profiles and furnace tube temperatures. On the other hand, changes in the process gas and tube skin temperatures do not markedly affect the flue gas side variables. Hence, to a good approximation, in the dynamic case, the process gas side equations may be decoupled from the flue gas side analysis if the latter is the immediate source of interest.

In all the test runs made on the unsteady state model, the magnitude of the input disturbances assumed is far greater than would be experienced under normal operating conditions. Where these circumstances could arise is when changes in the process gas flow and burner fuel input are not properly synchronised. A sudden fall in the process gas throughput could lead to a rapid increase in tube wall temperatures if no compensating reduction of fuel input is made; similarly, prior changes in the heat sink can bring about severe

thermal shock conditions in the refractory walls. These abnormal conditions are most liable to occur during start-up and shutdown of the reformer.

Unlike the steady state case it was not possible to verify the dynamic model with plant data logged during routine unsteady state operation. Instead, a number of special tests were performed, whereby small changes in burner fuel input were made, keeping other variables as steady as possible. The transient responses of the tube skin, exit make gas and exit flue gas temperatures were logged. It was found that the values predicted by the dynamic model from first principles were at variance with the recorded data. However, if the initial steady state model values of the measured quantities were forced to agree with the data (by suitable parameter adjustment) and the transient response alone identified, the fit of the model was seen to be considerably better.

The other important aspect of this work is the analysis of the refractory spalling problem. This effect is due to thermal shock experienced by the refractory during unsteady state operation. The analysis at present is of a preliminary nature only but it is based on conservative assumptions regarding the composition of the slab and the consequent stresses induced therein. It is seen that the stress profiles are such that large stresses are induced on the hot face of the wall during transient conditions but the stress in the slab interior is substantially less. Given that the mechanical strength of the fireclay material is an order of magnitude greater in compression than in tension, this leads to the conclusion that mechanical failure due to rapid heating of the refractory is very unlikely. Conversely, quenching effects such as might occur during plant shutdown are of far more serious consequence because then the hot face is under tension.

10.2 Possible Areas of Further Work.

With the advent of North Sea Gas, reforming plant for town gas making is being phased out fairly rapidly. The remaining plant will be used primarily to supply peak load demand so that the unsteady state nature of its operation will become even more apparent. Moreover, it seems probable that the unsteady state operation of furnaces in other chemical plants will assume increasing importance, particularly those which are closely inter-related with other units in a manufacturing complex. The techniques used to develop this model can readily be applied to similar systems.

With increasing interest in furnace dynamics there will come increasing demand for optimisation and control studies in both steady and unsteady states. The need is for detailed, comprehensive models based on a mathematical interpretation of the physical processes taking place. If the model is to form part of the actual control or optimisation algorithm it must be used repeatedly in each iteration of the computation. A major requirement here, then is for rapid computer run times for the model.

Techniques of model reduction must, therefore, be brought to bear to reduce the dimensionality of the problem whilst retaining the essential detail.

NOTATION

A_i absorptivity of band i

A_f cross sectional area of furnace box

A_t total surface area of tubes

A_w total cross sectional area of tube metal wall

a_t half furnace tube surface area per unit volume

a_w cross sectional area of tube metal per unit volume of furnace

a_s catalyst pellet surface area per unit volume of furnace

B beam length for radiation heat transfer

C_p process gas specific heat

C_g flue gas specific heat

C_t tube metal specific heat

C_r refractory specific heat

C_s catalyst pellet specific heat

ΔC_p difference in molar specific heats of products and reactants of process gas

d_s effective catalyst pellet diameter

E Young's modulus of elasticity for refractory slab

E_i source emission of radiation in the i^{th} band

F_r area of refractory surface associated with unit area of tube plane

$\underline{f}$ state vector function

G_p superficial mass flowrate of process gas

G_g " " " " flue gas

G_{pt} " " flow of process gas referred to the empty tube cross-sectional area

H_p enthalpy of process gas stream

H_g enthalpy of flue gas stream

ΔH^o_{298} heat of reaction of process gas at 298^oK

ΔH_{Tp} heat of reaction of process gas at prevailing temperature

H_{fi} standard heat of formation of component i

H^*_g total heat input to furnace

h_{tc} overall tube skin-process gas heat transfer coefficient, assuming isothermal bed.

h_i coefficient of heat transfer through film of fluid adjacent to tube inside wall.

h_{rs} coefficient for radiant heat transfer between tube skin and catalyst pellets.

h_{rv} coefficient for radiant heat transfer between tube skin and process fluid.

h_{FC} overall catalyst pellet-process fluid heat transfer coefficient, if bed not assumed isothermal.

h_{FW} overall tube skin-process fluid heat transfer coefficient assuming absence of catalyst pellets.

h_{ri} heat transfer coefficient between flue gas and refractory wall

h_{ro} heat transfer coefficient between outside face of refractory and ambience.

I_a^+ downward component of radiation intensity that interacts with furnace gas.

I_a^- upward component of radiation intensity that interacts with furnace gas.

I_b^+ downward component of radiation intensity that does not interact with furnace gas.

I_b^- upward component of radiation intensity that does not interact with furnace gas.

ΔI^+ nett downward radiation flux

ΔI_t nett radiant flux to tubes.

K_e effective thermal conductivity for catalyst bed

K_{td} contribution to effective bed thermal conductivity by convective transport.

K_p thermal conductivity of process gas

K_r thermal conductivity of refractory slab.

K_s thermal conductivity of catalyst pellets

L total heated tube length

ℓ thickness of gas through which radiation beam passes

ℓ^1 penetration depth of flames

ℓ_r refractory slab thickness

M mean molecular weight of flue gases

M^1 heat flux to "mirror" in model 2

N_i moles of reactant i in fuel combustion

N_j moles of product j in combustion process

n number of carbon atoms in one molecule of hydrocarbon feedstock or fuel.

N_u Nussolt number for flow of process gas through catalyst bed.

Q Radiation heat flux within furnace enclosure

q(z) heat input to tubes at position z down the furnace

q_v nett downward heat flux component (model 2)

q_m heat flux from "mirror" to tube plane (model 2)

q_r heat flux emitted from refractory wall (model 2)

$q(\tau)$ instantaneous heat flux to refractory walls at time τ .

q^o heat flux to refractory wall during time step in which the refractory slab temperature and stress distributions are evaluated.

R gas constant

R_i tube inside radius

R_m logarithmic mean of inner and outer tube radii

Re Reynold's number for flow of process gas through catalyst bed.

R^1 total flux to refractory wall

T* theoretical flame temperature

T_a combustion air preheat temperature

T_{av} average catalyst bed temperature for estimating overall tube skin - process gas heat transfer coefficient.

T_p temperature of process gas

T_g temperature of flue gas

T_t temperature of tube skin

T_r temperature of refractory hot face
(Temperatures concerned with model 2)

T_i temperature that characterises heat input to furnace.

T_p^o value of T_p at z = 0

T_p^L value of T_p at z = L

T_e	"effective" flue gas temperature for purposes of computing heat flux to tubes.
T_A	ambient temperature
T_z	temperature at internal position within refractory slab
t	dummy variable of integration for expression for source radiation
U	process gas enthalpy per unit mass
$\underline{u}$	control vector
V_p	velocity of process gas
V_g	velocity of flue gas
V	temperature distribution through refractory slab wall
W_i	fraction of spectrum corresponding to the $i^{'th}$ absorption band
X_1	groups of terms defined by Eqs.(8.23) and (8.24)
X_2	
x_t	fraction of radiation passing through tube plane that is intercepted by tubes
x	distance from source of beam propagation
$\underline{x}$	state vector
x_{fi}	number of moles of component i in the reformer feed
y_{oi}	number of moles of component i in the product gas, at equilibrium
z	distance down furnace (downward direction positive).
α	thermal expansion coefficient of refractory slab
α_r	thermal diffusivity of refractory slab
α_λ	fraction of monochromatic beam absorbed by gas
β	volumetric absorption coefficient of flue gas
δ	bed voidage fraction
ε_p	emissivity of process gas
ε_g	emissivity of flue gas
ε_t	emissivity of tube wall
ε_r	emissivity of refractory slab
ε_s	emissivity of catalyst pellets
ε_g^r	flue gas emissivity on refractory wall side of tube plane (model 2)

ε_g^m flue gas emissivity on mirror side of tube plane (model 2)

ξ nett flux absorbed by refractory wall in unsteady state

η radiant energy source function

Θ time increment

θ time variable

κ flue gas mass absorption coefficient

μ_p viscosity of process gas

μ cos ϕ

ν Poisson's ratio for refractory wall

ρ_p density of process gas

ρ_g density of flue gas

ρ_t density of tube metal wall

ρ_r density of refractory wall

ρ_s density of catalyst pellets

σ Stefan-Boltzmann constant

σ_{xx} stress distribution in refractory wall

τ optical depth parameter

τ continuous time variable into which discrete increment Θ is subdivided

χ ratio of lb.-atoms of carbon in the process feed to its total mass

ψ fraction of the spectrum that can absorb and emit radiation

ϕ direction of propagation of beam to the normal

ω solid angle over which beam is propagated

APPENDIX A

To obtain a fundamental derivation of the monochromatic radiant intensity I_λ an energy balance is performed on a differential volume element of the medium. I_λ is a function only of the local temperature and optical parameters of the medium and does not depend on the convected flow of heat through the furnace which is described by the overall conservation equations. It is assumed that the medium is stationary, non-scattering and bounded by two infinite parallel plates. Only one-dimensional transfer perpendicular to the plates is considered.

As a monochromatic beam of intensity I_λ passes through an incremental slab of thickness dz, its intensity will diminish as a result of absorption by the medium but be augmented by thermal emission from the volume element. If the nett change in intensity is dI_λ, the following differential equation can be formulated:

$$\cos\phi \frac{dI_\lambda}{dz} = -\beta_\lambda I_\lambda + \frac{\beta_\lambda}{\pi} \eta_\lambda(z) \qquad \text{------- A.1)}$$

where ϕ is the angle between the incident beam and the normal to the parallel plates, and $\eta_\lambda(z)$ the thermal emission term. An "optical thickness" γ may be defined as

$$\gamma_\lambda = \int_0^z \beta_\lambda \, dz \; ; \quad \gamma_{o\lambda} = \int_0^L \beta_\lambda \, dz \qquad \text{------- (A.2.)}$$

Also $\mu = \cos\phi$ ------- (A.3.)

It is convenient to identify separately the flux intensities travelling in the forward and reverse directions. Thus in the forward hemisphere ($0 \leqslant \mu \leqslant 1$) beams are denoted by the superscript + and in the reverse hemisphere ($-1 \leqslant \mu \leqslant 0$) by the superscript - The equation of transfer then becomes :

$$\mu \frac{dI_\lambda^+}{d\gamma_\lambda} + I_\lambda^+ = \frac{\eta_\lambda(\gamma_\lambda)}{\pi}$$

$$\mu \frac{dI_\lambda^-}{d\gamma_\lambda} + I_\lambda^- = \frac{\eta_\lambda(\gamma_\lambda)}{\pi} \qquad \text{------- (A.4.)}$$

Boundary conditions for equations (A.4) are taken as,

$$I_\lambda^+(\tau_\lambda,\mu) = I_\lambda^+(o,\mu);\ \tau_\lambda = 0$$
$$I_\lambda^-(\tau_\lambda,\mu) = I_\lambda^-(\tau_{o\lambda},\mu);\ \tau_\lambda = \tau_{o\lambda} \qquad \text{------- (A.5.)}$$

Equations (A.4) are non-homogeneous linear equations which are most easily solved by introducing an integrating factor of the form

$$F(\tau_\lambda) = \exp\left(\int \frac{1}{\mu}\, d\tau_\lambda\right) = e^{\tau_\lambda/\mu} \qquad \text{------- (A.6)}$$

The general solution for I^+ then becomes

$$I_\lambda(\tau_\lambda,\mu) = e^{-\tau_\lambda/\mu}\left[\int_0^{\tau} e^{\tau_\lambda/\mu}\frac{\eta_\lambda(\tau_\lambda)}{\pi\mu}\, d\tau_\lambda + C_1\right] \qquad \text{------- (A.7)}$$

where the constant of integration is evaluated from the boundary conditions (A.5). Introducing the dummy variable t for the source function integration, the equation for I^+ is

$$I_\lambda^+(\tau_\lambda,\mu) = e^{-\tau_\lambda/\mu}\int_{t=o}^{\tau} \frac{e^{t/\mu}\eta_\lambda(t)\,dt}{\pi\mu} + I(0,\mu)$$

$$\text{i.e. } I_\lambda^+(\tau_\lambda,\mu) = I_\lambda^+(0,\mu)e^{-\frac{\tau_\lambda}{\mu}} + \frac{1}{\pi}\int \eta_\lambda(t)\, e^{-\frac{(\tau_\lambda - t)}{\mu}}\frac{dt}{\mu} \qquad \text{-----(A.8)}$$

Similarly, the general equation for I_λ^- is:

$$I_\lambda^-(\tau_\lambda,\mu) = e^{-\frac{\tau_\lambda}{\mu}}\left[\int_{\tau_{o\lambda}}^{\tau_\lambda} e^{\frac{\tau_\lambda}{\mu}}\frac{\eta_\lambda(\tau_\lambda)}{\pi\mu} + C_2\right] \qquad \text{------- (A.9)}$$

Substituting the second boundary condition of (A.5) into (A.9) gives the integration constant C_2 as $I_\lambda^-(\tau_{o\lambda},\mu)e^{\tau_{o\lambda}/\mu}$ and the full equation for I_λ^- becomes:

$$I_\lambda^-(\tau_\lambda,\mu) = I_\lambda^-(\tau_{o\lambda},\mu)e^{\frac{(\tau_{o\lambda}-\tau_\lambda)}{\mu}} - \frac{1}{\pi}\int_{\tau_\lambda}^{\tau_{o\lambda}} \eta_\lambda(t)\, e^{-\frac{(\tau_\lambda - t)}{\mu}}\frac{dt}{\mu} \qquad \text{------- (A.10)}$$

The first term on the right hand sides of Eqs. (A.8) and (A.10) represents the absorption of radiation originating at the two plates. The integral expressions represent the emission of flux over the path lengths of the beams.

APPENDIX B

Calculation of Chemical Equilibrium

Calculation of the equilibrium composition of a complex gas mixture entails, essentially the minimisation of the Gibbs Free Energy function at the particular temperature and pressure. WHITE *et al* (74) and NAPTHALI (75) treat the problem as an example of constrained optimisation using a steepest descent technique whilst others, such as ZELEZNIK (76) have demonstrated that the problem may be formulated as a classic linear programming exercise.

Consider a mixture of n chemical species containing y_i mols of the i^{th} species. The free energy (Gibbs) function may then be expressed as:

$$F(\underline{Y}) = \sum_{i=1}^{n} f_i \qquad \text{-------- (B.1)}$$

where $\underline{Y}$ = the set of compositions y_i and

$$f_i = y_i \left[\frac{F^o}{RT} + \ln P + \ln \left(\frac{y_i}{\sum y_i} \right) \right] \qquad \text{-------- (B.2)}$$

The standard free energy function F^o is usually obtained from tabulated values of the entropy (77). Determination of the equilibrium compositions is equivalent to finding the positive set of values for y_i which minimises Eq. (B.1) and satisfies the atom balance constraints

$$\sum_{i=1}^{n} a_{ij} y_i = b_j \qquad j = 1, 2, \ldots\ldots m \qquad \text{-------- (B.3)}$$

where there are m different types of atoms present in the mixture and a_{ij} is the matrix of coefficients indicating the number of atoms of element j in a molecule of species i . The total lb- atoms of element j originally present is denoted by b_j.

White *et al* perform the minimisation by a steepest descent technique using a quadratic approximation to locate the minimum along the direction of steepest descent and Lagrange multipliers to deal with the constraints. The problem is resolved into the solution of m + 1 linear algebric

equations in unknown Lagrange multipliers, the total number of moles being the other unknown. As such, the computation is almost trivial except that degenerate cases may arise where the rank of the matrix is less than m. Modifications to obviate this problem have been proposed by STOREY (78) and NAPHTALI (79).

It is necessary to specify in advance which chemical species are present in the mixture at equilibrium. In the present case these are chosen as CO, CO_2, H_2, H_2O and CH_4. In addition ethane was included, but its concentration was driven down to trace amounts at equilibrium. However, its inclusion in the program ensured that the matrix of atom balance equations (B.3) were linearly independent and the rank of matrix a_{ij} was equal to m, so that the degenerate case did not arise.

APPENDIX C: FORMULATION OF ONE - AND TWO - DIMENSIONAL MODELS FOR A TUBULAR REACTOR.

An energy balance on an elemental volume of a tubular reactor, neglecting radial gradients of velocity, temperature and composition leads to the differential equation

$$G_p C_p \frac{d T_p}{d z} = - G_p \psi \frac{\Delta H_{T_p}(z)}{L} + 2 a_t q(z) \quad \text{-------(C.1.)}$$

Constant pressure, physical properties and superficial mass velocity are assumed.

If the temperature is now permitted to vary in the radial as well as the axial direction, a term for radial heat transport is to be included (80), Viz,

$$G_p C_p \frac{\partial T_p}{\partial z} = K_e \left(\frac{\partial^2 T_p}{\partial r^2} + \frac{1}{r} \cdot \frac{\partial T_p}{\partial r} \right) - \frac{G_p \psi \Delta H_{T_p}(r,z)}{L} \quad \text{------ (C.2.)}$$

with boundary conditions:

$$\left. \frac{\partial T_p}{\partial r} \right|_{r=0} = 0 \quad \text{------- (C.3.)}$$

$$\left. \frac{\partial T_p}{\partial r} \right|_{r=R} = - \frac{q(z)}{K_e} \quad \text{------- (C.4.)}$$

Clearly, the energy equation is a partial differential one with the radial variable r as the additional independent variable.

The boundary condition (C.3) expresses the radial symmetry of the temperature profile and (C.4.) represents the heat input to the system and replaces the last term in Eq. (C.1.).

It would be very time consuming to have to compute ΔH_{T_p} directly at every point by the method described in Sec.3.2, so it is convenient to obtain ΔH_{T_p} as an algebric function of temperature for given process feed characteristics. A least squares polynomial function of sufficiently high degree to give low variance was employed (81). The equations then contain T_p as the only dependent variable provided that the heat input profile q (z) is specified.

Eq. (C.1.) may be integrated by almost any initial-value routine (the inlet temperature is specified). On the other hand, the boundary-value, two-dimensional model requires far more computational effort. LAPIDUS (82) describes how this may be done and highlights the stability problems that arise with parabolic partial differential equations, particularly with gradient-type (Neumann) boundary conditions.

APPENDIX D

RUN 1 : STANDARD FLOWSHEET CONDITIONS

NAPHTHA FEEDSTOCK AND FUEL

BURNER FUEL FLOWRATE	3072	LB PER HOUR
AIR TO FUEL RATIO	16.90	
PROCESS GAS FLOWRATE	44000	LB PER HOUR
STEAM TO CARBON RATIO	3.00	
THEORETICAL FLAME TEMPERATURE	2180.0	DEG K

DISTANCE DOWN FURNACE	FLUE GAS TEMP	REFRACTORY TEMP	TUBE SKIN TEMP	PROCESS GAS TEMP
0.0	1.0417E +3	1.0062E +3	6.3916E +2	3.9900E +2
1.1	1.0610E +3	1.0103E +3	6.7589E +2	4.4614E +2
2.1	1.1262E +3	1.0160E +3	7.1129E +2	4.8988E +2
3.2	1.1949E +3	1.0221E +3	7.4228E +2	5.3032E +2
4.2	1.2460E +3	1.0269E +3	7.6888E +2	5.6739E +2
5.3	1.2705E +3	1.0288E +3	7.9244E +2	6.0097E +2
6.4	1.2655E +3	1.0273E +3	8.1050E +2	6.3089E +2
7.4	1.2296E +3	1.0223E +3	8.2344E +2	6.5684E +2
8.5	1.1614E +3	1.0147E +3	8.3088E +2	6.7887E +2
9.5	1.1111E +3	1.0047E +3	8.3698E +2	6.9728E +2
10.6	1.0803E +3	9.9395E +2	8.3820E +2	7.1200E +2
11.7	1.0578E +3	9.8333E +2	8.3979E +2	7.2364E +2
12.7	1.0393E +3	9.7325E +2	8.3979E +2	7.3258E +2
13.8	1.0232E +3	9.6380E +2	8.3808E +2	7.3929E +2
14.8	1.0086E +3	9.5502E +2	8.3539E +2	7.4420E +2
15.9	9.9527E +2	9.4689E +2	8.3368E +2	7.4757E +2
17.0	9.8306E +2	9.3941E +2	8.3088E +2	7.4970E +2
18.0	9.7184E +2	9.3257E +2	8.2807E +2	7.5084E +2
19.1	9.6154E +2	9.2638E +2	8.2465E +2	7.5118E +2
20.1	9.5212E +2	9.2084E +2	8.2184E +2	7.5091E +2
21.2	9.4356E +2	9.1597E +2	8.1904E +2	7.5014E +2
22.3	9.3586E +2	9.1181E +2	8.1623E +2	7.4907E +2
23.3	9.2902E +2	9.0838E +2	8.1440E +2	7.4774E +2
24.4	9.2308E +2	9.0576E +2	8.1172E +2	7.4628E +2
25.4	9.1810E +2	9.0401E +2	8.1001E +2	7.4479E +2
26.5	9.1417E +2	9.0320E +2	8.0891E +2	7.4340E +2

HEAT FLUX PROFILES FOR RUN 1

DISTANCE DOWN FURNACE	NET VERTICAL FLUX	FLUX TO TUBES
0.0	8.9407E -8	1.8047E +4
1.1	-2.2660E +3	1.7283E +4
2.1	-3.6531E +3	1.6561E +4
3.2	-3.6144E +3	1.5915E +4
4.2	-2.2212E +3	1.5240E +4
5.3	1.0235E +2	1.4396E +4
6.4	2.7566E +3	1.3458E +4
7.4	5.0856E +3	1.2449E +4
8.5	6.4128E +3	1.1496E +4
9.5	6.6011E +3	1.0430E +4
10.6	6.3301E +3	9.5621E +3
11.7	5.9180E +3	8.7072E +3
12.7	5.4775E +3	7.9885E +3
13.8	5.0406E +3	7.4168E +3
14.8	4.6170E +3	6.9528E +3
15.9	4.2114E +3	6.4950E +3
17.0	3.8159E +3	6.1436E +3
18.0	3.4273E +3	5.8409E +3
19.1	3.0409E +3	5.6148E +3
20.1	2.6524E +3	5.4039E +3
21.2	2.2577E +3	5.2380E +3
22.3	1.8493E +3	5.1172E +3
23.3	1.4293E +3	4.9967E +3
24.4	9.8393E +2	4.9655E +3
25.4	5.1154E +2	4.9402E +3
26.5	-2.9802E -8	4.9430E +3

RUN 2: MAXIMUM THROUGHPUT

NAPHTHA FEEDSTOCK, NATURAL GAS FUEL

BURNER FUEL FLOWRATE	3380	LB PER HOUR
AIR TO FUEL RATIO	19.30	
PROCESS GAS FLOWRATE	48400	LB PER HOUR
STEAM TO CARBON RATIO	3.00	
THEORETICAL FLAME TEMPERATURE	2260.0	DEG K

DISTANCE DOWN FURNACE	FLUE GAS TEMP	REFRACTORY TEMP	TUBE SKIN TEMP	PROCESS GAS TEMP
0.0	1.0846" +3	1.0475" +3	6.7028" +2	3.9900" +2
1.1	1.1048" +3	1.0517" +3	7.0848" +2	4.4754" +2
2.1	1.1726" +3	1.0577" +3	7.4240" +2	4.9256" +2
3.2	1.2440" +3	1.0640" +3	7.7450" +2	5.3430" +2
4.2	1.2969" +3	1.0689" +3	8.0318" +2	5.7258" +2
5.3	1.3222" +3	1.0708" +3	8.2465" +2	6.0729" +2
6.4	1.3168" +3	1.0690" +3	8.4271" +2	6.3824" +2
7.4	1.2793" +3	1.0636" +3	8.5455" +2	6.6520" +2
8.5	1.2083" +3	1.0555" +3	8.6346" +2	6.8822" +2
9.5	1.1558" +3	1.0449" +3	8.6798" +2	7.0727" +2
10.6	1.1237" +3	1.0334" +3	8.6907" +2	7.2265" +2
11.7	1.1002" +3	1.0221" +3	8.6907" +2	7.3491" +2
12.7	1.0807" +3	1.0114" +3	8.6748" +2	7.4438" +2
13.8	1.0637" +3	1.0013" +3	8.6639" +2	7.5157" +2
14.8	1.0483" +3	9.9190" +2	8.6456" +2	7.5685" +2
15.9	1.0342" +3	9.8320" +2	8.6175" +2	7.6044" +2
17.0	1.0212" +3	9.7518" +2	8.5895" +2	7.6282" +2
18.0	1.0093" +3	9.6786" +2	8.5455" +2	7.6404" +2
19.1	9.9835" +2	9.6121" +2	8.5163" +2	7.6455" +2
20.1	9.8832" +2	9.5526" +2	8.4882" +2	7.6435" +2
21.2	9.7920" +2	9.5003" +2	8.4540" +2	7.6361" +2
22.3	9.7098" +2	9.4555" +2	8.4260" +2	7.6250" +2
23.3	9.6368" +2	9.4186" +2	8.3979" +2	7.6113" +2
24.4	9.5733" +2	9.3905" +2	8.3649" +2	7.5967" +2
25.4	9.5201" +2	9.3715" +2	8.3539" +2	7.5816" +2
26.5	9.4781" +2	9.3630" +2	8.3368" +2	7.5666" +2

HEAT FLUX PROFILES FOR RUN 2

DISTANCE DOWN FURNACE	NET VERTICAL FLUX	FLUX TO TUBES
0.0	5.9605* -8	2.0442* +4
1.1	-2.5727* +3	1.9560* +4
2.1	-4.1337* +3	1.8837* +4
3.2	-4.0595* +3	1.8102* +4
4.2	-2.4305* +3	1.7278* +4
5.3	2.5814* +2	1.6447* +4
6.4	3.3208* +3	1.5402* +4
7.4	5.9964* +3	1.4321* +4
8.5	7.5152* +3	1.3153* +4
9.5	7.7315* +3	1.2017* +4
10.6	7.4156* +3	1.1015* +4
11.7	6.9331* +3	1.0110* +4
12.7	6.4152* +3	9.3576* +3
13.8	5.9047* +3	8.6484* +3
14.8	5.4092* +3	8.0476* +3
15.9	4.9364* +3	7.5639* +3
17.0	4.4719* +3	7.1402* +3
18.0	4.0187* +3	6.8575* +3
19.1	3.5630* +3	6.5510* +3
20.1	3.1074* +3	6.2915* +3
21.2	2.6455* +3	6.1163* +3
22.3	2.1708* +3	5.9620* +3
23.3	1.6768* +3	5.8619* +3
24.4	1.1523* +3	5.8437* +3
25.4	5.9708* +2	5.7757* +3
26.5	0.0000	5.8051* +3

RUN 3 : MINIMUM THROUGHPUT

NAPHTHA FEEDSTOCK, NATURAL GAS FUEL

BURNER FUEL FLOWRATE	1225	LB PER HOUR
AIR TO FUEL RATIO	19.30	
PROCESS GAS FLOWRATE	17600	LB PER HOUR
STEAM TO CARBON RATIO	3.00	
THEORETICAL FLAME TEMPERATURE	2260.0	DEG K

DISTANCE DOWN FURNACE	FLUE GAS TEMP	REFRACTORY TEMP	TUBE SKIN TEMP	PROCESS GAS TEMP
0.0	9.3357" +2	9.0931" +2	5.7278" +2	3.9900" +2
1.1	9.5330" +2	9.1229" +2	6.3757" +2	4.8277" +2
2.1	1.0054" +3	9.1662" +2	6.9213" +2	5.5444" +2
3.2	1.0487" +3	9.2128" +2	7.3508" +2	6.1449" +2
4.2	1.0745" +3	9.2462" +2	7.6888" +2	6.6383" +2
5.3	1.0810" +3	9.2554" +2	7.9536" +2	7.0357" +2
6.4	1.0679" +3	9.2366" +2	8.1440" +2	7.3438" +2
7.4	1.0344" +3	9.1925" +2	8.2624" +2	7.5743" +2
8.5	9.7981" +2	9.1332" +2	8.3356" +2	7.7405" +2
9.5	9.5153" +2	9.0596" +2	8.3539" +2	7.8511" +2
10.6	9.3659" +2	8.9861" +2	8.3649" +2	7.9215" +2
11.7	9.2467" +2	8.9178" +2	8.3539" +2	7.9581" +2
12.7	9.1412" +2	8.8546" +2	8.3368" +2	7.9721" +2
13.8	9.0460" +2	8.7963" +2	8.3088" +2	7.9707" +2
14.8	8.9594" +2	8.7424" +2	8.2795" +2	7.9579" +2
15.9	8.8807" +2	8.6928" +2	8.2515" +2	7.9365" +2
17.0	8.8091" +2	8.6474" +2	8.2075" +2	7.9086" +2
18.0	8.7442" +2	8.6058" +2	8.1782" +2	7.8803" +2
19.1	8.6855" +2	8.5682" +2	8.1440" +2	7.8490" +2
20.1	8.6329" +2	8.5350" +2	8.1001" +2	7.8190" +2
21.2	8.5863" +2	8.5058" +2	8.0720" +2	7.7909" +2
22.3	8.5457" +2	8.4812" +2	8.0440" +2	7.7643" +2
23.3	8.5113" +2	8.4614" +2	8.0159" +2	7.7399" +2
24.4	8.4833" +2	8.4467" +2	7.9988" +2	7.7168" +2
25.4	8.4623" +2	8.4374" +2	7.9866" +2	7.6980" +2
26.5	8.4488" +2	8.4342" +2	7.9695" +2	7.6813" +2

HEAT FLUX PROFILES FOR RUN 3

DISTANCE DOWN FURNACE	NET VERTICAL FLUX	FLUX TO TUBES
0.0	7.4506E -8	1.3111E +4
1.1	-1.5663E +3	1.1692E +4
2.1	-2.3140E +3	1.0319E +4
3.2	-2.0872E +3	9.1049E +3
4.2	-1.1234E +3	7.9885E +3
5.3	2.4904E +2	6.9153E +3
6.4	1.6877E +3	5.9308E +3
7.4	2.8347E +3	5.0946E +3
8.5	3.3266E +3	4.3752E +3
9.5	3.2147E +3	3.8421E +3
10.6	2.9970E +3	3.3538E +3
11.7	2.7902E +3	3.0119E +3
12.7	2.5991E +3	2.7362E +3
13.8	2.4168E +3	2.5470E +3
14.8	2.2415E +3	2.3919E +3
15.9	2.0712E +3	2.2567E +3
17.0	1.9019E +3	2.2224E +3
18.0	1.7265E +3	2.1394E +3
19.1	1.5490E +3	2.1023E +3
20.1	1.3602E +3	2.1328E +3
21.2	1.1634E +3	2.1110E +3
22.3	9.5609E +2	2.1127E +3
23.3	7.3673E +2	2.1388E +3
24.4	5.0806E +2	2.1407E +3
25.4	2.6187E +2	2.1481E +3
26.5	-2.9802E -8	2.2082E +3

Run 4 : Steam / Carbon Ratio 2:1

Naphtha Feedstock, Nat. Gas Fuel

BURNER FUEL FLOWRATE	1840	LB PER HOUR
AIR TO FUEL RATIO	16.90	
PROCESS GAS FLOWRATE	26400	LB PER HOUR
STEAM TO CARBON RATIO	2.00	
THEORETICAL FLAME TEMPERATURE	2180.0	DEG K

DISTANCE DOWN FURNACE	FLUE GAS TEMP	REFRACTORY TEMP	TUBE SKIN TEMP	PROCESS GAS TEMP
0.0	9.6374" +2	9.3416" +2	5.8901" +2	3.9900" +2
1.1	9.8340" +2	9.3765" +2	6.3916" +2	4.6247" +2
2.1	1.0428" +3	9.4255" +2	6.8310" +2	5.1931" +2
3.2	1.0982" +3	9.4773" +2	7.2032" +2	5.6951" +2
4.2	1.1346" +3	9.5151" +2	7.5241" +2	6.1324" +2
5.3	1.1476" +3	9.5268" +2	7.7621" +2	6.5040" +2
6.4	1.1363" +3	9.5064" +2	7.9524" +2	6.8120" +2
7.4	1.1001" +3	9.4562" +2	8.0720" +2	7.0594" +2
8.5	1.0377" +3	9.3860" +2	8.1611" +2	7.2519" +2
9.5	9.9848" +2	9.2973" +2	8.2063" +2	7.3936" +2
10.6	9.7665" +2	9.2056" +2	8.2075" +2	7.4937" +2
11.7	9.6039" +2	9.1181" +2	8.2075" +2	7.5603" +2
12.7	9.4652" +2	9.0364" +2	8.2063" +2	7.6012" +2
13.8	9.3410" +2	8.9607" +2	8.1782" +2	7.6209" +2
14.8	9.2281" +2	8.8907" +2	8.1452" +2	7.6263" +2
15.9	9.1247" +2	8.8259" +2	8.1160" +2	7.6208" +2
17.0	9.0302" +2	8.7665" +2	8.0720" +2	7.6080" +2
18.0	8.9438" +2	8.7121" +2	8.0428" +2	7.5902" +2
19.1	8.8652" +2	8.6632" +2	7.9988" +2	7.5683" +2
20.1	8.7940" +2	8.6194" +2	7.9695" +2	7.5448" +2
21.2	8.7301" +2	8.5811" +2	7.9415" +2	7.5194" +2
22.3	8.6736" +2	8.5487" +2	7.8975" +2	7.4931" +2
23.3	8.6246" +2	8.5221" +2	7.8792" +2	7.4687" +2
24.4	8.5834" +2	8.5021" +2	7.8524" +2	7.4451" +2
25.4	8.5507" +2	8.4892" +2	7.8341" +2	7.4248" +2
26.5	8.5271" +2	8.4840" +2	7.8231" +2	7.4070" +2

HEAT FLUX PROFILES FOR RUN 4

DISTANCE DOWN FURNACE	NET VERTICAL FLUX	FLUX TO TUBES
0.0	7.4506E -8	1.4284E +4
1.1	-1.7528E +3	1.3234E +4
2.1	-2.6898E +3	1.2249E +4
3.2	-2.4910E +3	1.1336E +4
4.2	-1.3439E +3	1.0387E +4
5.3	3.7668E +2	9.4993E +3
6.4	2.2333E +3	8.5419E +3
7.4	3.7665E +3	7.6701E +3
8.5	4.5208E +3	6.7987E +3
9.5	4.4837E +3	6.0180E +3
10.6	4.2133E +3	5.4389E +3
11.7	3.9120E +3	4.9041E +3
12.7	3.6215E +3	4.4206E +3
13.8	3.3484E +3	4.1096E +3
14.8	3.0864E +3	3.8612E +3
15.9	2.8338E +3	3.6310E +3
17.0	2.5818E +3	3.5030E +3
18.0	2.3308E +3	3.3383E +3
19.1	2.0763E +3	3.2720E +3
20.1	1.8165E +3	3.1687E +3
21.2	1.5517E +3	3.0905E +3
22.3	1.2762E +3	3.1138E +3
23.3	9.8692E +2	3.0552E +3
24.4	6.8140E +2	3.0683E +3
25.4	3.5240E +2	3.0805E +3
26.5	-1.4901E -8	3.1009E +3

RUN 5 ; STEAM/CARBON RATIO 2:1

NATURAL GAS FEEDSTOCK AND FUEL

BURNER FUEL FLOWRATE	1840	LB PER HOUR
AIR TO FUEL RATIO	16.90	
PROCESS GAS FLOWRATE	26400	LB PER HOUR
STEAM TO CARBON RATIO	2.00	
THEORETICAL FLAME TEMPERATURE	2180.0	DEG K

DISTANCE DOWN FURNACE	FLUE GAS TEMP	REFRACTORY TEMP	TUBE SKIN TEMP	PROCESS GAS TEMP
0.0	9.4701E +2	9.1505E +2	5.7717E +2	3.9900E +2
1.1	9.6721E +2	9.1881E +2	6.2110E +2	4.5434E +2
2.1	1.0287E +3	9.2388E +2	6.5954E +2	5.0385E +2
3.2	1.0863E +3	9.2911E +2	6.9493E +2	5.4773E +2
4.2	1.1242E +3	9.3277E +2	7.2312E +2	5.8583E +2
5.3	1.1379E +3	9.3358E +2	7.4509E +2	6.1817E +2
6.4	1.1263E +3	9.3094E +2	7.6144E +2	6.4490E +2
7.4	1.0888E +3	9.2503E +2	7.7218E +2	6.6628E +2
8.5	1.0241E +3	9.1695E +2	7.7780E +2	6.8257E +2
9.5	9.8244E +2	9.0680E +2	7.8060E +2	6.9435E +2
10.6	9.5867E +2	8.9626E +2	7.7901E +2	7.0219E +2
11.7	9.4068E +2	8.8612E +2	7.7780E +2	7.0702E +2
12.7	9.2517E +2	8.7660E +2	7.7450E +2	7.0947E +2
13.8	9.1117E +2	8.6769E +2	7.7059E +2	7.1009E +2
14.8	8.9832E +2	8.5940E +2	7.6608E +2	7.0940E +2
15.9	8.8649E +2	8.5170E +2	7.6156E +2	7.0774E +2
17.0	8.7557E +2	8.4459E +2	7.5705E +2	7.0532E +2
18.0	8.6552E +2	8.3807E +2	7.5253E +2	7.0240E +2
19.1	8.5630E +2	8.3213E +2	7.4851E +2	6.9926E +2
20.1	8.4789E +2	8.2682E +2	7.4350E +2	6.9591E +2
21.2	8.4028E +2	8.2215E +2	7.3960E +2	6.9245E +2
22.3	8.3349E +2	8.1817E +2	7.3508E +2	6.8905E +2
23.3	8.2755E +2	8.1491E +2	7.3166E +2	6.8585E +2
24.4	8.2252E +2	8.1245E +2	7.2885E +2	6.8283E +2
25.4	8.1849E +2	8.1086E +2	7.2605E +2	6.8004E +2
26.5	8.1555E +2	8.1023E +2	7.2434E +2	6.7757E +2

HEAT FLUX PROFILES FOR RUN 5

DISTANCE DOWN FURNACE	NET VERTICAL FLUX	FLUX TO TUBES
0.0	5.9605E -8	1.3360E +4
1.1	-1.6505E +3	1.2531E +4
2.1	-2.5132E +3	1.1779E +4
3.2	-2.2532E +3	1.1003E +4
4.2	-1.0466E +3	1.0264E +4
5.3	7.3156E +2	9.5000E +3
6.4	2.6350E +3	8.6891E +3
7.4	4.2014E +3	7.8782E +3
8.5	4.9742E +3	7.1429E +3
9.5	4.9366E +3	6.4102E +3
10.6	4.6567E +3	5.8568E +3
11.7	4.3362E +3	5.3265E +3
12.7	4.0204E +3	4.9322E +3
13.8	3.7189E +3	4.6082E +3
14.8	3.4276E +3	4.3510E +3
15.9	3.1434E +3	4.1318E +3
17.0	2.8650E +3	3.9480E +3
18.0	2.5881E +3	3.7979E +3
19.1	2.3059E +3	3.6610E +3
20.1	2.0183E +3	3.5953E +3
21.2	1.7253E +3	3.5189E +3
22.3	1.4192E +3	3.4990E +3
23.3	1.0958E +3	3.4725E +3
24.4	7.5524E +2	3.4606E +3
25.4	3.9136E +2	3.4892E +3
26.5	-1.4901E -8	3.5219E +3

RUN 6 : STEAM/CARBON RATIO 4:1

NATURAL GAS FEEDSTOCK AND FUEL

BURNER FUEL FLOWRATE	1840	LB PER HOUR
AIR TO FUEL RATIO	16.90	
PROCESS GAS FLOWRATE	26400	LB PER HOUR
STEAM TO CARBON RATIO	4.00	
THEORETICAL FLAME TEMPERATURE	2180.0	DEG K

DISTANCE DOWN FURNACE	FLUE GAS TEMP	REFRACTORY TEMP	TUBE SKIN TEMP	PROCESS GAS TEMP
0.0	9.5138E +2	9.2017E +2	5.8010E +2	3.9900E +2
1.1	9.7143E +2	9.2387E +2	6.2452E +2	4.5420E +2
2.1	1.0324E +3	9.2889E +2	6.6394E +2	5.0366E +2
3.2	1.0894E +3	9.3414E +2	6.9676E +2	5.4785E +2
4.2	1.1269E +3	9.3787E +2	7.2605E +2	5.8689E +2
5.3	1.1404E +3	9.3884E +2	7.4960E +2	6.2083E +2
6.4	1.1289E +3	9.3648E +2	7.6608E +2	6.4953E +2
7.4	1.0918E +3	9.3095E +2	7.7951E +2	6.7317E +2
8.5	1.0278E +3	9.2334E +2	7.8633E +2	6.9182E +2
9.5	9.8697E +2	9.1375E +2	7.9134E +2	7.0608E +2
10.6	9.6391E +2	9.0383E +2	7.9244E +2	7.1628E +2
11.7	9.4662E +2	8.9435E +2	7.9244E +2	7.2331E +2
12.7	9.3181E +2	8.8548E +2	7.9134E +2	7.2776E +2
13.8	9.1851E +2	8.7725E +2	7.8804E +2	7.3009E +2
14.8	9.0639E +2	8.6961E +2	7.8524E +2	7.3098E +2
15.9	8.9527E +2	8.6255E +2	7.8231E +2	7.3060E +2
17.0	8.8506E +2	8.5606E +2	7.7792E +2	7.2920E +2
18.0	8.7571E +2	8.5012E +2	7.7340E +2	7.2725E +2
19.1	8.6716E +2	8.4472E +2	7.7047E +2	7.2494E +2
20.1	8.5939E +2	8.3991E +2	7.6608E +2	7.2215E +2
21.2	8.5239E +2	8.3568E +2	7.6315E +2	7.1926E +2
22.3	8.4616E +2	8.3208E +2	7.5876E +2	7.1621E +2
23.3	8.4074E +2	8.2913E +2	7.5693E +2	7.1333E +2
24.4	8.3615E +2	8.2691E +2	7.5412E +2	7.1043E +2
25.4	8.3248E +2	8.2548E +2	7.5082E +2	7.0768E +2
26.5	8.2981E +2	8.2490E +2	7.4960E +2	7.0531E +2

HEAT FLUX PROFILES FOR RUN 6

DISTANCE DOWN FURNACE	NET VERTICAL FLUX	FLUX TO TUBES
0.0	2.9802E -8	1.3609E +4
1.1	-1.6790E +3	1.2754E +4
2.1	-2.5680E +3	1.1963E +4
3.2	-2.3389E +3	1.1262E +4
4.2	-1.1662E +3	1.0486E +4
5.3	5.7264E +2	9.6639E +3
6.4	2.4395E +3	8.8556E +3
7.4	3.9777E +3	7.9436E +3
8.5	4.7302E +3	7.1732E +3
9.5	4.6790E +3	6.3653E +3
10.6	4.3950E +3	5.7216E +3
11.7	4.0757E +3	5.1665E +3
12.7	3.7666E +3	4.7076E +3
13.8	3.4764E +3	4.3913E +3
14.8	3.1980E +3	4.0943E +3
15.9	2.9320E +3	3.8402E +3
17.0	2.6733E +3	3.6842E +3
18.0	2.4125E +3	3.5651E +3
19.1	2.1490E +3	3.4104E +3
20.1	1.8837E +3	3.3482E +3
21.2	1.6089E +3	3.2560E +3
22.3	1.3244E +3	3.2555E +3
23.3	1.0231E +3	3.1840E +3
24.4	7.0593E +2	3.1873E +3
25.4	3.6737E +2	3.2477E +3
26.5	-1.4901E -8	3.2670E +3

RUN 7 : AIR/FUEL RATIO 16.5 : 1

NAPHTHA FEEDSTOCK AND FUEL

BURNER FUEL FLOWRATE	2460	LB PER HOUR
AIR TO FUEL RATIO	16.50	
PROCESS GAS FLOWRATE	35200	LB PER HOUR
STEAM TO CARBON RATIO	3.00	
THEORETICAL FLAME TEMPERATURE	2225.0	DEG K

DISTANCE DOWN FURNACE	FLUE GAS TEMP	REFRACTORY TEMP	TUBE SKIN TEMP	PROCESS GAS TEMP
0.0	1.0146E +3	9.8128E +2	6.2110E +2	3.9900E +2
1.1	1.0348E +3	9.8506E +2	6.6394E +2	4.5332E +2
2.1	1.0996E +3	9.9038E +2	7.0225E +2	5.0298E +2
3.2	1.1637E +3	9.9601E +2	7.3667E +2	5.4811E +2
4.2	1.2083E +3	1.0002E +3	7.6596E +2	5.8875E +2
5.3	1.2267E +3	1.0016E +3	7.8975E +2	6.2488E +2
6.4	1.2173E +3	9.9963E +2	8.0879E +2	6.5626E +2
7.4	1.1792E +3	9.9434E +2	8.2075E +2	6.8276E +2
8.5	1.1111E +3	9.8675E +2	8.3076E +2	7.0473E +2
9.5	1.0646E +3	9.7702E +2	8.3527E +2	7.2225E +2
10.6	1.0377E +3	9.6674E +2	8.3808E +2	7.3587E +2
11.7	1.0180E +3	9.5681E +2	8.3820E +2	7.4610E +2
12.7	1.0016E +3	9.4749E +2	8.3808E +2	7.5358E +2
13.8	9.8716E +2	9.3882E +2	8.3698E +2	7.5880E +2
14.8	9.7405E +2	9.3081E +2	8.3368E +2	7.6214E +2
15.9	9.6207E +2	9.2342E +2	8.3088E +2	7.6406E +2
17.0	9.5111E +2	9.1663E +2	8.2807E +2	7.6486E +2
18.0	9.4107E +2	9.1044E +2	8.2465E +2	7.6487E +2
19.1	9.3191E +2	9.0484E +2	8.2184E +2	7.6420E +2
20.1	9.2358E +2	8.9985E +2	8.1904E +2	7.6299E +2
21.2	9.1607E +2	8.9548E +2	8.1611E +2	7.6138E +2
22.3	9.0937E +2	8.9176E +2	8.1281E +2	7.5954E +2
23.3	9.0350E +2	8.8873E +2	8.1001E +2	7.5762E +2
24.4	8.9850E +2	8.8641E +2	8.0879E +2	7.5571E +2
25.4	8.9441E +2	8.8490E +2	8.0708E +2	7.5376E +2
26.5	8.9132E +2	8.8427E +2	8.0440E +2	7.5194E +2

HEAT FLUX PROFILES FOR RUN 7

DISTANCE DOWN FURNACE	NET VERTICAL FLUX	FLUX TO TUBES
0.0	8.9407E -8	1.6689E +4
1.1	-2.0842E +3	1.5766E +4
2.1	-3.2654E +3	1.4935E +4
3.2	-3.0976E +3	1.4127E +4
4.2	-1.7329E +3	1.3295E +4
5.3	3.9203E +2	1.2398E +4
6.4	2.7366E +3	1.1394E +4
7.4	4.7207E +3	1.0441E +4
8.5	5.7614E +3	9.4012E +3
9.5	5.7952E +3	8.4803E +3
10.6	5.4793E +3	7.6193E +3
11.7	5.0841E +3	6.9343E +3
12.7	4.6879E +3	6.3168E +3
13.8	4.3092E +3	5.8044E +3
14.8	3.9503E +3	5.4548E +3
15.9	3.6065E +3	5.1279E +3
17.0	3.2729E +3	4.8452E +3
18.0	2.9402E +3	4.6345E +3
19.1	2.6099E +3	4.4341E +3
20.1	2.2786E +3	4.2728E +3
21.2	1.9420E +3	4.1559E +3
22.3	1.5931E +3	4.0955E +3
23.3	1.2280E +3	4.0519E +3
24.4	8.4372E +2	3.9764E +3
25.4	4.3792E +2	3.9693E +3
26.5	-2.9802E -8	4.0563E +3

Run 8 : AIR/FUEL RATIO 19.5:1

NAPHTHA FEEDSTOCK AND FUEL

BURNER FUEL FLOWRATE	2460	LB PER HOUR
AIR TO FUEL RATIO	19.50	
PROCESS GAS FLOWRATE	35200	LB PER HOUR
STEAM TO CARBON RATIO	3.00	
THEORETICAL FLAME TEMPERATURE	1945.0	DEG K

DISTANCE DOWN FURNACE	FLUE GAS TEMP	REFRACTORY TEMP	TUBE SKIN TEMP	PROCESS GAS TEMP
0.0	9.6120" +2	9.3046" +2	5.8730" +2	3.9900" +2
1.1	9.7724" +2	9.3430" +2	6.2293" +2	4.4505" +2
2.1	1.0323" +3	9.3988" +2	6.5832" +2	4.8756" +2
3.2	1.0915" +3	9.4605" +2	6.8944" +2	5.2668" +2
4.2	1.1369" +3	9.5110" +2	7.1702" +2	5.6242" +2
5.3	1.1603" +3	9.5369" +2	7.4119" +2	5.9460" +2
6.4	1.1582" +3	9.5312" +2	7.5876" +2	6.2310" +2
7.4	1.1294" +3	9.4936" +2	7.7328" +2	6.4779" +2
8.5	1.0727" +3	9.4327" +2	7.8341" +2	6.6855" +2
9.5	1.0299" +3	9.3505" +2	7.8963" +2	6.8554" +2
10.6	1.0034" +3	9.2608" +2	7.9256" +2	6.9914" +2
11.7	9.8386" +2	9.1723" +2	7.9524" +2	7.0975" +2
12.7	9.6785" +2	9.0885" +2	7.9536" +2	7.1775" +2
13.8	9.5388" +2	9.0100" +2	7.9536" +2	7.2371" +2
14.8	9.4133" +2	8.9370" +2	7.9524" +2	7.2787" +2
15.9	9.2991" +2	8.8697" +2	7.9256" +2	7.3058" +2
17.0	9.1946" +2	8.8077" +2	7.9085" +2	7.3219" +2
18.0	9.0987" +2	8.7509" +2	7.8963" +2	7.3295" +2
19.1	9.0107" +2	8.6995" +2	7.8683" +2	7.3291" +2
20.1	8.9304" +2	8.6535" +2	7.8353" +2	7.3238" +2
21.2	8.8573" +2	8.6128" +2	7.8231" +2	7.3146" +2
22.3	8.7915" +2	8.5780" +2	7.7901" +2	7.3020" +2
23.3	8.7329" +2	8.5491" +2	7.7780" +2	7.2886" +2
24.4	8.6818" +2	8.5269" +2	7.7609" +2	7.2736" +2
25.4	8.6387" +2	8.5120" +2	7.7340" +2	7.2583" +2
26.5	8.6043" +2	8.5047" +2	7.7328" +2	7.2444" +2

HEAT FLUX PROFILES FOR RUN 8

DISTANCE DOWN FURNACE	NET VERTICAL FLUX	FLUX TO TUBES
0.0	5.9605E -8	1.4088E +4
1.1	-1.7775E +3	1.3455E +4
2.1	-2.9149E +3	1.2833E +4
3.2	-3.0053E +3	1.2275E +4
4.2	-2.0830E +3	1.1677E +4
5.3	-4.3777E +2	1.0966E +4
6.4	1.4919E +3	1.0244E +4
7.4	3.2201E +3	9.4005E +3
8.5	4.2414E +3	8.5713E +3
9.5	4.4353E +3	7.7699E +3
10.6	4.2795E +3	7.0729E +3
11.7	4.0146E +3	6.4058E +3
12.7	3.7251E +3	5.8917E +3
13.8	3.4365E +3	5.4251E +3
14.8	3.1603E +3	5.0051E +3
15.9	2.8917E +3	4.7386E +3
17.0	2.6298E +3	4.4644E +3
18.0	2.3709E +3	4.2027E +3
19.1	2.1138E +3	4.0438E +3
20.1	1.8504E +3	3.9377E +3
21.2	1.5822E +3	3.7725E +3
22.3	1.3025E +3	3.7292E +3
23.3	1.0073E +3	3.6294E +3
24.4	6.9629E +2	3.5858E +3
25.4	3.6274E +2	3.6208E +3
26.5	-1.4901E -8	3.5882E +3

Run 9 : Combustion air preheat 300°C

Naphtha feedstock and fuel

BURNER FUEL FLOWRATE	2460	LB PER HOUR
AIR TO FUEL RATIO	16.90	
PROCESS GAS FLOWRATE	35200	LB PER HOUR
STEAM TO CARBON RATIO	3.00	
THEORETICAL FLAME TEMPERATURE	2130.0	DEG K

DISTANCE DOWN FURNACE	FLUE GAS TEMP	REFRACTORY TEMP	TUBE SKIN TEMP	PROCESS GAS TEMP
0.0	9.9089m +2	9.5828m +2	6.0536m +2	3.9900m +2
1.1	1.0098m +3	9.6213m +2	6.4490m +2	4.4946m +2
2.1	1.0715m +3	9.6753m +2	6.8200m +2	4.9583m +2
3.2	1.1336m +3	9.7330m +2	7.1421m +2	5.3818m +2
4.2	1.1779m +3	9.7769m +2	7.4399m +2	5.7658m +2
5.3	1.1972m +3	9.7939m +2	7.6767m +2	6.1087m +2
6.4	1.1897m +3	9.7772m +2	7.8512m +2	6.4087m +2
7.4	1.1543m +3	9.7276m +2	7.9866m +2	6.6650m +2
8.5	1.0898m +3	9.6552m +2	8.0720m +2	6.8782m +2
9.5	1.0447m +3	9.5614m +2	8.1331m +2	7.0511m +2
10.6	1.0181m +3	9.4617m +2	8.1611m +2	7.1855m +2
11.7	9.9859m +2	9.3653m +2	8.1623m +2	7.2879m +2
12.7	9.8239m +2	9.2746m +2	8.1623m +2	7.3645m +2
13.8	9.6811m +2	9.1902m +2	8.1611m +2	7.4187m +2
14.8	9.5520m +2	9.1122m +2	8.1440m +2	7.4547m +2
15.9	9.4341m +2	9.0403m +2	8.1172m +2	7.4763m +2
17.0	9.3262m +2	8.9743m +2	8.0891m +2	7.4873m +2
18.0	9.2274m +2	8.9140m +2	8.0708m +2	7.4888m +2
19.1	9.1371m +2	8.8595m +2	8.0428m +2	7.4828m +2
20.1	9.0549m +2	8.8108m +2	8.0147m +2	7.4725m +2
21.2	8.9806m +2	8.7681m +2	7.9866m +2	7.4580m +2
22.3	8.9142m +2	8.7317m +2	7.9536m +2	7.4410m +2
23.3	8.8558m +2	8.7019m +2	7.9256m +2	7.4233m +2
24.4	8.8057m +2	8.6790m +2	7.9134m +2	7.4049m +2
25.4	8.7644m +2	8.6639m +2	7.8963m +2	7.3867m +2
26.5	8.7327m +2	8.6573m +2	7.8792m +2	7.3697m +2

HEAT FLUX PROFILES FOR RUN 9

DISTANCE DOWN FURNACE	NET VERTICAL FLUX	FLUX TO TUBES
0.0	0.0000	1.5482E +4
1.1	-1.9343E +3	1.4703E +4
2.1	-3.0691E +3	1.3967E +4
3.2	-2.9714E +3	1.3297E +4
4.2	-1.7572E +3	1.2518E +4
5.3	1.8583E +2	1.1701E +4
6.4	2.3552E +3	1.0849E +4
7.4	4.2130E +3	9.9036E +3
8.5	5.2111E +3	9.0120E +3
9.5	5.2740E +3	8.0891E +3
10.6	5.0022E +3	7.2932E +3
11.7	4.6466E +3	6.6600E +3
12.7	4.2826E +3	6.0830E +3
13.8	3.9366E +3	5.5633E +3
14.8	3.6075E +3	5.1676E +3
15.9	3.2922E +3	4.8626E +3
17.0	2.9837E +3	4.6043E +3
18.0	2.6856E +3	4.3394E +3
19.1	2.3900E +3	4.1568E +3
20.1	2.0872E +3	4.0100E +3
21.2	1.7811E +3	3.8987E +3
22.3	1.4636E +3	3.8453E +3
23.3	1.1282E +3	3.8065E +3
24.4	7.7812E +2	3.7361E +3
25.4	4.0402E +2	3.7296E +3
26.5	-2.9802E -8	3.7686E +3

RUN 10 : COMBUSTION AIR PREHEAT 400°C

NAPHTHA FEEDSTOCK AND FUEL

BURNER FUEL FLOWRATE	2460	LB PER HOUR
AIR TO FUEL RATIO	16.90	
PROCESS GAS FLOWRATE	35200	LB PER HOUR
STEAM TO CARBON RATIO	3.00	
THEORETICAL FLAME TEMPERATURE	2230.0	DEG K

DISTANCE DOWN FURNACE	FLUE GAS TEMP	REFRACTORY TEMP	TUBE SKIN TEMP	PROCESS GAS TEMP
0.0	1.0212E +3	9.8785E +2	6.2562E +2	3.9900E +2
1.1	1.0415E +3	9.9167E +2	6.6857E +2	4.5441E +2
2.1	1.1064E +3	9.9698E +2	7.0848E +2	5.0505E +2
3.2	1.1707E +3	1.0026E +3	7.4240E +2	5.5101E +2
4.2	1.2155E +3	1.0068E +3	7.7169E +2	5.9237E +2
5.3	1.2342E +3	1.0083E +3	7.9695E +2	6.2907E +2
6.4	1.2249E +3	1.0063E +3	8.1452E +2	6.6082E +2
7.4	1.1869E +3	1.0011E +3	8.2807E +2	6.8782E +2
8.5	1.1187E +3	9.9352E +2	8.3649E +2	7.0999E +2
9.5	1.0720E +3	9.8381E +2	8.4260E +2	7.2781E +2
10.6	1.0449E +3	9.7356E +2	8.4381E +2	7.4160E +2
11.7	1.0252E +3	9.6365E +2	8.4540E +2	7.5195E +2
12.7	1.0088E +3	9.5435E +2	8.4381E +2	7.5941E +2
13.8	9.9428E +2	9.4570E +2	8.4271E +2	7.6464E +2
14.8	9.8115E +2	9.3768E +2	8.4150E +2	7.6800E +2
15.9	9.6916E +2	9.3030E +2	8.3820E +2	7.6987E +2
17.0	9.5819E +2	9.2351E +2	8.3527E +2	7.7067E +2
18.0	9.4814E +2	9.1732E +2	8.3247E +2	7.7056E +2
19.1	9.3896E +2	9.1172E +2	8.2966E +2	7.6973E +2
20.1	9.3062E +2	9.0673E +2	8.2624E +2	7.6833E +2
21.2	9.2309E +2	9.0236E +2	8.2184E +2	7.6669E +2
22.3	9.1637E +2	8.9864E +2	8.1904E +2	7.6491E +2
23.3	9.1049E +2	8.9558E +2	8.1782E +2	7.6292E +2
24.4	9.0546E +2	8.9329E +2	8.1452E +2	7.6084E +2
25.4	9.0136E +2	8.9176E +2	8.1331E +2	7.5886E +2
26.5	8.9825E +2	8.9112E +2	8.1160E +2	7.5706E +2

HEAT FLUX PROFILES FOR RUN 10

DISTANCE DOWN FURNACE	NET VERTICAL FLUX	FLUX TO TUBES
0.0	5.9605E +3	1.7046E +4
1.1	-2.1183E +3	1.6108E +4
2.1	-3.3262E +3	1.5211E +4
3.2	-3.1650E +3	1.4406E +4
4.2	-1.7855E +3	1.3562E +4
5.3	3.7453E +2	1.2586E +4
6.4	2.7609E +3	1.1635E +4
7.4	4.7789E +3	1.0591E +4
8.5	5.8452E +3	9.6152E +3
9.5	5.8846E +3	8.6004E +3
10.6	5.5637E +3	7.8083E +3
11.7	5.1654E +3	7.0376E +3
12.7	4.7648E +3	6.4864E +3
13.8	4.3806E +3	5.9659E +3
14.8	4.0178E +3	5.5046E +3
15.9	3.6690E +3	5.1979E +3
17.0	3.3278E +3	4.9172E +3
18.0	2.9932E +3	4.6730E +3
19.1	2.6616E +3	4.4694E +3
20.1	2.3283E +3	4.3353E +3
21.2	1.9814E +3	4.2872E +3
22.3	1.6220E +3	4.2017E +3
23.3	1.2524E +3	4.0812E +3
24.4	8.6225E +2	4.1034E +3
25.4	4.4785E +2	4.0724E +3
26.5	-2.9802E -8	4.1148E +3

REFERENCES

1. SPIERS, H.M., "Technical Data on Fuel", 6th ed. (1962).
2. "Gas Making", published by The British Petroleum Company Ltd.
4. MESSING, R.F. and BRADLEY, J.W., Chem. Eng. 67 No.13, p 74 (1960).
5. Pet. Ref. 38 No.11, p 280 (1959)
6. REDMAN, J., J. Inst. Fuel, 36 p 329 (1963).
7. DENT, F.J., Inst. Gas Eng. and Inst. of Fuel Conf., Hastings, (1962)
9. DENT, F.J., COCKERHAM, R.G. and THOMPSON, B.H., 7th International Gas Conf., The Hague.
10. THIBODEAU, R.D. and STEVENS, W.F., Chem. Proc. Eng. 46, p 410 (1965)
11. KIPINIAK, W., "Dynamic Optimisation and Control", John Wiley, (1961).
12. TURNER, K., PhD Dissertation, University of Leeds (1970).
14. TOPSOE, HALDOR, J. Inst. Gas Eng. 6 p 401 (1966)
15. LOBO, W.E. and EVANS, J.E., Trans. Am. Inst. Chem.Eng. 35 p 743 (1939)
16. McADAMS, W., "Heat Transmission", Mc-Graw Hill, (1954).
17. HOTTEL, H.C., J. Inst. Fuel 34, p 220 (1961).
18. HOTTEL, H.C. and SAROFIM, A.F., Inst. J. Heat Mass Transf., 8, p 1153, (1965).
19. CHANDRASEKHAR, S., "Radiative Transfer", Dover Publications, (1960)
20. KOURGANOFF, V., "Basic Methods in Transfer Problems", Oxford Univ. Press (1952).
21. USISKIN, C.M. and SPARROW, E.M., Int. J. Heat Mass Transf., 1 p 28 (1960).
22. VISKANTA, R. and GROSH, R.J. Internat. J. Heat and Mass Transfer, 1, p 81, (1960).
23. WIEBELT, J.A., "Engineering Radiation Heat Transfer", Holt, Reinhart and Winston, (1966).
24. CESS, R.D., Adv. in Heat Transfer, 1 p 1, (1964).
25. CHEN, J.C., Am. Inst. Chem. Eng. Journal, 10, p 253, (1964).
26. VISKANTA, R., Advances in Heat Transfer, 3, Academic Press, (1966).

27. HIRSCHFELDER, J.O., CURTIS, C.F. and BIRD, R.B., "Molecular Theory of Gases and Liquids", Wiley, (1954).

28. EDDINGTON, A.S., "The Internal Constitution of the stars", Dover Publications, (1959).

29. HOTTEL, H.C., Proc. of 1961-62 Heat Transfer Conf. ASME Special Lecture, (1963).

30. HOTTEL, H.C., Notes on Radiant Heat Transmission, Chem. Eng. Department, MIT, (1938).

31. ROESLER, F.C., Chem. Eng. Sci., 22 p 1325, (1967).

32. CRIB, G.S., Brit. Chem. Eng., 9, p 366, (1964).

33. FOX, J.M. and VARZE, J.C., Ind. Eng. Chem. 40, p 65, (1964).

34. SOMER, T.G., Brit. Chem. Eng. 8, p 466, (1963).

35. DENT, F.J., Gas World, 161, p 275, (1965).

36. LIHOU, D.A., Chem. Proc. Eng. 46, p 487, (1965).

37. COCKERHAM, R.G., PERCIVAL, G., and YARWOOD, T., J.Inst. Gas Eng., 5, p 109, (1965).

38. ANDREW, S.P.S. Private Communication

39. ANDREW, S.P.S., Paper delivered at the AGM of the Society of Chemical Industry, (1964).

40. DODGE, W.F., "Chemical Engineering Thermodynamics", McGraw-Hill, (1944).

41. THRING, M.W., Chem. Proc. Eng. 46, p 544, (1965).

42. FROMENT, G.F., Ind. Eng. Chem., 59, p 18, (1967).

43. CRESSWELL, D.L., PhD Dissertation, University of Leeds, (1969).

44. McGREAVY. C. and TURNER, K., 19th Canadian Chemical Engineering Conference, Symposium on Catalysis, (1969).

45. THRING, M.W., "The Science of Flames and Furnaces", Chapman and Hall, (1962).

46. JAKOB, M., Proc. Phys. Roy. Soc., 59, p 726, (1947).

47. HOTTEL, H.C., J.Inst. Fuel, 34, p 220, (1961).

48. LEVA, M., Ind. Eng. Chem., 40, p 747, (1948).

49. YAGI, S. and WAKAO, N., Am. Inst. Chem. Eng. Journal, 5, p 79, (1959).

50. FELIX, T.R., PhD Thesis, University of Wisconsin, (1951).

51. PLAUTZ, D.A., and JOHNSTONE, H.F., Am. Inst. Chem. Eng. Journal, 1, p 193, (1955).

52. YAGI, S. AND KUNII.,D., Am. Inst. Chem. Eng. Journal, 6, p 97,(1960).

53. Ibid. 3, p 373, (1957).

54. ARGO, W.B. and SMITH, J.M., Chem. Eng. Prog., 49, p 443, (1953).

55. BEEK, J., Adv. in Chem. Eng. p 203, (1962).

56. FAHIEN, R.W. and SMITH, J.M., Am. Inst. Chem. Eng.Journal, 1, p 25, (1955).

57. HOUGEN et al, Am. Inst. Chem. Eng. Journal, 41, p 445, (1943).

58. WILDE, D.J., "Optimum Seeking Methods", Prentice-Hall, (1964).

59. KIEFER, J., Proc. Am. Math. Soc., 4, p 502, (1953).

60. GILL, S., Proc. Camb. Phil. Soc., 47, p 96, (1951).

61. HACKETT, R.S., Paper at Amsterdam Conference. "Application of Automation in the Process Industries", Inst. Chem. Eng., (1967).

64. PORT, F.J., ScD Thesis, Massachusetts Inst. of Technology, (1940).

65. CHAO, K.C., Am. Inst. Chem. Eng. Journal, 9, p 555, (1963).

66. ROSS, G., Trans. Inst. Chem. Eng. 45, p CE272, (1967).

67. PENNINGTON, R.H., "Introductory Computer Methods and Numerical Analysis", Collier, Macmillan, (1965).

68. JURSIK, J., Control. Eng. p 61, (1963).

69. IDA, E.S., Control Eng. p 107, (1962).

70. ECKERT, E.R.G. and DRAKE, R.M., "Heat and Mass Transfer", McGraw-Hill, (1959).

71. HOP, A.G., Paper at Amsterdam Conference, "Application of Automation in the Process Industries", (1967).

72. SAVAS, E.S., "Computer Control of Industrial Processes", McGraw-Hill, (1965).

73. CARBERRY, J.J., Chem. Proc. Eng., p 306, (1963).

74. WHITE, W.B., JOHNSON, S.M. and DANTZIG, G.B., J. Chem. Phys. 28, p 751, (1958).

75. NAPHTALI, L.M. J. Chem. Phys., 31, p 263, (1959).

76. ZELEZNIK, F.J., Ind. Eng. Chem., 60, p 27, (1968).

77. LEWIS, G.N. and RANDALL, M. "Thermodynamics", McGraw-Hill, (1961).

78. STOREY, S.H. and VAN ZEGGEREN, Can. J. Chem. Eng., 42, p 54, (1964).

79. NAPHTALI, L.M., Ind. Eng. Chem., 53, p 387, (1966).

80. SMITH, J.M., "Chemical Engineering Kinetics", McGraw-Hill.

81. GUEST, P.G., "Numerical Methods of Curve Fitting", Camb. Univ. Press, (1961).

82. LAPIDUS, L., "Digital Computation for Chemical Engineers", McGraw-Hill, (1962).

83. BOLEY, B.A. and WEINER, G.H., "Theory of Thermal Stresses", Wiley(1960).

84. HASSELMAN, D.P.H., J. Amer. Ceram. Soc., 46, p 229, (1963).

85. GRIFFITH, A.A., Phil. Trans. Roy. Soc., A221, p 163, (1920).

86. KINGERY, W.D., J. Amer. Ceram. Soc., 38, p 3, (1955).

87. HASSELMAN, D.P.H., J. Amer. Ceram. Soc., 50, p 454, (1967).